AD-A122 026 MEASUREMENTS OF SWARM PARAMETERS IN CHLORINE-BEARING MOLECULES(U) WESTINGHOUSE RESEARCH AND DEVELOPMENT CENTER PITTSBURGH PA D K DAVIES AUG 82 DYD-11008-CE

UNCLASSIFIED AFWAL-TR-82-2083 F33615-79-C-2074 F/G 20/8 NL

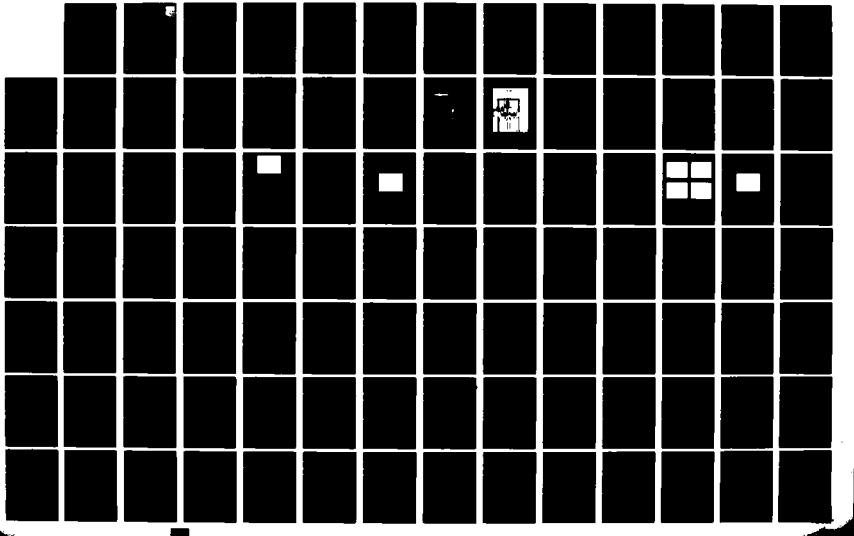

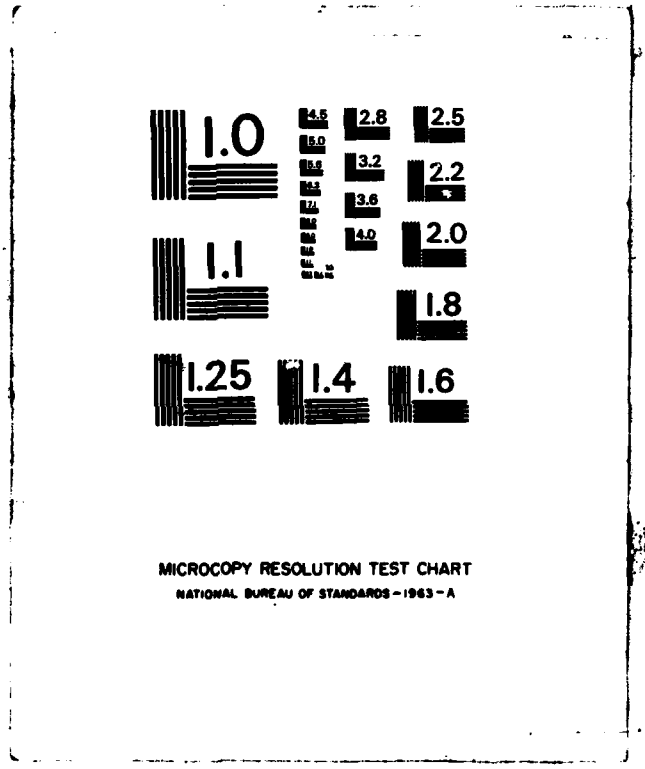
1.0
1.1
1.25
1.4
1.6
1.8
2.0
2.2
2.5
2.8
3.2
3.6
4.0
4.5
5.0
5.6
6.3
7.1
MICROCOPY RESOLUTION TEST CHART
NATIONAL BUREAU OF STANDARDS - 1963 - A

AFWAL-TR-82-2083

MEASUREMENTS OF SWARM PARAMETERS IN CHLORINE-BEARING MOLECULES

D. K. Davies

Westinghouse Electric Corporation
Research and Development Center
1310 Beulah Road
Pittsburgh, PA 15235

August 1982

Final Report for Period 15 August 1979 - 31 December 1981

AERO PROPULSION LABORATORY
AIR FORCE WRIGHT AERONAUTICAL LABORATORIES
AIR FORCE SYSTEMS COMMAND
WRIGHT-PATTERSON AIR FORCE BASE, OHIO 45433

NOTICE

When Government drawings, specifications, or other data are used for any purpose other than in connection with a definitely related Government procurement operation, the United States Government thereby incurs no responsibility nor any obligation whatsoever; and the fact that the government may have formulated, furnished, or in any way supplied the said drawings, specifications, or other data, is not to be regarded by implication or otherwise as in any manner licensing the holder or any other person or corporation, or conveying any rights or permission to manufacture use, or sell any patented invention that may in any way be related thereto.

This report has been reviewed by the Office of Public Affairs (ASD/PA) and is releasable to the National Technical Information Service (NTIS). At NTIS, it will be available to the general public, including foreign nations.

This technical report has been reviewed and is approved for publication.

Gary L. Duke

GARY L. DUKE, Capt, USAF
TAM, Plasma Physics

Joseph Wise

JOSEPH F. WISE, Chief
Energy Conversion Branch
Aerospace Power Division

FOR THE COMMANDER

James D. Reams

JAMES D. REAMS
Chief, Aerospace Power Division
Aero Propulsion Laboratory

"If your address has changed, if you wish to be removed from our mailing list, or if the addressee is no longer employed by your organization please notify AFWAL/POOC, W-PAFB, OH 45433 to help us maintain a current mailing list".

Copies of this report should not be returned unless return is required by security considerations, contractual obligations, or notice on a specific document.

UNCLASSIFIED

SECURITY CLASSIFICATION OF THIS PAGE (When Data Entered)

REPORT DOCUMENTATION PAGE		READ INSTRUCTIONS BEFORE COMPLETING FORM
1. REPORT NUMBER AFWAL-TR-82-2083	2. GOVT ACCESSION NO. AD-A122026	3. RECIPIENT'S CATALOG NUMBER
4. TITLE (and Subtitle) MEASUREMENTS OF SWARM PARAMETERS IN CHLORINE-BEARING MOLECULES		5. TYPE OF REPORT & PERIOD COVERED FINAL REPORT 15 AUG 79 - 31 DEC 81 6. PERFORMING ORG. REPORT NUMBER DYD-11008-CE
7. AUTHOR(s) D. K. Davies		8. CONTRACT OR GRANT NUMBER(s) F33615-79-C-2074
9. PERFORMING ORGANIZATION NAME AND ADDRESS Westinghouse Electric Corporation Research and Development Center 1310 Beulah Road Pittsburgh PA 15235		10. PROGRAM ELEMENT, PROJECT, TASK AREA & WORK UNIT NUMBERS Task 2301 Project S2 Work Unit 23
11. CONTROLLING OFFICE NAME AND ADDRESS Aero Propulsion Laboratory (POOC) Air Force Wright Aeronautical Laboratories (AFSC) Wright-Patterson Air Force Base, OH 45433		12. REPORT DATE August 1982 13. NUMBER OF PAGES 94
14. MONITORING AGENCY NAME & ADDRESS(if different from Controlling Office)		15. SECURITY CLASS. (of this report) UNCLASSIFIED 15a. DECLASSIFICATION/DOWNGRADING SCHEDULE

16. DISTRIBUTION STATEMENT (of this Report)

Approved for public release; distribution unlimited

17. DISTRIBUTION STATEMENT (of the abstract entered in Block 20, if different from Report)

18. SUPPLEMENTARY NOTES

19. KEY WORDS (Continue on reverse side if necessary and identify by block number)

Drift Tube, HCl, CCl_4, Cl_2, BCl_3, ionization, attachment, drift velocity, ion mobility, electron collision cross sections, Hydrochloric acid, carbon-tetrachloride, chlorine, boron trichloride.

20. ABSTRACT (Continue on reverse side if necessary and identify by block number)

Precision measurements of swarm parameters have been measured over an extended range of electron mean energy in chlorine-bearing gases relevant to the xenon chloride excimer laser system. These measurements were accomplished using a pulsed drift tube specifically designed to handle corrosive gases.

Experimental measurements of electron drift velocity, attachment and ionization coefficients together with positive and negative-ion mobilities have

DD FORM 1 JAN 73 1473 EDITION OF 1 NOV 65 IS OBSOLETE

UNCLASSIFIED

SECURITY CLASSIFICATION OF THIS PAGE (When Data Entered)

been made in pure HCl over the range of E/N (ratio of electric field to gas number density) from 3 to 300 x 10^{-17} Vcm^2. A set of electron collision cross sections has been derived which is consistent with the measured swarm parameters. Combination of this set of cross sections with the known set for nitrogen has resolved an apparent discrepancy in the attachment rate coefficient between the present measurements and other measurements in HCl/N_2 mixtures.

Measurements of swarm parameters in pure CCl_4 have been made over the range of E/N from 300 to 950 x 10^{-17} V-cm^2. Measurements of electron drift velocity were possible only over the limited range of E/N from 850 to 950 x 10^{-17} V-cm^2. The lack of sufficient data in CCl_4 prevented a meaningful derivation of a cross section set for CCl_4.

Considerable effort was expended to obtain swarm data in pure Cl_2. Attempts to achieve a higher yield photocathode than a semi-transparent gold cathode are documented. A new louvered photocathode was designed. Together with higher intensity UV exciting sources, usable current waveforms were finally recorded in Cl_2. The results of a literature search on swarm parameters and electron impact cross sections are summarized for Cl_2 and BCl_3.

FOREWARD

This final report was prepared by the Westinghouse R&D Center, 1310 Beulah Road, Pittsburgh, PA 15235, under Contract No. F33615-79-C-2074, Project 2301, Task S2, Work Unit 23, with Capt. Gary L. Duke (AFWAL/POOC-3) as Government Project Monitor. The technical effort described in this report was conducted by D. K. Davies and accomplished during the period 15 August 1979 through 31 December 1981. The author is particularly indebted to P. J. Chantry and M. A. Biondi for many fruitful discussions during the course of the work. The assistance of L. E. Kline in operating the Boltzmann code and for supplying cross-section data for Xe and Ne is also gratefully acknowledged. Thanks are also due to W. M. Uhlig for the careful construction and assembly of the experimental system, to J. R. Auld for the preparation of the $CC\ell_4$ sample, and to G. W. Sherwin and T. G. Ketterer for their fine technical support. It was a pleasure to interact with Major R. D. Franklin and Capt. G. L. Duke in their capacities as Program Manager for this contract. Finally, a debt of gratitude is owed to A. V. Phelps for his interest in and encouragement of this work.

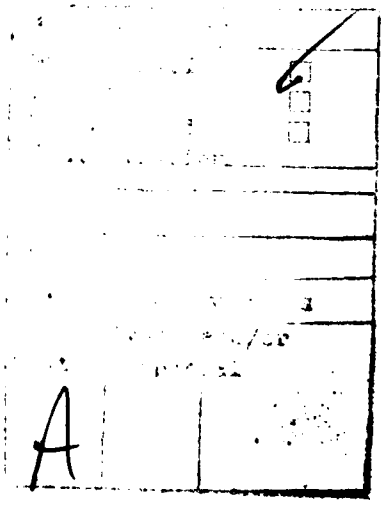

CONTENTS

CONTENTS CONCLUDED

ILLUSTRATIONS

ILLUSTRATIONS CONTINUED

ILLUSTRATIONS CONTINUED

ILLUSTRATIONS CONCLUDED

TABLES

SUMMARY

PROGRAM OBJECTIVES AND APPROACH

The major objective of the present contract was to provide precision measurements of electron drift velocity together with attachment and ionization coefficients over an extended range of electron mean energy in chlorine-bearing gases relevant to the xenon chloride excimer laser system. Specifically, in order of importance, the gases to be studied were $HC\ell$, $C\ell_2$, $CC\ell_4$, and $BC\ell_3$. A second objective was to derive a set of electron collision cross sections consistent with the measured swarm parameters.

The measurements of swarm parameters have been carried out using a pulsed drift tube specifically designed to handle corrosive gases. The technique involves the injection of a pulse of electrons into a region of uniform field E containing the gas under study at a density N. Collisions of these electrons with the gas molecules during their drift to the anode result, in general, in a distribution of electrons, negative ions, and positive ions in the drift space. The swarm parameters are then determined directly from measurements of the time-resolved currents of electrons and negative ions arriving at the anode and of positive ions arriving at the cathode. The ability of the present drift tube to resolve the arrival spectra of each charged species leads to the most direct interpretation of the measurements particularly at high values of E/N above the onset of ionization. A set of collision cross sections consistent with the measured swarm parameters is obtained from iterative solutions of the Boltzmann transport equation. The input trial cross sections required for numerical integration of the Boltzmann equation are adjusted until agreement between predicted and measured swarm parameters is attained.

ACCOMPLISHMENTS

During the early phases of the contract, a gas-handling system was designed and constructed for the safe handling of the reactive and toxic gases under study. In particular, the expended gas samples from the drift tube are trapped out in a valved high-pressure cylinder thereby avoiding the necessity for special vacuum pumps to exhaust the gases. The system has proved to be hazard-free and has been used routinely for measurements in the gases

studied. A full description of this system together with a detailed account of the experimental apparatus and procedure for the determination of the swarm parameters and derived cross sections is given in Section 2.

Experimental measurements of electron drift velocity, attachment and ionization coefficients together with positive and negative-ion mobilities have been made in pure HCℓ over the range of E/N from 3 to 300 x 10^{-17} V cm^2 corresponding to electron mean energies from thermal to < 6 eV. A set of electron collision cross sections including those for momentum transfer, rotational, vibrational, and electronic excitation, attachment and ionization has been derived which is consistent with the measured swarm parameters. Combination of this set of cross sections with the known set for nitrogen has resolved an apparent discrepancy in the attachment rate coefficient between the present measurements in pure HCℓ and other measurements in $HC\ell/N_2$ mixtures. The derived set of cross sections for HCℓ has also been used in combination with cross section sets for Ne and Xe to predict rate coefficients in a typical excimer laser gas mixture. The results of the investigation in HCℓ are given in Section 3.

Measurements of swarm parameters in pure $CC\ell_4$ have been carried out over the range of E/N from 300 to 950 x 10^{-17} V cm^2. The attachment rate coefficient in $CC\ell_4$ is very large as evidenced by the high value of the limiting E/N (≈ 880 x 10^{-17} V cm^2). Consequently, measurements of electron drift velocity have been possible only over the limited range of E/N from 850 to 950 x 10^{-17} V cm^2 for which ionization in the drift space allows sufficient transmission of the electron current through the drift space for detection. The lack of sufficient data on cross sections in $CC\ell_4$ has prevented a meaningful derivation of a cross section set for $CC\ell_4$ to be made. The investigation in $CC\ell_4$ is described in Section 4.

Considerable effort has been expended to obtain swarm data in pure $C\ell_2$ and is documented in Section 5. On introducing $C\ell_2$ into the drift tube the photo-electron yield from the semi-transparent gold cathode is reduced by four orders of magnitude compared with that obtained with HCℓ or $CC\ell_4$. Attempts to achieve a higher yield by replacing the thin-film gold cathode with films of different material compatible with $C\ell_2$ have been unsuccessful. However, towards the end of the contract period, the use of a different type of cathode structure together with different UV exciting sources having a higher

intensity particularly at the shorter wavelengths have allowed usable current waveforms to be recorded in pure $C\ell_2$. Unfortunately, the large effort expended to overcome the unforeseen technical difficulties with $C\ell_2$ left no time to conduct systematic swarm measurements in $C\ell_2$. For the same reason, no measurements have been made in $BC\ell_3$.

SUGGESTED FURTHER WORK

Although the present work in HCℓ has provided an extensive data base for this gas previously unavailable, there remain some details worthy of further attention. Specifically, to separate the effects of rotational excitation from elastic scattering at low electron mean energies, further measurements of electron drift velocity in mixtures of HCℓ with other buffer gases, such as N_2, whose cross sections are well established would be desirable. The enhancement of the dissociative attachment rate in HCℓ from rotationally excited levels has been predicted to be as pronounced as that from vibrationally excited levels. In addition measurements of electronic excitation rate coefficients (e.g., for the B and C states) would be desirable to place stronger confidence on the rate coefficient for the A state. This latter rate is considered to be important since it leads to dissociation of HCℓ, the dissociated atoms being particularly efficient in de-exciting vibrationally excited states of HCℓ from which enhanced dissociative attachment is known to occur.

The successful solution to the problems associated with the operation of the drift tube in the presence of pure $C\ell_2$ now enables measurements of swarm parameters in $C\ell_2$ to be carried out. The availability of data on $C\ell_2$ would allow the effects of $C\ell_2$ build-up in excimer laser gas mixtures on the performance of the laser to be modelled.

As pointed out in Section 6, the prediction of swarm properties in mixtures of the chlorine-donor molecule with xenon and neon is hampered by the uncertainty in the momentum transfer cross sections in Xe and Ne for electron energies above 7 eV. Thus, to overcome these uncertainties, it is proposed that a systematic set of measurements of electron drift velocity be made in pure Xe and pure Ne over an extended range of E/N. In addition, measurements of D_L/μ_e in Xe at low E/N would be desirable to improve the precision of the momentum transfer cross section in Xe in the region of the Ramsauer minimum.

1. INTRODUCTION

1.1 BACKGROUND

Assessment of the potential efficiency and scalability of laser systems requires a considerable body of basic data concerning the interaction of electrons and photons with the various gas species involved. The steady-state operating conditions of the laser discharge are determined by a balance between electron production and electron loss processes. In the case of the rare gas-chloride excimer laser system the chlorine-donor molecule is usually an attaching gas and electron attachment represents the dominant electron loss mechanism. In addition, an important channel for formation of the upper lasing state of the exciplex proceeds via reactions of the atomic negative ion, produced by dissociative attachment, of the chlorine-donor gas with rare gas ions. For efficient laser energy output, attempts are made to operate the discharge under conditions where the electron energy distribution is optimized for production of the upper lasing state. Control of the operating conditions of the discharge is obtained by proper choice of the constituent species in the mixture, by the relative proportions of the species in the mixture, and by additional sources of electron production in the gas such as irradiation by high-energy electrons.

The electron energy distribution as a function of applied field may be predicted from a solution of the Boltzmann transport equation provided all the cross sections for collisions of electrons with the constituent species of the gas mixture are known. Knowledge of the distribution function then enables the production and loss rates of electrons to be determined and, together with other reaction-rate data, allows prediction of the production rate of the upper lasing level. In the case of the rare gas-chloride lasing systems, the cross sections for the rare gas constituents are reasonably established although some uncertainty still exists for electron energies $\gtrsim$ 1 eV. However, limited studies have been made of the chlorinated molecules due to the high level of chemical reactivity and/or toxicity of most of the molecules of interest.

The emphasis on the molecule HCl in the present work stems from its emergence as the leading candidate for use in the XeCl system. CCl_4 and BCl_3 are potential substitutes for HCl as chlorine-donor molecules. Although

chlorine has also been used as a chlorine donor in the XeCl system, its potential applicability in this role is considered to be limited because of its large optical absorption cross section at the lasing wavelength. Nevertheless, because of this property, data on chlorine are of importance since molecular chlorine is known to arise from impurity build-up in systems employing other chlorine-donor molecules.

1.2 CONTRACT OBJECTIVES

The major objective of the present contract was to measure electron swarm parameters, i.e., electron drift velocity, attachment coefficient, and ionization coefficient, in the four chlorine-bearing molecules HCl, Cl_2, CCl_4, and BCl_3, over as wide a range of electron mean energy as possible.

A minor objective of the contract was to determine a set of electron collision cross sections for each of the four gases consistent with the measured swarm parameters.

1.3 GENERAL METHODOLOGY

The method adopted for determining the electron transport and swarm parameters is the time-resolved measurement of electron and ion waveforms using a pulsed drift tube. In this method, a pulse of electrons is injected from the cathode into a region of uniform electric field E containing a gas of known density N. In general, a distribution of electrons, negative ions, and positive ions is created in the drift space as a result of collisions of electrons with gas molecules during the drift time of electrons to the anode. The electron transport and swarm parameters are then determined directly from measurements of the time-resolved currents of electrons and negative ions arriving at the anode and of positive ions arriving at the cathode. Resolution of the arrival spectra of each charged species leads to the most direct interpretation of the measurements and is the approach used in the present apparatus.

Determination of a set of electron collision cross sections consistent with the measured swarm parameters is obtained from iterative solutions of the Boltzmann transport equation using a two-term spherical harmonics expansion

model for the distribution function. In this method, the input trial cross sections, required for numerical integration of the Boltzmann equation, are adjusted until agreement between predicted and measured swarm parameters is attained.

2. EXPERIMENTAL PROCEDURE

2.1 DRIFT TUBE

A sectional drawing of the drift tube chamber is shown in Figure 1 and a photograph of the internal structure in Figure 2. A uniform-field drift region is maintained between the semi-transparent cathode and anode by a set of ten annular guard rings 0.16 cm thick having an external diameter of 8.9 cm and internal diameter of 5.1 cm. The guard rings are separated by precision spherical sapphire spacers such that the centers of the rings are accurately spaced 0.5 cm apart. Both anode and cathode are electrically shielded from the drift region by a highly transparent etched grid[1] located 0.1 cm from the surface of each electrode. Each grid is 0.0025 cm thick and contains 20 lines/cm with a line thickness of 0.0033 cm giving an optical transparency of 87%.

The cathode consists of a plate with a bevelled sapphire disc insert, 1.6 cm in diameter, centered along the axis of the drift tube and with its surface coplanar with the surface of the plate adjacent to the drift region. The bevelled edge and lip of the sapphire are coated with gold to a thickness of 1400 Å prior to its insertion in the support plate. After assembly, the entire surface of the plate and insert adjacent to the drift region are coated with gold to a thickness of 300 Å. Electrical contact between the thin gold-film photocathode and the support plate is provided through the thicker gold film deposited on the lip and edge of the sapphire insert.

The anode and its associated grid structure are coupled to the chamber envelope via a linear bellows drive enabling the drift distance to be varied. A stop attached to the guard ring farthest from the cathode is positioned such that at the maximum drift distance, the anode grid is coplanar with the center plane of this guard ring and is indicated by electrical continuity between the guard ring and anode grid. Thus, decreasing the drift distance in increments of 0.5 cm ensures that the anode grid is coplanar with each successive guard ring thereby minimizing distortions of the electric field. Increments in drift distance are accurately measured using a high-resolution (0.0002 cm/division) micrometer indexed to the drive outside the

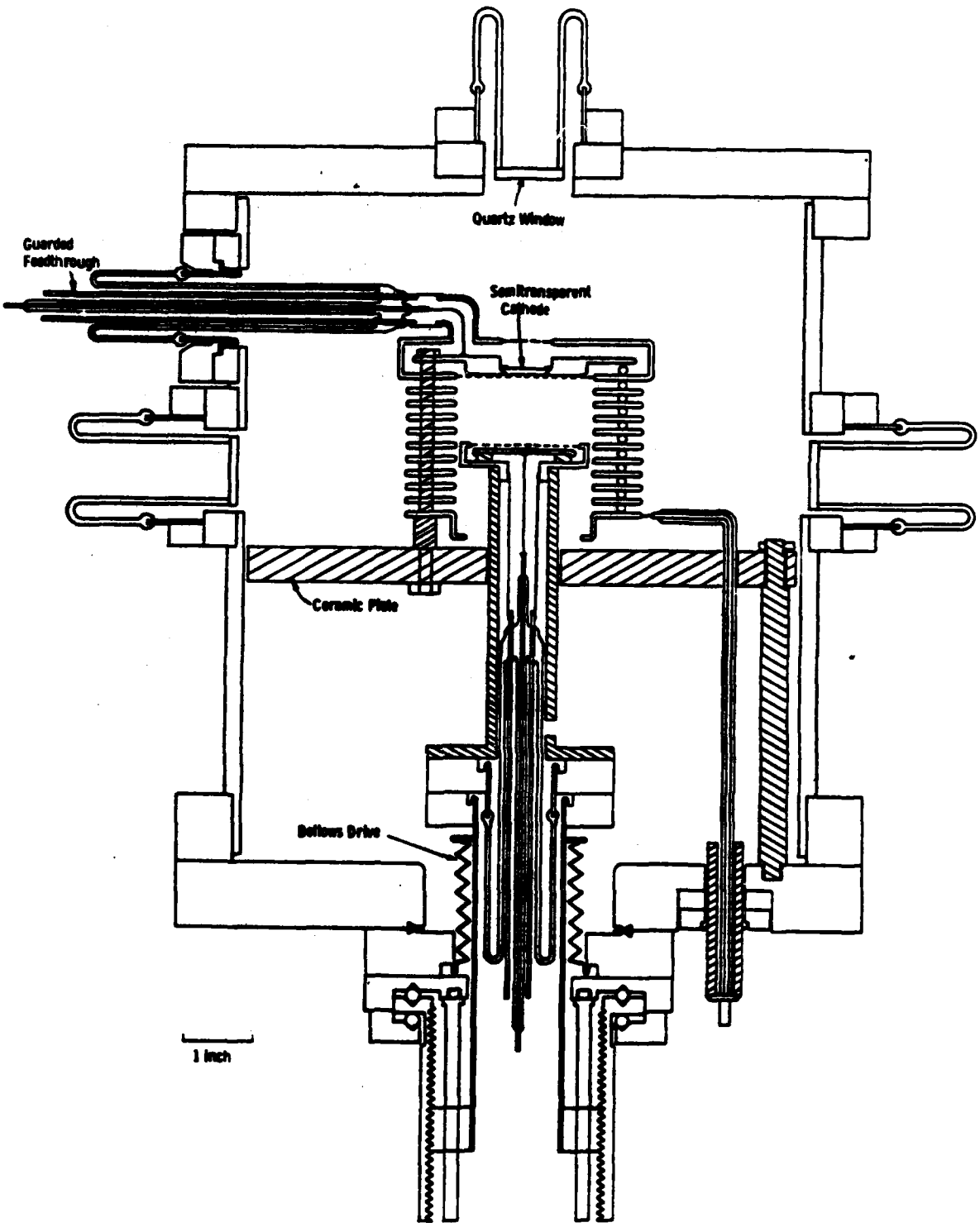

Fig. 1 - Sectional drawing of the drift tube.

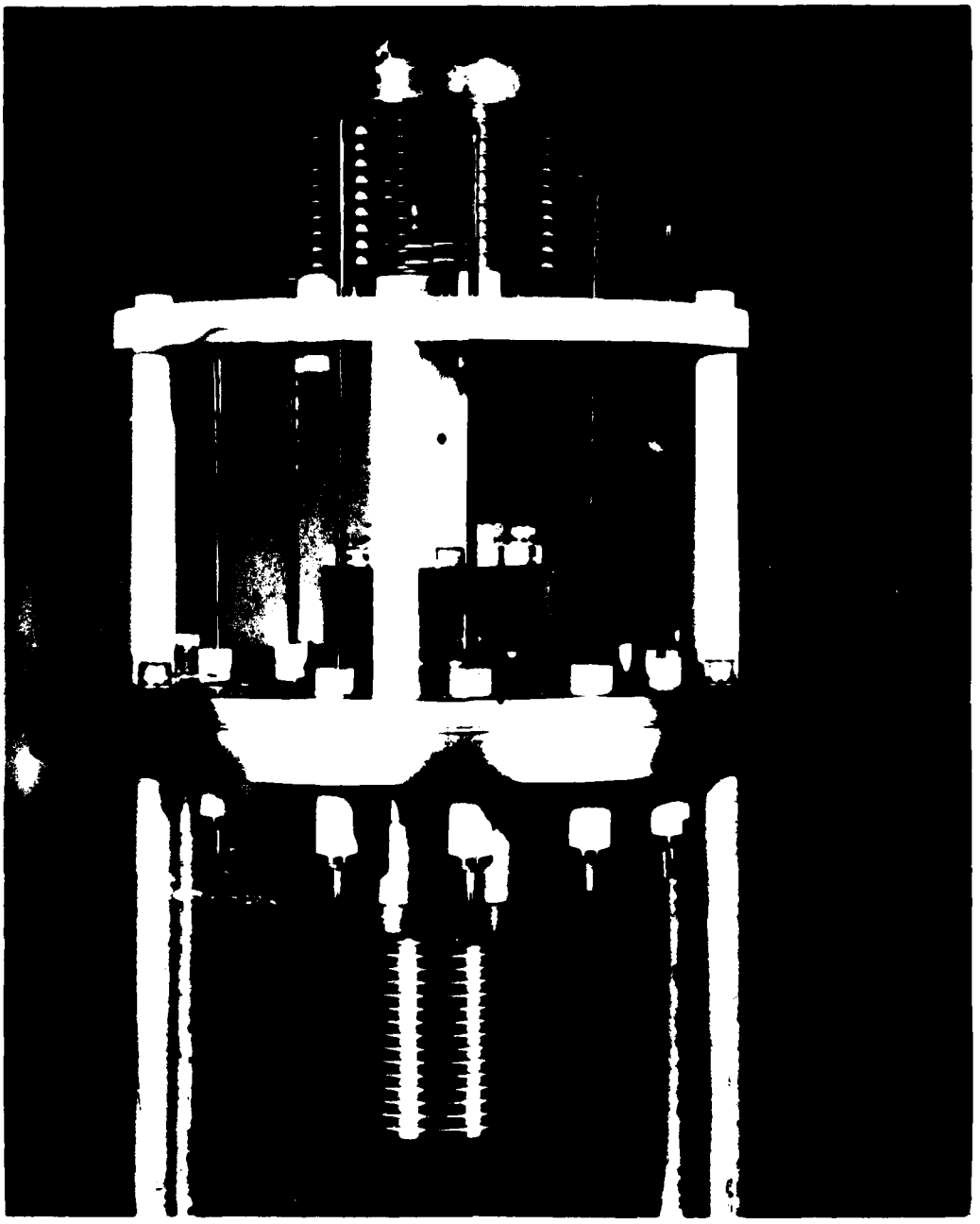

Fig. 2 - Photograph of the internal structure of the drift tube.

chamber envelope. In this way the total drift distance between anode and cathode may be varied from 0.7 cm to 5.2 cm.

The tube is designed so that either the cathode or anode may be connected to high potential. Connection to each guard ring is made by an insulated lead to a separate vacuum feedthrough in the chamber envelope.

The stainless steel chamber enclosing the drift tube also contains three quartz windows, one to provide optical access colinear with the axis of the drift tube and two for providing an optical path through the annular guard rings transverse to the axis of the drift tube.

2.2 VACUUM AND GAS HANDLING SYSTEM

The chamber is connected to an ultra high vacuum and gas handling system shown in Figure 3. Materials used for fabrication of the drift tube and its associated vacuum system have been chosen to be compatible with corrosive gases. All system components within the dashed rectangle in Figure 3 are baked during vacuum processing of the system prior to admission of gas to the chamber. Following a bakeout of the system at 350°C for 20 hr, the residual pressure is reduced to the low 10^{-9}-Torr range.

The gas pressure in the chamber is measured using a system of two differential Baratron[2] gauges having a combined specified accuracy of ±0.1% over the range from 0.1 Torr to 1000 Torr. The reference side of each gauge may be separately evacuated to a pressure $< 10^{-6}$ Torr using the ion pump. Alternately, the reference side of the 10-Torr gauge (which is connected to the measurement side of the 1000-Torr gauge) may be pressurized from the nitrogen supply. Thus, for pressures in the range 0.1 Torr to 10 Torr the pressure is measured directly using the 10-Torr gauge with its reference side evacuated. For pressures greater than 10 Torr, the 10-Torr gauge is used as a null indicator (differential pressure $< 10^{-3}$ Torr) by allowing nitrogen into its reference side and reading the pressure directly with the 1000-Torr gauge. Comparisons of the two gauges over the limited pressure range where both gauges are within their specified accuracy limits show consistency to ±0.1%.

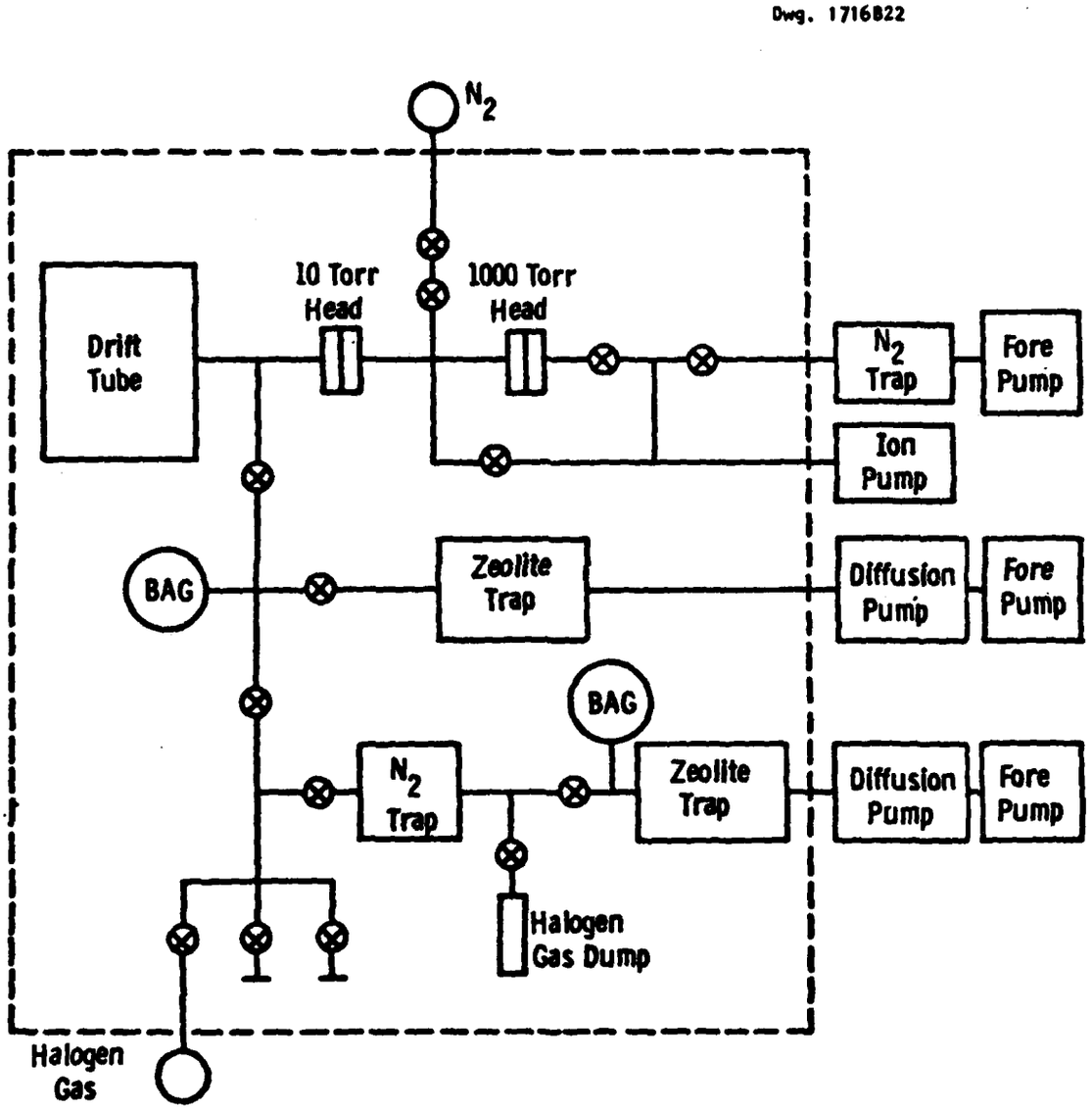

Fig. 3 - Schematic drawing of the vacuum and gas-handling system.

In order to avoid exhausting heavy loads of corrosive gas from the drift tube through the vacuum pumps, a halogen gas dump has been incorporated in the gas system. This consists of a valved stainless-steel cylinder having a volume of 100 cc and capable of withstanding internal pressures up to 1000 psi. After cooling the cylinder to liquid-nitrogen temperature the halogen gas sample in the drift tube is transferred to the cylinder, the pressure in the drift tube dropping to a value ~ 10^{-2} Torr in 1 to 2 hours. The valve on the cylinder is then closed and the residual gas in the drift tube is exhausted through the vacuum pumps. Between transfers, the valved-off cylinder may be allowed to warm to room temperature provided the saturated vapor pressure of the halogen gas is less than the pressure rating of the cylinder, which is the case for all four chlorine-bearing molecules in the present study.

2.3 OPTICAL ABSORPTION SYSTEM

The study of reactive gases in a static system is complicated by possible changes in gas density and/or gas composition. Thus, it is desirable to provide a means of monitoring the halogen gas density in the drift tube during measurements of current waveforms. A convenient method for many molecules is that of optical absorption in the ultraviolet region of the spectrum and is the method adopted in the present investigation.

The system shown in Figure 4 is a conventional dual-beam system comprising a probing beam (A), coupled along a path of length 21.5 cm through the drift region transverse to the drift tube axis via the quartz windows in the chamber envelope, and a reference beam (B). Both optical paths are of equal length and the intensities of both beams are made approximately equal by using metal screen attenuators in one of the beams. All optical components are made of quartz and are enclosed in sealed metal housings attached to the drift tube with O-ring seals. By flowing nitrogen through the housings, unwanted absorption in the far UV by oxygen and water vapor in the atmosphere is removed. The light source used is a mercury lamp (Ultra-Violet Products Model 11SC-2) which emits a number of convenient lines in the ultraviolet region which are selected using appropriate interference filters.

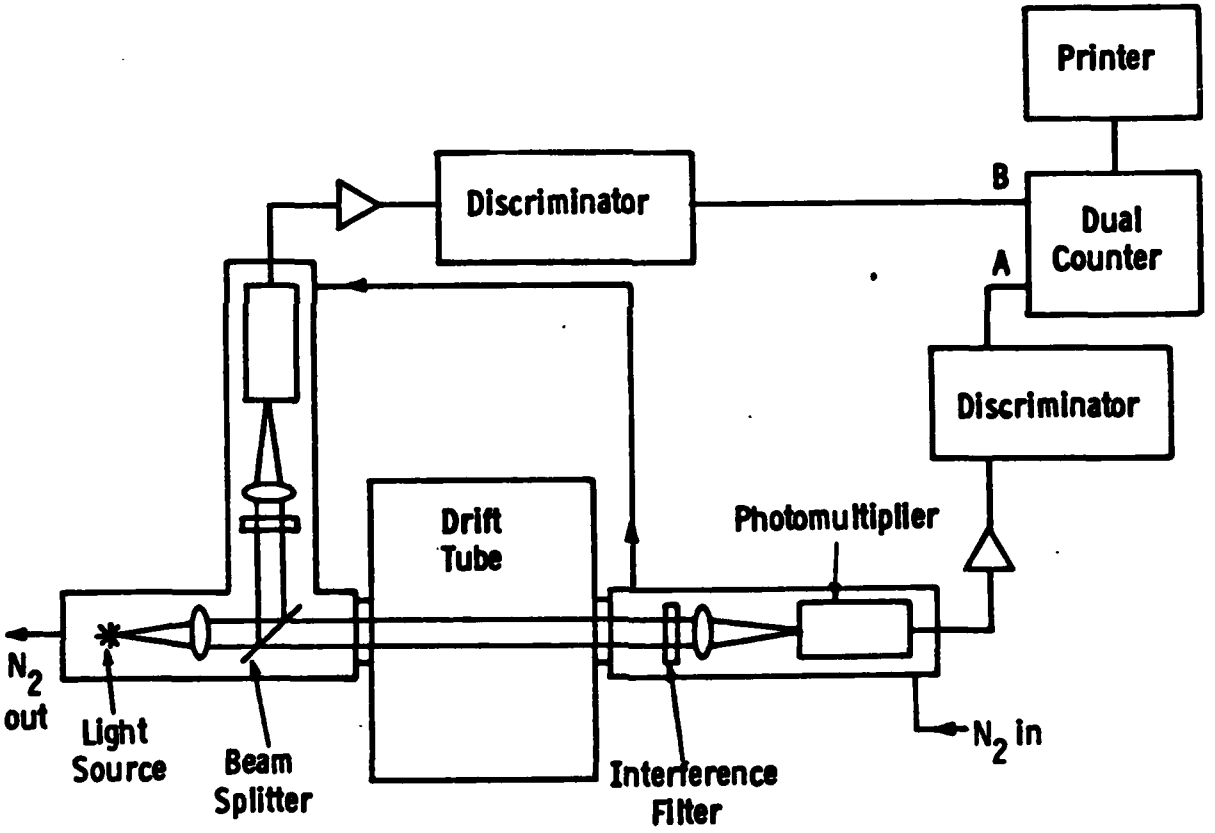

Fig. 4 - Schematic drawing of the optical absorption monitoring system.

Photon counting is used in the electronic readout of the system. The output from each photomultiplier (EMI type 6256S) is fed through an amplifier (LeCroy Model VV100B) having a gain of 20 dB and a bandwidth of 230 MHz to a discriminator (LeCroy Model LD 601C) having a pulse-pair resolution of 9 nsec followed by a 320 MHz decade prescaler (Fairchild Model 95H90) and then to one channel of a dual-channel counter (Ortec Model 9315). The counter is arranged so that both channels remain active until a predetermined number of counts (10^8) have been accumulated in the reference channel B at which time the counter is stopped, the contents of both channels printed and the counter reset for the next count cycle. The use of a wide bandwidth system enables a cycle time ~ 10 sec to be attained with a statistical variation in the transmitted count ~ 1 part in 10^4. Thus, a continual record of the optical transmission through the drift region is obtained at intervals ~ 10 sec. In practice, the fluctuation in the transmitted count is higher than the statistical variation. The overall stability in the system corresponds to a variation in the transmitted signal of ±3 parts in 10^4 over an 8 hour period. To achieve this stability, it is found necessary to operate both photomultipliers from a common power supply and to set each photomultiplier voltage at a value where the gradients of the gain versus voltage characteristics of both photomultipliers are matched.

In the case of HCℓ, the transmission is monitored at the wavelength 1849 Å where the absorption cross section is[3] 1.3×10^{-19} cm^2. For $Cℓ_2$, transmission at 3650 Å is monitored where the absorption cross section is[4] 9.0×10^{-20} cm^2. Thus, for both gases, densities down to ~ 4×10^{15} cm^{-3} (corresponding to an absorption ~ 1% over the optical path length) may be accurately monitored.

2.4 MEASUREMENT CIRCUITRY

The experimental arrangement used for the measurement of current waveforms from the drift tube is shown schematically in Figure 5 and is a modification of that used by Stelman et al.[5] A chain of 0.1% precision resistors across a bipolar DC power supply is used to derive the potentials applied to the drift tube, and the potential difference between the cathode and anode is measured to better than ±0.1% using a digital voltmeter. A pulse of UV radiation from

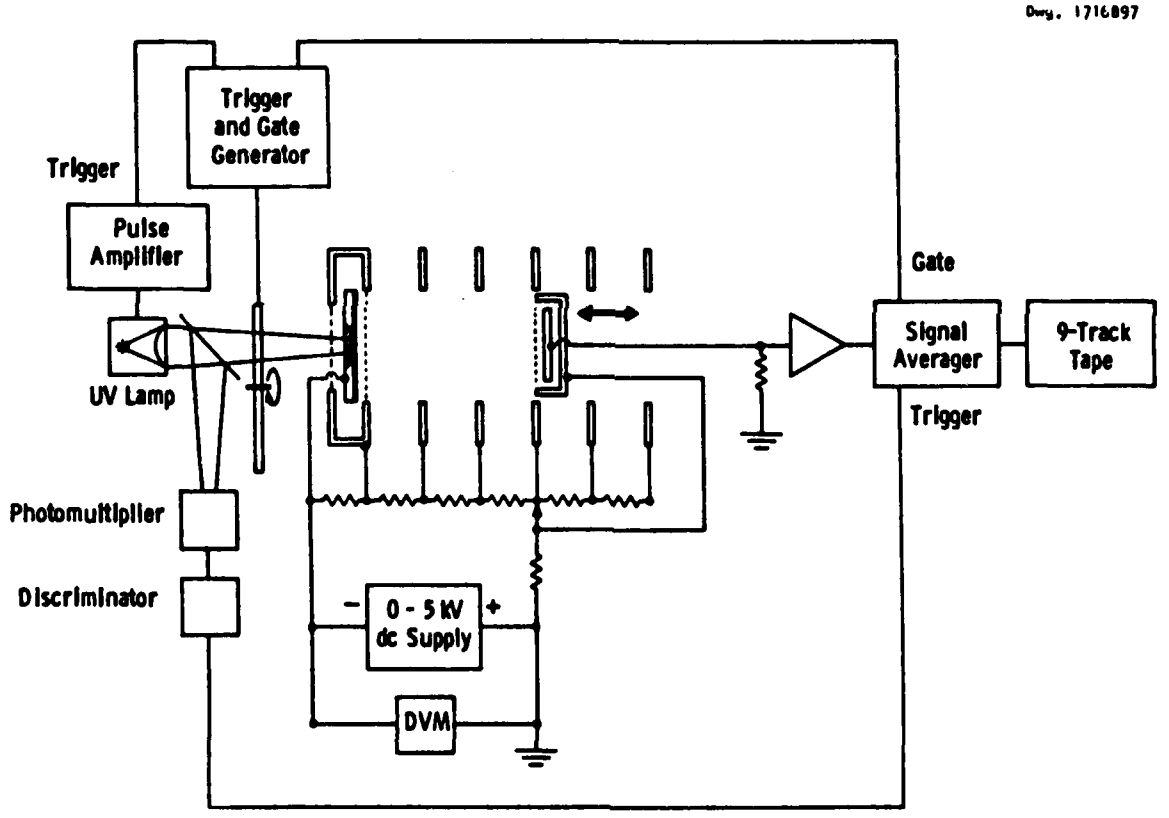

Fig. 5 - Experimental arrangement of the system for measuring current waveforms.

an externally mounted source illuminates the rear surface of the semi-transparent cathode via the quartz window in the chamber envelope. This provides the initial photoelectron pulse emitted to the drift region. The resulting arrival-time currents of electrons and negative ions at the anode or of positive ions at the cathode are detected when they pass through the grid immediately adjacent to each collecting electrode. The electrode current signal is amplified and fed to a waveform digitizer (Biomation Model 6500) and signal averager (Nicolet Model 1070) and eventually stored on 9-track tape (Kennedy Model 9700). Data are accumulated in the signal averager at a repetition rate ~ 30-100 pulses/sec until the signal/noise ratio has attained a satisfactory value. Typically this requires the summation of between 10^4 and 10^5 digitized current waveforms.

Although the signal averager is effective in improving the ratio of true signal to random noise, sources of non-random (systematic) noise and DC drift are unaffected. Despite careful shielding non-random noise, particularly that associated with pick-up from the pulsed light source, remains significant. In order to remove this source of noise from the signal accumulated from many repetitions of the experiment it has been found necessary to arrange the transfer of data from the waveform digitizer to the signal averager so that alternate pulses are added to and subtracted from the data already stored in the signal averager. A synchronized shutter between the pulsed light source and the drift tube is arranged so that during the add cycle the light pulse from the UV source is transmitted into the drift tube, while during the subtract cycle the light pulse is blocked. This scheme removes from the accumulated signal all components of the background which occur repetitively in synchronism with the pulsed light source, including any DC component. In the present application it has also been found necessary to ensure that the chopper wheel presents the same electrical screening profile in both the add/open position and subtract/blocked position. This is achieved using a metal wheel consisting of all open segments with alternate segments masked by non-conducting opaque material.

Three different pulsed UV sources have been used during the course of the present investigation for liberating the initial photoelectron pulse from the cathode. For the measurements of electron drift velocity a spark discharge

source (Xenon Corporation Model 437A Nanopulser with a Type N-789B Head) has been used operating in air with an input energy ~ 1 mJ/pulse. The UV output from this source has a risetime of 10 nsec and a halfwidth of 20 nsec and liberates ~ 10^5 photoelectrons/pulse from the cathode.

For measurements of ion mobility, attachment, and ionization two different sources have been used. The earlier measurements were carried out using a deuterium lamp pulsed at a peak current ~ 4A. The rise and fall times of the radiation pulse are ~ 20 nsec with a pulse width which may be varied over the range from 70 nsec to 150 μsec. For the longer pulse durations the photoelectron yield/pulse is comparable to the spark discharge source. Later measurements were carried out using a pulsed xenon lamp (EGG Type FX-265 UV) operated at input energies over the range from 10 mJ/pulse to 100 mJ/pulse. Over this range the risetime of the UV output varies from 65 nsec to 185 nsec and the halfwidth varies from 145 nsec to 385 nsec giving a cathode photoemission in the range from 10^6 to 2 x 10^7 electrons/pulse. The higher intensity from this source compared with the deuterium source results in a significant improvement in the signal/noise ratio of the measured ion waveforms.

The configuration shown in Figure 5 corresponds to that used for measuring electron and negative ion signals arriving at the anode. For measurements of positive ion signals arriving at the cathode, the measuring circuitry is transferred to the cathode and the ground of the DC supply is transferred to the negative side. The ability of the present system to resolve the individual negative ion and positive ion components under conditions where attachment and ionization are occurring simultaneously simplifies the determination of the attachment and ionization coefficients as discussed in Section 2.5. For these measurements, normalization of the positive ion and negative ion signals to the initial photoelectron current is necessary. This is accomplished by monitoring the UV radiation entering the drift tube. A fraction of the UV output from the lamp is diverted by a suprasil quartz beamsplitter, placed between the chopper wheel and the drift tube, onto a photomultiplier. The output from the photomultiplier is fed to a gated current integrator whose gate width is adjusted to be slightly longer than the UV pulse duration. The input to the integrator is arranged to be active for

the same number of preset cycles for which the signal averager is accumulating current waveforms. Preliminary measurements were carried out to verify the correspondence between the UV signal and the total charge collected from the drift tube. These showed proportionality to within 1% justifying the normalization procedure adopted.

2.5 DETERMINATION OF SWARM PARAMETERS

2.5.1 Electron Waveforms

Under conditions where the duration (δt) of the initial electron pulse leaving the cathode is such that $\delta t \ll d/w_e$, where d is the total drift distance and w_e is the electron drift velocity, solution of the continuity equation for electrons leads to the following expression[6,7] for the time-dependent electron current [I_e (d,t)] arriving at the anode:

$$I_e(d,t) = [Q_o w_e/(4\pi D_L t)^{1/2}] \exp[-(d - w_e t)^2/4D_L t + (\alpha - \eta)w_e t]. \quad (1)$$

In Equation (1) Q_o is the initial net electron charge released from the cathode, D_L is the longitudinal diffusion coefficient, α is the ionization coefficient and η is the attachment coefficient. From Equation (1) the time τ_e corresponding to the arrival time at the anode of the peak of the electron current pulse is given to first order by

$$\tau_e \simeq (d/w_e)\ [1 - D_L/w_e d + 2D_L\ (\alpha - \eta)/w_e]. \quad (2)$$

By making measurements of τ_e as a function of d, errors due to the finite width of the pulse, end effects, and (to first order) diffusion effects are eliminated. However, effects due to attachment and ionization are not removed since, from Equation (2), the slope of the linear plot of τ_e versus d is given by $[1 + 2D_L\ (\alpha - \eta)/w_e]/w_e$, in contrast to the value $1/w_e$ obtaining in the absence of ionization or attachment. Thus, the true value of w_e is less than d/τ_e if $\eta > \alpha$ and larger than d/τ_e if $\alpha > \eta$. Usually, experimental conditions are chosen so that $D_L\ |\alpha - \eta|/w_e \ll 1$ making the correction to w_e negligibly small.

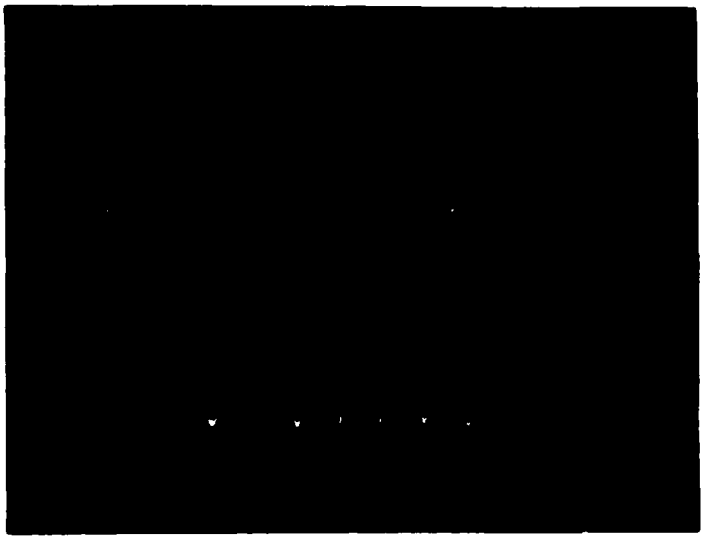

(a)

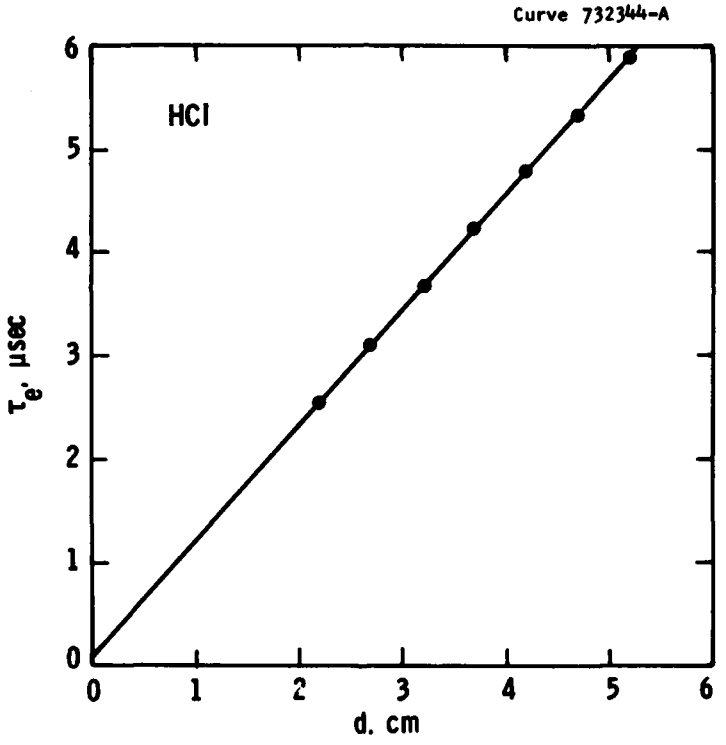

(b)

Fig. 6 - Sample of the raw data used for the determination of electron drift velocity. (a) Analog presentation of stored digital data corresponding to seven superimposed electron current waveforms taken in HCℓ at drift distances ranging from 2.2 cm to 5.2 cm in increments of 0.5 cm. The time scale is 10 nsec/point (∿ 800 nsec/division). (b) Plot of τ_e versus d derived from the data shown in the photograph. The line represents a linear regression fit to the experimental points. $E/N = 2.000 \times 10^{-16}$ V cm^2, $N = 6.49 \times 10^{16}$ cm^{-3}.

In general, seven different drift distances have been used for the determination of w_e at each value of E/N. A typical example of the raw data is shown in Figure 6, corresponding to data taken in HCℓ at a value of $E/N = 2.000 \times 10^{-16}$ V cm^2 and a gas density $N = 6.49 \times 10^{16}$ cm^{-3}. The upper part of the figure is an analog presentation of the stored digital data corresponding to seven superimposed electron waveforms taken at drift distances ranging from 2.2 cm to 5.2 cm in increments of 0.5 cm. The magnified peaks show the resolution attained in the measurements. The lower part of the figure shows a plot of the arrival time τ_e of the peak of the waveform as a function of drift distance, these data being obtained from the stored digital values corresponding to the waveforms shown in the photograph. In all cases the plots are found to be linear and the values of w_e are obtained directly from the slope of the linear regression fit to each plot. For every plot analyzed the experimental points differ from the linear regression fit by less than ±1% and in most cases by less than ±0.5%.

2.5.2 Ion Waveforms

Under conditions where the duration (δt) of the initial electron pulse is such that $\delta t \ll d/w_\pm$ (where w_+ and w_- are the drift velocities of positive ions and negative ions, respectively) solution of the continuity equation for negative ions leads to the following expression[8] for the time-dependent negative ion current [$I_-(d,t)$] arriving at the anode:

$$I_-(d,t) = Q_o \eta w_- \exp[(\alpha - \eta)(d - w_- t)] \quad \text{for } 0 < t < d/w_-,$$
$$I_-(d,t) = 0 \quad \text{for } t > d/w_- . \tag{3}$$

Similarly, the time-dependent positive ion current $I_+(0,t)$ arriving at the cathode is given by

$$I_+(0,t) = Q_o \alpha w_+ \exp[(\alpha - \eta) w_+ t] \quad \text{for } 0 < t < d/w_+,$$
$$I_+(0,t) = 0 \quad \text{for } t > d/w_+ . \tag{4}$$

The positive and negative ion transit times, τ_+ and τ_-, respectively, are readily determined from the ion current waveforms as described above for the

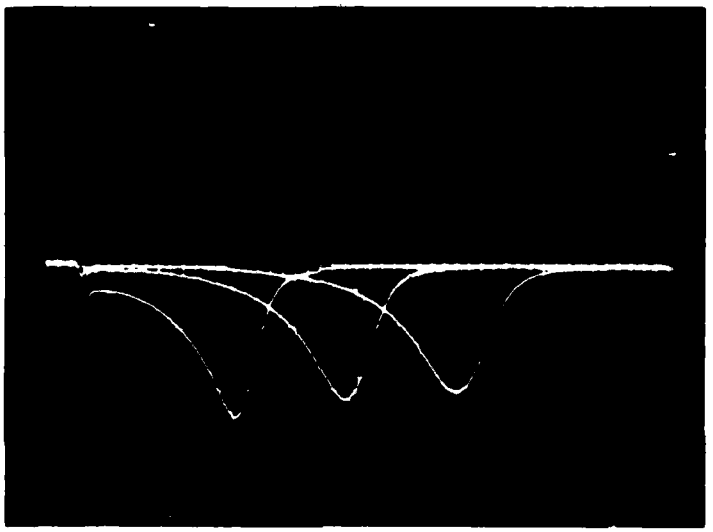

Fig. 7 - Sample of raw data showing total anode current waveforms. The photograph shows an analog presentation of stored digital data corresponding to three superimposed waveforms taken in $CC\ell_4$ at drift distances of 2.2 cm, 3.7 cm, and 5.2 cm. The time scale is 50 nsec/point ($\sim$ 5 μsec/division). $E/N = 7.00 \times 10^{-15}$ V cm^2, $N = 1.718 \times 10^{16}$ cm^{-3}.

case of electrons. Examples of total current waveforms collected at the anode are given in Figure 7. Here, three superimposed waveforms are shown taken in $CC\ell_4$ at drift distances of 2.2 cm, 3.7 cm, and 5.2 cm at a constant value of $E/N = 7.00 \times 10^{-15}$ V cm^2 and a value of $N = 1.718 \times 10^{16}$ cm^{-3}. For each waveform the first peak represents the collected current due to electrons which have crossed the drift space without suffering attaching collisions and the second peak is due to the collected current of negative ions formed in the drift region. Similar measurements of the total collected current at the cathode enable the positive ion component as a function of drift distance to be recorded at values of E/N where $\alpha > 0$. Thus, the values of w_+ and w_- are given from the slopes of the linear plots of τ_+ versus d, and τ_- versus d, respectively. The ion reduced mobilities μ_o^+ and μ_o^- are defined by the relations

$$\mu_o^+ = w_+/(E/N)N_o; \; \mu_o^- = w_-/(E/N)N_o, \tag{5}$$

where N_o is the gas number density corresponding to 760 Torr at 273°K, i.e., $N_o = 2.688 \times 10^{19}$ cm^{-3}.

The net ionization coefficient $(\alpha - \eta)$ may be determined from either the positive ion or negative ion waveforms. In practice, greater precision is obtained if the positive ion waveform is used when $\alpha > \eta$, and the negative ion waveform is used when $\eta > \alpha$.

Under conditions where only a single ion species is present, plots of $\ell n\, I_-(d,t)$ versus t or $\ell n\, I_+(0,t)$ versus t are linear and from Equations (3) and (4), have slopes $(\alpha - \eta)w_-$ and $(\alpha - \eta)w_+$, respectively. Thus, knowing w_- and w_+, $(\alpha - \eta)$ is determined. Figure 8 shows an anode current waveform recorded in $HC\ell$ replotted in semi-log form (inverted for convenience) using the stored digital data. For the sake of clarity every twentieth point only has been plotted. The slope $(\eta - \alpha)\, w_-$ is determined from a regression fit to the experimental points on the rising portion of the ion current waveform. Such a fit is shown by the straight line drawn in Figure 8. For all the waveforms analyzed the experimental points differ from the regression fit by less than ±3%.

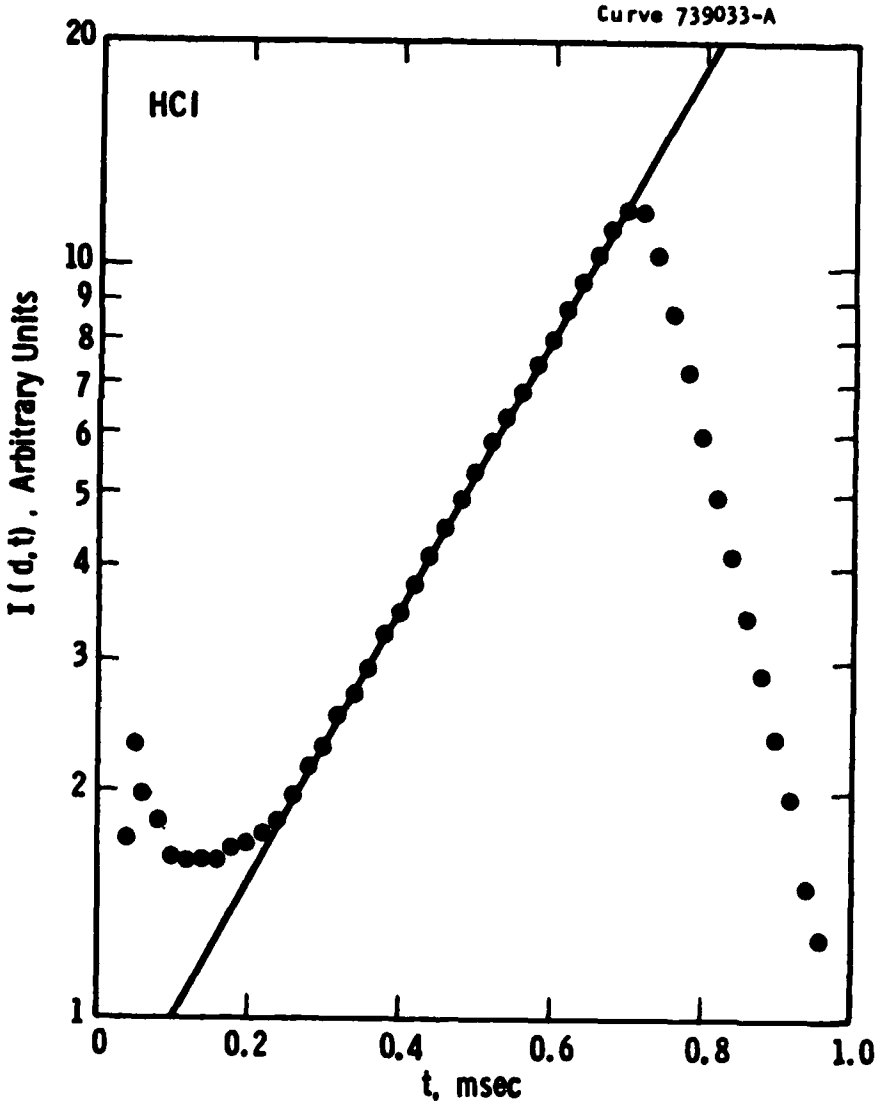

Fig. 8 - Semi-log plot of I_- (d,t) versus t obtained using the stored digital data corresponding to an anode current waveform recorded in HCℓ. The straight line is a regression fit to the experimental points on the rising portion of the negative-ion signal. $E/N = 4.00 \times 10^{-16}$ V cm^2, $N = 1.098 \times 10^{17}$ cm^{-3}, d = 5.2 cm.

For situations where more than one ion species is present, the ion current waveforms are no longer purely exponential and $(\alpha - \eta)$ is more conveniently determined from the integrals of the current waveforms, i.e., from the charge collected. In the analysis of the charge waveforms, account must be taken of the different transmissions of the grids for electrons and ions.

Thus, at the anode, the charge of electrons Q_e^A, negative ions Q_-^A and total charge Q_T^A collected are given by

$$Q_e^A = f_1^2 \, Q_o \exp(\alpha - \eta)d, \tag{6}$$

$$Q_-^A = [f_1 f_2 \, Q_o \, \eta/(\alpha - \eta)] \, [\exp(\alpha - \eta)d - 1], \tag{7}$$

$$Q_T^A = Q_o \, [\{[f_1 f_2 \, \eta/(\alpha - \eta)] + f_1^2\} \exp(\alpha - \eta)d - f_1 f_2 \, \eta/(\alpha - \eta)], \tag{8}$$

where f_1 and f_2 are the fractions of electrons and ions, respectively, transmitted by each grid. Writing $y^A = Q_T^A/Q_e^A$, it follows from Equations (6) and (8) that

$$y_{d + \Delta d}^A = y_d^A \exp{-(\alpha - \eta)\Delta d} + \{1 + (f_2/f_1)[\eta/(\alpha - \eta)]\}[1 - \exp{-(\alpha - \eta)\Delta d}], \tag{9}$$

where y_d^A and $y_{d+\Delta d}^A$ are the charge ratios at the drift distances d and $d + \Delta d$, respectively. Thus, by making measurements of the charge ratio Q_T^A/Q_e^A at a sequence of drift distances differing by a constant increment Δd, keeping E/N constant, the net ionization coefficient $(\alpha - \eta)$ is determined from the slope $\exp - (\alpha - \eta)\Delta d$ of the linear plot of $y_{d+\Delta d}^A$ versus y_d^A.

Similarly, at the cathode, the total charge Q_T^C collected is comprised of the initial electron charge leaving Q_e^C and the returning positive ion charge Q_+^C. The resulting expressions for Q_e^C, Q_+^C and Q_T^C are given by

$$Q_e^C = Q_o, \tag{10}$$

$$Q_+^C = [f_1 f_2 \, Q_o \, \alpha/(\alpha - \eta)] \, [\exp(\alpha - \eta)d - 1], \tag{11}$$

$$Q_T^C = Q_o \, \{[f_1 f_2 \, \alpha/(\alpha - \eta)] \exp(\alpha - \eta)d - f_1 f_2 \, \eta/(\alpha - \eta)\} \, , \tag{12}$$

leading to the corresponding expression for the charge ratio $y_d^C = Q_T^C/Q_e^C$ given by

$$y_{d+\Delta d}^C = y_d^C \exp(\alpha - \eta)\Delta d + [1 - f_1 f_2\, \alpha/(\alpha - \eta)]\,[1 - \exp(\alpha - \eta)\Delta d]. \qquad (13)$$

The net ionization coefficient $(\alpha - \eta)$ is then determined from the slope $\exp(\alpha - \eta)\Delta d$ of the linear plot of $y_{d+\Delta d}^C$ versus y_d^C.

The ratio α/η is determined directly from the ratio of $(Q_+^C/Q_o)/(Q_-^A/Q_o)$ where normalization of the charge Q_+^C and Q_-^A collected at the cathode and anode is made to the charge Q_o (or more correctly to a charge proportional to Q_o) as discussed in Section 2.4. Thus, knowing $(\alpha - \eta)$ and α/η, the individual coefficients α and η are determined.

For given values of E/N and Q_o, it is noted that the total charge Q_T^C collected at the cathode is larger than that collected at the anode Q_T^A by an amount $(f_1 f_2 - f_1^2) \exp(\alpha - \eta)d$. For perfectly transmitting grids, i.e., for $f_1 = f_2 = 1$, the expressions given by Equations (8) and (12) both reduce to the well-known form describing spatial current growth between planar electrodes under steady-state conditions.

Examples of total current waveforms collected at both the cathode and anode are shown in Figure 9 together with the corresponding integrated (or charge) waveforms at values of E/N where $\alpha < \eta$ and $\alpha > \eta$. The cathode waveforms show the initial electron current leaving the cathode followed by the positive- ion current arriving at the cathode. The anode waveforms show the attenuated (or amplified) electron current arriving at the anode followed by the negative-ion current. These data clearly show the ability of the present drift tube to resolve the individual electron, negative-ion, and positive-ion components of the total current under conditions where all three components are present simultaneously. It is noted that the negative-ion and positive-ion mobilities are significantly different. This is generally the case for all the gases studied which is in contrast to the assumption often made that the mobilities are equal in this range of E/N.

At the limiting value of E/N, at which $\alpha = \eta$, Equations (3) and (4) show that $I_-(d,t)$ and $I_+(0,t)$ are constant for $t < d/w_-$ and $t < d/w_+$, respectively,

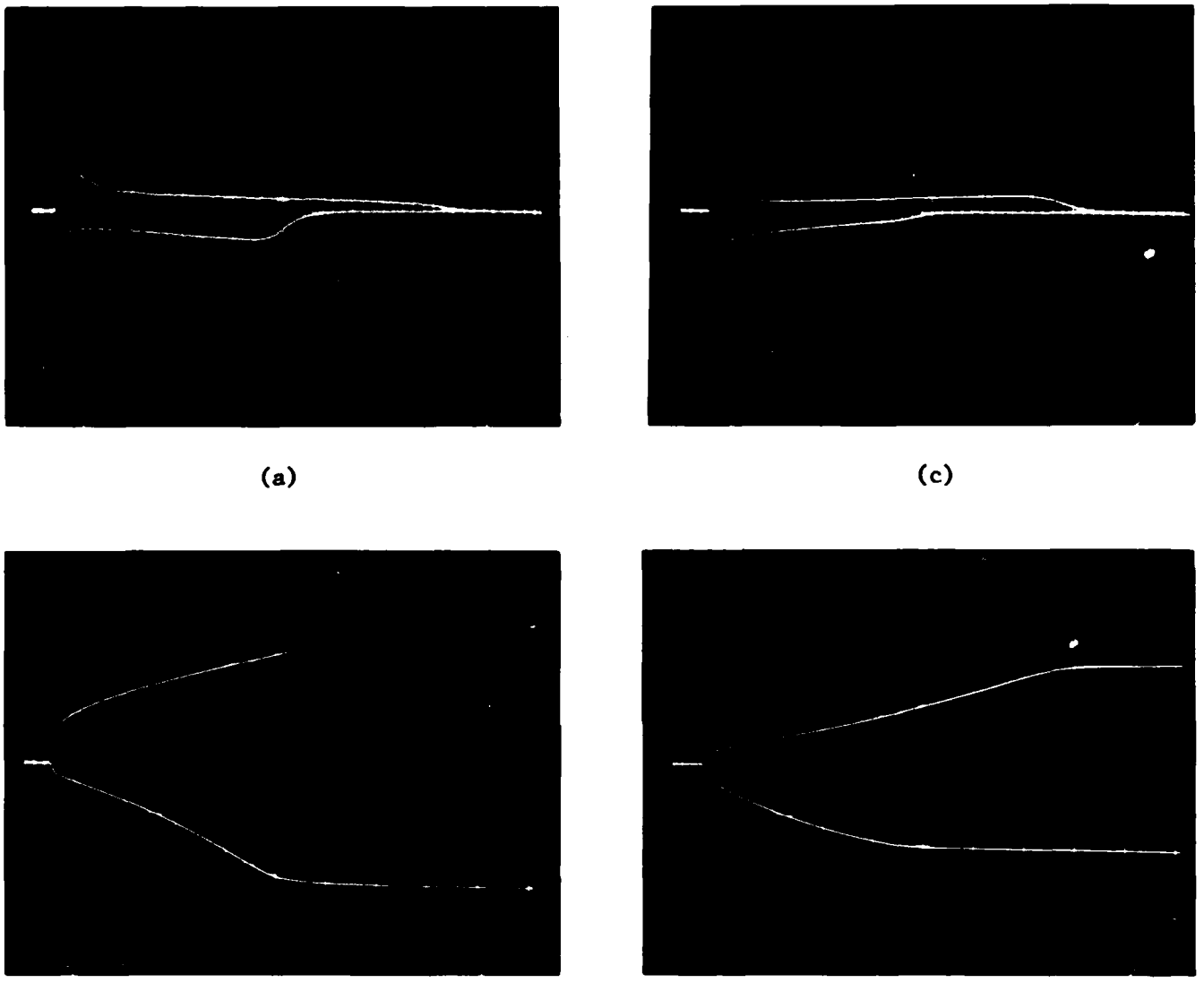

Fig. 9 - Sample of total anode and cathode waveforms taken in $CC\ell_4$ at a drift distance of 5.2 cm for values of $E/N = 8.50 \times 10^{-15}$ V cm^2 where $\alpha < \eta$ [(a), (b)], and $E/N = 9.50 \times 10^{-15}$ V cm^2 where $\alpha > \eta$ [(c), (d)]. Photographs (a) and (c) show the superimposed cathode (upper) and anode (lower) current waveforms and photographs (b) and (d) the corresponding integrated current (or charge) waveforms. The time scale is 100 nsec/point ($\sim$ 6 μsec/division). (a) and (b): $N = 1.092 \times 10^{16}$ cm^{-3}, (c) and (d): $N = 9.45 \times 10^{15}$ cm^{-3}.

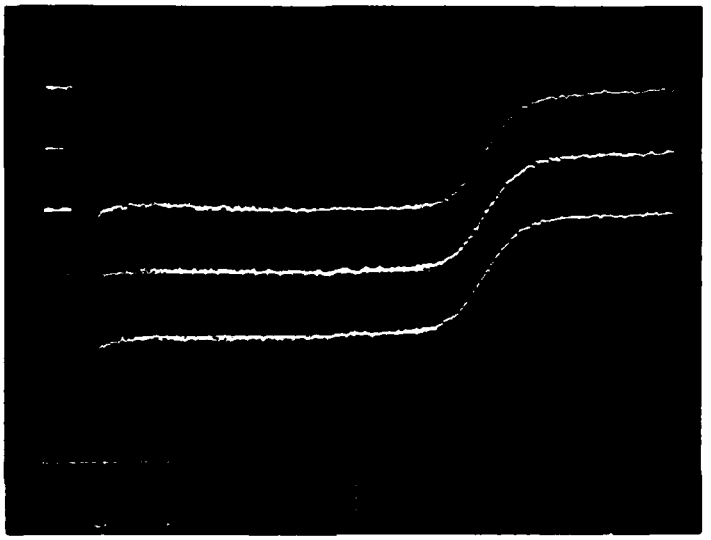

Fig. 10 - Three superimposed anode current waveforms taken in $CC\ell_4$ for values of E/N in the vicinity of the limiting value. The waveforms have been expanded to show the negative-ion components more clearly (the electron component peaks are off scale). The time scale is 100 nsec/point ($\sim$ 4 μsec/division). $N = 1.118 \times 10^{16}$ cm^{-3}, d = 5.2 cm. Upper: $E/N = 8.78 \times 10^{-15}$ V cm^2, Center: $E/N = 8.80 \times 10^{-15}$ V cm^2 (the limiting value), Lower: $E/N = 8.82 \times 10^{-15}$ V cm^2.

and from Equations (7) and (11), $Q_{-}^{A} = Q_{+}^{C} = f_1 f_2 Q_o \eta d$. Thus, the limiting value of E/N may be determined precisely from measurements of the ion component of the total current waveforms, as shown in Figure 10. Here, three superimposed anode waveforms are shown taken in $CC\ell_4$ at a drift distance of 5.2 cm and a density of 1.118×10^{16} cm^{-3} for values of $E/N = 8.80 \times 10^{-15}$ V cm^2, the limiting value (center), $E/N = 8.78 \times 10^{-15}$ V cm^2 (upper), and $E/N = 8.82 \times 10^{-15}$ V cm^2 (lower).

For values of E/N below the onset of ionization, $\alpha = 0$ and Equation (3) reduces to

$$I_{-}(d,t) = Q_o \eta w_{-} \exp[-\eta(d - w_{-}t)] \quad \text{for } 0 \leq t \leq d/w_{-},$$

$$I_{-}(d,t) = 0 \quad \text{for } t > d/w_{-}. \tag{14}$$

Under conditions where only a single negative ion species is present, the attachment coefficient is determined from the slope ηw_{-} of a plot of $\ell n\ I_{-}(d,t)$ versus t, and the determined value of w_{-}. If more than one negative ion species is present, the attachment coefficient is determined from the charge waveform and Equation (9) reduces to

$$y^{A}_{d+\Delta d} = y^{A}_{d} \exp \eta\Delta d - \{1 - (f_2/f_1)\} \quad (\exp \eta\Delta d - 1). \tag{15}$$

Thus, η is determined from the slope $\exp \eta\Delta d$ of a plot of $y^{A}_{d+\Delta d}$ versus y^{A}_{d}.

The above analysis demonstrates clearly that differential measurements are mandatory if meaningful values (free from grid transmission effects) of both $(\alpha - \eta)$ and η are to be obtained from charge waveforms derived from a drift tube of this type. As pointed out previously, the charge waveforms are the most convenient data to use when more than one ion species is present. Neglect of grid transmission effects not only leads to incorrect values of the coefficients but also to an incorrect functional dependence of the coefficients on E/N since the value of f_2/f_1 is also a function of E/N. The present measurements in pure $HC\ell$ (an example of a gas in which only a single negative ion species is observed, cf. Section 3.2) have shown that values of η determined from the current waveforms and from the charge waveforms agree to within the uncertainty of the measurements when proper account is taken of grid

transmission effects. The determination of the parameters η, α and w_e, as functions of E/N enables the rate coefficients for attachment $k_a = \eta w_e/N$ (for a two-body process) or $k_a = \eta w_e/N^2$ (for a three-body process) and for ionization $k_i = \alpha w_e/N$ to be determined as functions of E/N.

2.6 DETERMINATION OF ELECTRON COLLISION CROSS SECTIONS

The method used to determine electron collision cross sections from the measured swarm parameters is that developed by Phelps and co-workers.[9,10] In this method, the Boltzmann transport equation is numerically integrated using trial input cross sections for momentum transfer, rotational excitation, vibrational excitation, electronic excitation, attachment and ionization to obtain the electron energy distribution function. Convolution of the distribution function with the appropriate cross section enables the swarm parameters to be predicted as a function of electron mean energy (or E/N). The trial cross sections are adjusted iteratively until agreement between predicted and measured swarm parameters is obtained.

The Boltzmann transport equation for a pure gas is given by

$$\frac{E^2}{3}\frac{d}{d\varepsilon}\left(\frac{\varepsilon}{NQ_m}\frac{df}{d\varepsilon}\right) + \frac{2m}{M}\frac{d}{d\varepsilon}\left(\varepsilon^2 NQ_m f\right) + \frac{2mkT}{Me}\frac{d}{d\varepsilon}\left(\varepsilon^2 NQ_m \frac{df}{d\varepsilon}\right)$$

$$+ \sum_j (\varepsilon + \varepsilon_j)\, f(\varepsilon + \varepsilon_j)\, NQ_j(\varepsilon + \varepsilon_j) - \varepsilon f(\varepsilon)\, N \sum_j Q_j(\varepsilon)$$

$$+ \sum_j (\varepsilon - \varepsilon_j)\, f(\varepsilon - \varepsilon_j)\, NQ_{-j}(\varepsilon - \varepsilon_j) - \varepsilon f(\varepsilon)\, N \sum_j Q_{-j}(\varepsilon) = 0. \qquad (16)$$

In Equation (16), $\varepsilon^{1/2} f(\varepsilon)$ is the electron distribution function, e and m are the electron charge and mass, respectively, M is the molecular mass, k is Boltzmann's constant, ε ($= mv^2/2e$, where v is the electron speed) is the electron energy, Q_m is the momentum transfer cross section, and Q_j and Q_{-j} are cross sections for the inelastic loss and gain, respectively, from the jth inelastic process. Included in Q_j and Q_{-j} is a factor to account for fractional population and statistical weights.

The first term in Equation (16) accounts for the gain in energy due to the electric field E. The second term, involving the factor 2m/M, accounts for elastic energy losses due to collisions with gas molecules. The third term involving the temperature T, enables account to be taken of the gain in energy of low-energy electrons which collide with fast moving thermal gas molecules. The first term involving a summation over Q_j accounts for electrons of energy $\varepsilon + \varepsilon_j$ losing energy ε_j and the second term in Q_j accounts for electrons of energy ε losing energy ε_j. The remaining terms in Q_{-j} represent electrons gaining energy ε_j due to collisions of the second kind.

In the present analysis, rotational excitation is included using the continuous approximation, introduced by Frost and Phelps.[9] In this approximation rotational terms are omitted from the summations involving Q_j and Q_{-j} in Equation (16) and introduced in the second and third terms by replacing Q_m with Q_m' where

$$Q_m' = Q_m + (M/2m\varepsilon)C. \tag{17}$$

In the case where rotational transitions occur as a result of the electric quadrupole moment of the molecule, the quantity C in Equation (17) is given by[9]

$$C = 32\,\pi\,B_o\,q_4^2\,a_o^2/15, \tag{18}$$

where B_o is the rotational constant of the molecule in eV, q_4 is the quadrupole moment of the molecule in units of ea_o^2, and a_o is the first Bohr radius in cm. For molecules having a permanent electric dipole moment, C is given by[11]

$$C = 8\pi 2^{7/4}\,\Gamma\,(15/8)R_y B_o^{7/8} q_2^2\,a_o^2/3(kT/e)^{1/8}\varepsilon^{3/4}, \tag{19}$$

where R_y is Rydberg's constant in eV, and q_2 is the dipole moment of the molecule in units of ea_o. The continuous approximation is expected to be valid for values of electron mean energy greater than a few kT/e.[9,11]

Once the distribution function f is obtained for a given E/N, the swarm parameters are determined from

$$w_e = \frac{8\pi e^2}{3m^2} \frac{E}{N} \int_o^\infty \frac{\varepsilon}{Q_m} \frac{df}{d\varepsilon} \, d\varepsilon, \tag{20}$$

$$D_T = \frac{8\pi e^2}{3m^2 N} \int_o^\infty \frac{\varepsilon f}{Q_m} \, d\varepsilon, \tag{21}$$

$$\frac{\nu_a}{N} = \frac{8\pi e^2}{m^2} \int_o^\infty Q_a \varepsilon f \, d\varepsilon, \tag{22}$$

$$\nu_i/N = \frac{8\pi e^2}{m^2} \int_o^\infty Q_i \, \varepsilon f \, d\varepsilon, \tag{23}$$

where Q_a and Q_i are the attachment and ionization cross sections, respectively. Similarly, rate coefficients for other inelastic processes are given by

$$\nu_j/N = \frac{8\pi e^2}{m^2} \int_o^\infty Q_j \, \varepsilon f \, d\varepsilon. \tag{24}$$

In addition, the longitudinal diffusion coefficient D_L is determined[12,13] in terms of integrals over f and the cross sections. The power P_j delivered by each electron to the inelastic level j is evaluated from

$$P_j/N = \frac{8\pi e^2}{m^2} \varepsilon_j \int_o^\infty Q_j \, \varepsilon f \, d\varepsilon, \tag{25}$$

where ε_j is the energy loss of the jth level in eV. In Equations (20) to (25) f is normalized by

$$\int 4\pi \, v^2 \, f \, dv = 1. \tag{26}$$

For gas mixtures, Equation (16) is modified to average the collision frequencies among the different molecules. Thus, for the first term Q_m is replaced by Q_1 where

$$Q_1 = \sum_n Q_m^n G^n, \tag{27}$$

where Q_m^n and G_n are the momentum transfer cross section and mole fraction, respectively, of the nth gas. For the second and third terms Q_m is replaced by Q_2 where, by analogy with Equation (17),

$$Q_2 = \sum_n M Q_m^n G^n/M^n + (M/2m\varepsilon) C^n G^n, \tag{28}$$

where M^n is the mass of the molecule of the nth gas, $M = \sum_n M^n G^n$, and C^n is the rotational parameter, defined by Equation (18) or (19), for the nth gas. The terms in Equation (16) involving the inelastic cross sections Q_j are each reduced by the mole fraction of the gas associated with each particular cross section.

The computer code used to solve the Boltzmann equation and evaluate the swarm paramters is that documented by Luft.[14] Approximations made in this code are:

(i) the distribution function is represented by a spherical expansion of Legendre polynomials truncated after the first two terms

(ii) attachment and ionization are treated as energy loss processes ignoring the loss or gain of an electron in the attachment or ionization event, respectively

(iii) collisions of the second kind involving vibrational and electronic states are neglected.

The two-term expansion model has been found to be a good approximation for gases having inelastic contributions to the total cross section which are small compared with the momentum transfer cross section. An analysis of nitrogen, a gas having a large vibrational cross section whose peak value approaches the momentum transfer cross section, has recently been carried out by Pitchford and Phelps[15] using a multi-term expansion (up to six terms) for the distribution function. They find that the predicted values of electron drift velocity are

insensitive (within 2%) to the number of terms greater than two and that values of D_T/μ_e are lower by up to 10% for a six-term expansion compared with a two-term expansion. However, values of excitation rate coefficients are up to 30% larger for a six-term expansion compared with a two-term expansion.

On the other hand, inclusion in the analysis of the extra electron produced in an ionizing collision leads to lower values of the predicted ionization rate coefficient.[16] Thus, the inclusion of the additional electron produced in ionization in a multi-term expansion code leads to mutually compensating effects and results, in the case of nitrogen, in predicted values of the ionization rate coefficient which are within 10% of those predicted using the two-term expansion code neglecting the extra electron. Inclusion of the loss of an electron in an attaching collision is likely to be most important in gases which have large attachment cross sections at low electron energy that make significant contributions to the total energy-loss spectrum.

With respect to the third approximation, collisions of the second kind can be neglected for electron mean energies above thermal since the terms involving such collisions (i.e., terms in Q_{-j}) are insignificant compared with the other terms in Equation (16).

The question of the uniqueness and the uncertainty of the derived cross sections is dependent on the complexity of the gas in question and on the degree of available knowledge of the cross sections themselves, particularly concerning the onset energy and shape of the cross sections. Thus, for example, cross sections for atomic gases may often be more precisely determined than for molecular gases because of the absence of rotational and vibrational excitation processes. Nevertheless, use of the approximate two-term expansion Boltzmann code to determine a set of collision cross sections which are consistent with measured swarm parameters is of value in many applications. Such an application is appropriate in the context of the present investigation where predictions of swarm parameters in mixtures of the halogen-donor gas with rare gases is required. The success of such an approach has been demonstrated previously for CO_2-laser gas mixtures.[17]

3. RESULTS OF MEASUREMENTS IN HCℓ

The present measurements have been carried out with electronic grade HCℓ supplied by Matheson Co. The gas is quoted by the manufacturer as being 99.99% pure, the major impurities being N_2: 50 ppm, O_2: 10 ppm, CO_2: <15 ppm, and CH_4: < 5 ppm.

3.1 ELECTRON DRIFT VELOCITY

A summary of the measurements of electron drift velocity as a function of E/N is given in the log-log plot of Figure 11 and the values are also tabulated in Table 1. The present data, denoted by the solid points, cover the range of E/N from 3 to 200 x 10^{-17} V cm^2. The values have an estimated uncertainty of ±1%. No corrections to the data have been made at high values of E/N to account for ionization and attachment effects (cf. Section 2.5.1); these corrections would be less than the quoted uncertainty. These measurements have been carried out using values of gas density in the range from 1.68 to 30.2 x 10^{16} cm^{-3}. The scatter in the values of w_e at a given E/N determined at different gas densities is within ±1%.

For values of E/N less than 7 x 10^{-17} V cm^2, the electron mobility is constant and equal to 141 cm^2/sec V. Estimates of D_L/μ_e from the width of the electron waveforms confirm that this value is characteristic of electrons in thermal equilibrium with the gas. For values of E/N greater than 7 x 10^{-17} V cm^2, the electron mobility increases initially with increasing values of E/N, a characteristic behavior in gases having a Ramsauer minimum in the momentum transfer cross section. The observed structure in the data at values of E/N from 50 to 80 x 10^{-17} V cm^2 is associated with structure in the momentum transfer coss section and is discussed further in Section 3.4.

The present data are compared in Figure 11 with the only previous measurements, those of Bailey and Duncanson,[18] denoted by the open points. These values differ from the present results by amounts varying up to ±55%. The solid line in Figure 11 represents the predictions of the Boltzmann code using the set of cross sections discussed in Section 3.4.

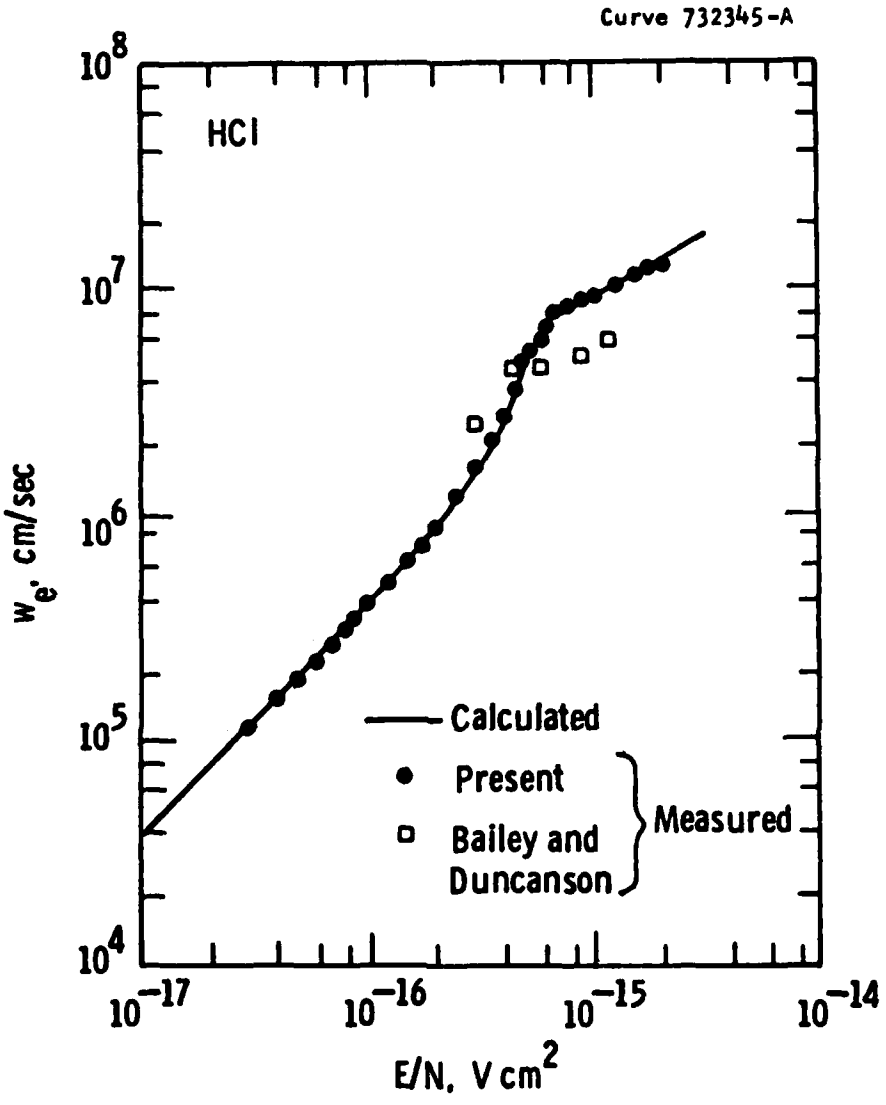

Fig. 11 - Comparison of the present values (solid points) of electron drift velocity in HCℓ as a function of E/N with previous measurements (open points). The solid line represents the predicted values obtained from the Boltzmann code using the set of cross sections discussed in Section 3.4.

TABLE 1. SUMMARY OF VALUES OF THE SWARM PARAMETERS DETERMINED FOR HCℓ.[a]

E/N 10^{-17} V cm^2	w_e 10^6 cm/sec	η/N 10^{-18} cm^2	α/N 10^{-18} cm^2	$(\alpha-\eta)/N$ 10^{-18} cm2	α/η	ν_a/N 10^{-12} cm^3/sec	ν_i/N 10^{-12} cm^3/sec	μ_o^- cm^2/sec V	μ_o^+ cm^2/sec V
3.00	0.113								
4.00	0.152								
5.00	0.190								
6.00	0.229								
7.00	0.267								
8.00	0.312								
9.00	0.352								
10.00	0.395								
12.50	0.501								
15.00	0.616								
17.50	0.742								
20.00	0.897								
25.00	1.21	0.40 ± 3%				0.48 ± 4%		0.697	
30.00	1.61	1.76 ± 3%				2.83 ± 4%		0.695	
35.00	2.16	3.81 ± 3%				8.2 ± 4%		0.694	
40.0	2.74	5.3 ± 3%				14.5 ± 4%		0.698	
45.0	3.62								
50.0	4.83	8.9 ± 3%				43 ± 4%		0.704	
55.0	5.39								
60.0	6.00	10.8 ± 3%				65 ± 4%		0.702	
65.0	7.21								
70.0	7.94	11.0 ± 3%				87 ± 4%		0.709	
80.0	8.45	10.6 ± 3%				90 ± 4%		0.711	
90.0	8.90	10.1 ± 3%				90 ± 4%		0.707	
100.0	9.26	8.8 ± 3%				81 ± 4%		0.712	
125.0	10.6	6.4 ± 3%	1.00 ± 5%	-5.4	0.156	68 ± 4%	10.6 ± 6%	0.725	
150.0	11.6	4.9 ± 5%	2.9 ± 8%	-2.01	0.59	57 ± 6%	33 ± 9%	0.721	
163.0				0	1.00				
175.0	12.0	4.1 ± 10%	6.0 ± 7%	1.88	1.46	49 ± 11%	72 ± 8%		0.948
200.0	12.6	3.9 ± 6%	10.1 ± 4%	6.2	2.58	49 ± 7%	129 ± 5%	0.764	1.02
225.0		4.0 ± 6%	15.9 ± 4%	11.9	4.0				1.05
250.0		3.8 ± 6%	21.2 ± 3%	17.4	5.6			0.769	1.09
275.0		3.5 ± 6%	27.8 ± 3%	24.3	7.9				1.09
300.0		3.5 ± 6%	34.5 ± 3%	31.0	9.9			0.811	1.10

[a]Estimated uncertainties in the measured quantities are:

E/N: ± 0.2%
w_e, μ_o^-, μ_o^+ : ± 1%
$(\alpha - \eta)/N$: ± 3%
α/η : ± 2%
η/N, α/N, ν_a/N, ν_i/N: As noted in table.

3.2 ION MOBILITIES

The negative-ion mobility has been determined from measurements of the negative-ion component of the total anode-collected current. As in the case for electrons, ion waveforms have been recorded at seven values of drift distance for each value of E/N. Only one negative-ion species is observed, based on the single exponential dependence of negative-ion current with time. A summary of the values of reduced negative-ion mobility are given in Figure 12 and in Table 1; the uncertainty in these measurements is estimated to be ±1%. The low-field mobility value is found to be 0.70 cm^2/sec V which is in very good agreement with the value of 0.71 cm^2/sec V measured previously by McDaniel and McDowell[19] at a value of E/N = 3.3×10^{-17} V cm^2.

Negative ions are formed by electron impact on HCℓ according to the processes:

$$e + HC\ell \rightarrow C\ell^- + H \tag{29}$$

$$e + HC\ell \rightarrow H^- + C\ell \tag{30}$$

$$e + HC\ell \rightarrow H^+ + C\ell^- \tag{31}$$

with onset energies of 0.67 eV, 5.6 eV, and 14.6 eV, respectively. From the discussion presented in Section 3.4, there is little doubt that the parent ion associated with the present measurements is $C\ell^-$ formed by reaction (29); however, the identity of the final ion observed is undetermined. Observations of cluster ions of $C\ell^-$ with HCℓ have been reported[20] at values of E/N corresponding to the onset of reaction (29).

The positive-ion mobility has been determined from measurements of the positive-ion component of the cathode-collected current using the same procedure as described above for negative ions. The variation of the positive-ion current with time is not described by a single exponential and thereby indicates the presence of more than one positive-ion species. The values given in Figure 12 and Table 1 correspond to the slowest ion, the only species clearly resolved in the present measurements. The uncertainty in these values is ±1%.

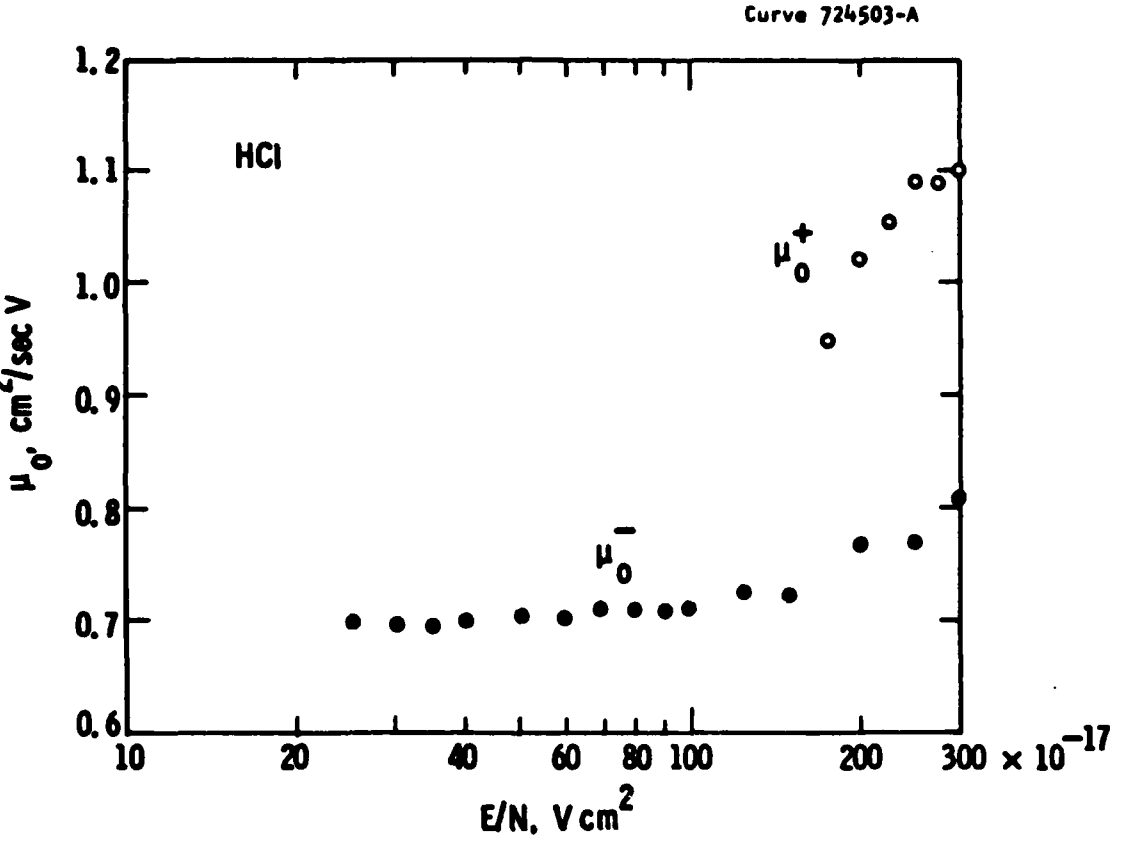

Fig. 12 - Measurements of the reduced negative-ion mobility (solid points) and positive-ion mobility (open points) in HCℓ as a function of E/N. The values of μ_o^+ refer to the slowest positive ion observed.

Positive ions produced by electron impact on HCℓ are formed at the lowest values of electron energy as a result of the reactions:

$$e + HC\ell \rightarrow HC\ell^+ + 2e \tag{32}$$

$$e + HC\ell \rightarrow H^+ + C\ell^- \tag{33}$$

having onset energies of 12.74 eV and 14.6 eV, respectively. The identity of the positive-ion species whose mobility is determined in the present measurements is uncertain but is most likely to correspond either to $HC\ell^+$ or to clusters of $HC\ell^+$ with HCℓ.

3.3 ATTACHMENT AND IONIZATION COEFFICEINTS

The values of the net ionization coefficient $(\alpha - \eta)/N$ determined as a function of E/N from either the negative-ion or positive-ion waveforms are given in Table 1 and plotted as absolute values in Figure 13. The limiting value of E/N, $(E/N)^*$, at which $\alpha = \eta$, is determined to be $163 \pm 1 \times 10^{-17}$ V cm^2 and is denoted by the dashed line in Figure 13. For values of $E/N < 100 \times 10^{-17}$ V cm^2 no positive ions are detected and the data in this region correspond to pure attachment coefficients. For values of E/N from 100 to 300×10^{-17} V cm^2 both negative and positive ions are observed. For values of $E/N > (E/N)^*$, the net ionization coefficients have been determined from the positive-ion charge waveforms. For values of $E/N < (E/N)^*$, the values of $(\alpha - \eta)/N$ determined from either the negative-ion current waveforms or the negative-ion charge waveforms agree to within the uncertainty of the measurements which is estimated to be ±3%.

The present measurements are compared in Figure 13 with the only other sets of previous measurements, those of Bailey and Duncanson[18] for $E/N < (E/N)^*$, and those of Townsend[21] for $E/N > (E/N)^*$. The present measurements differ significantly from these previous data by amounts ranging up to a factor of two.

Measurements of the ratio α/η as a function of E/N over the range 100 to 300×10^{-17} V cm^2 are shown in Figure 14 and also in Table 1. These values have been determined, at a given E/N, from the ratio of the

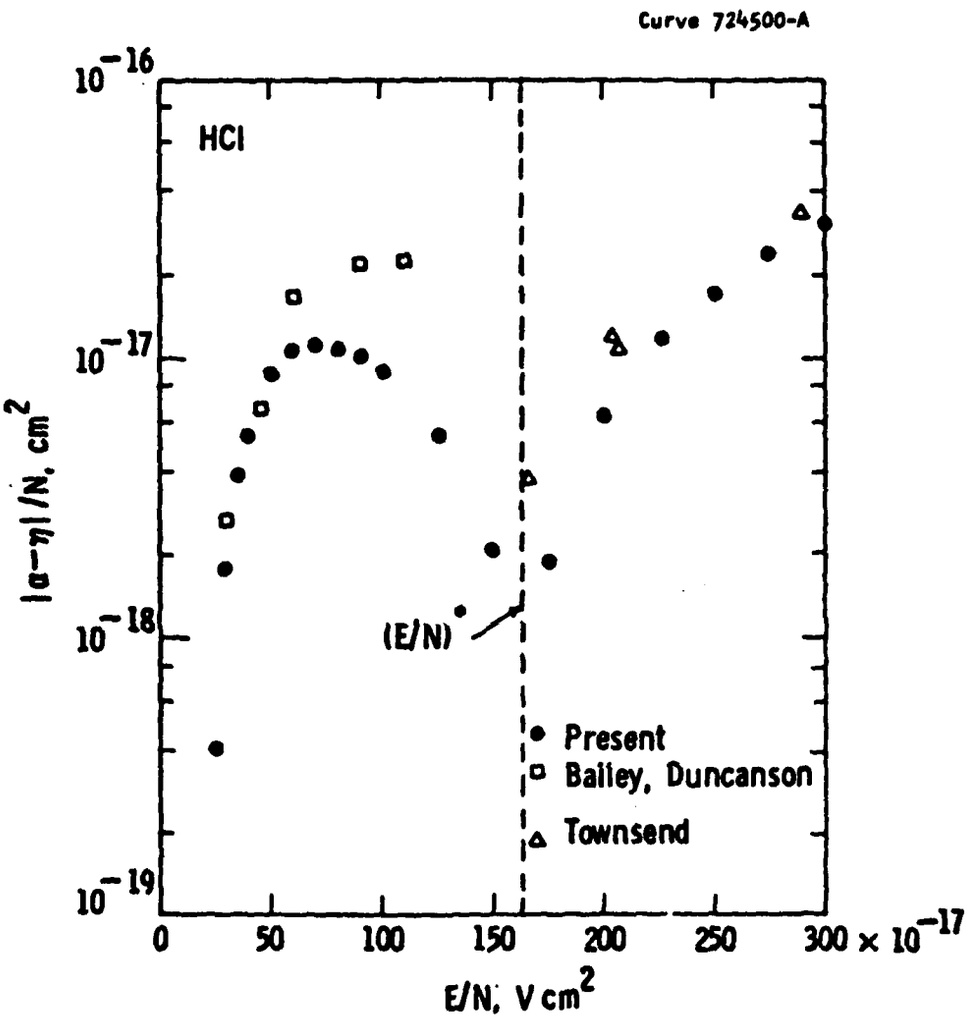

Fig. 13 - Comparison of the present values (solid points) of the net ionization coefficient $(\alpha - \eta)/N$ in HCℓ as a function of E/N with previous measurements (open points).

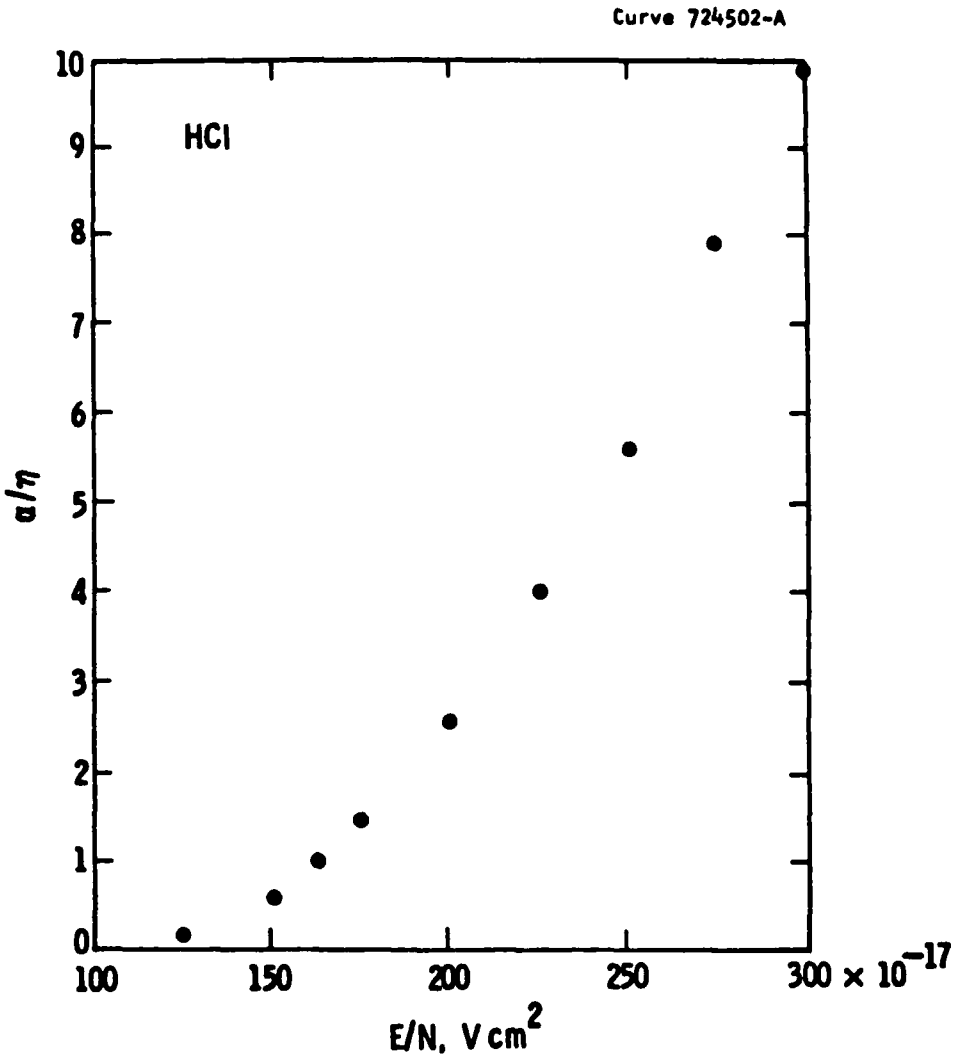

Fig. 14 - Present measurements of the ratio α/η in HCl as a function of E/N.

positive-ion charge to the negative-ion charge (normalized to the initial electron charge leaving the cathode) collected at the same value of the drift distance, i.e., $(Q_+^C/Q_o)/(Q_-^A/Q_o) \equiv \alpha/\eta$. In the event that the pair-production process described by reaction (31) proves to be significant (as discussed in Section 3.4), the values of α/η will require modification since inclusion of the pair-production process in the analysis given in Section 2.5.2 leads to

$$(Q_+^C/Q_o)/(Q_-^A/Q_o) \equiv (\alpha + p)/(\eta + p). \tag{34}$$

In Equation (34), p is a coefficient defined (analagously to α and η) as the number of positive and negative ions produced by the pair-production process per cm drift of electrons in the field direction. In a swarm experiment, the only possible means of distinguishing pair production from attachment or ionization is by identification of the ions if the ion species produced in the separate processes are different. In any event, the uncertainty in the values of the ratio $(Q_+^C/Q_o)/(Q_-^A/Q_o)$, identified with α/η in the present analysis, is estimated to be ±2%.

The values of α/N and η/N given in Figure 15 and Table 1 are obtained by combining the values of $(\alpha - \eta)/N$ and α/η. It should be emphasized that the possible uncertainty introduced by the interpretation of $(Q_+^C/Q_o)/(Q_-^A/Q_o)$ applies only for values of $E/N > 100 \times 10^{-17}$ V cm^2 since the onset for pair production occurs at a higher electron energy than that for ionization. Neglecting this ambiguity, the uncertainties in the values of α/η and η/N are given in Table 1. The measured values of α/N (in cm^2) are described to within ±4% by the relation

$$\alpha/N = 4.43 \times 10^{-16} \exp[-757/(E/N)], \tag{35}$$

where E/N is in units of 10^{-17} V cm^2, as shown in Figure 16.

The rate coefficients for attachment and ionziation, determined by combining the values of α/N and η/N with the values of electron drift velocity, are shown in Figure 17 and are also given together with their estimated uncertainties in Table 1. Despite a careful search, no negative ions could be detected for values of $E/N < 20 \times 10^{-17}$ V cm^2. An upper limit

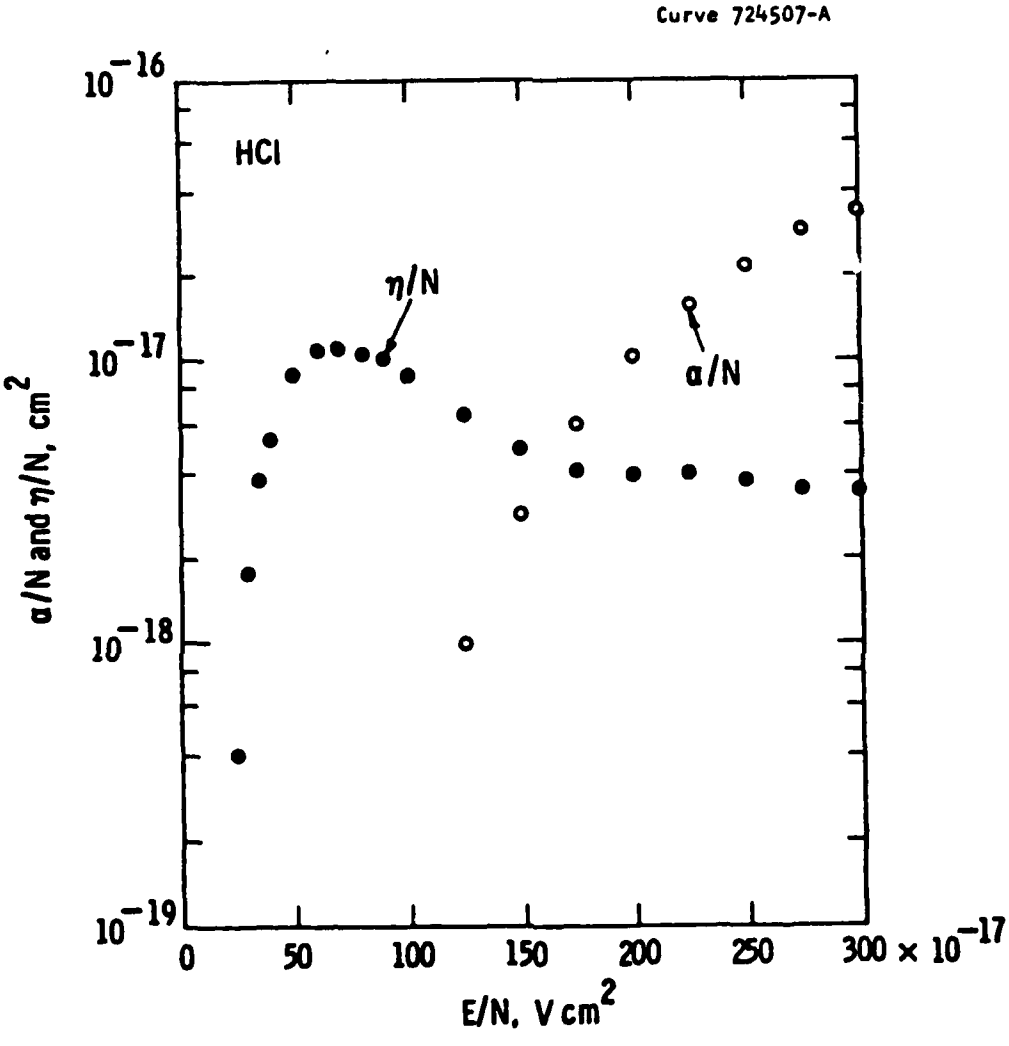

Fig. 15 - Values of the ionization (α/N) and attachment (η/N) coefficients in HCℓ as a function of E/N measured in the present study.

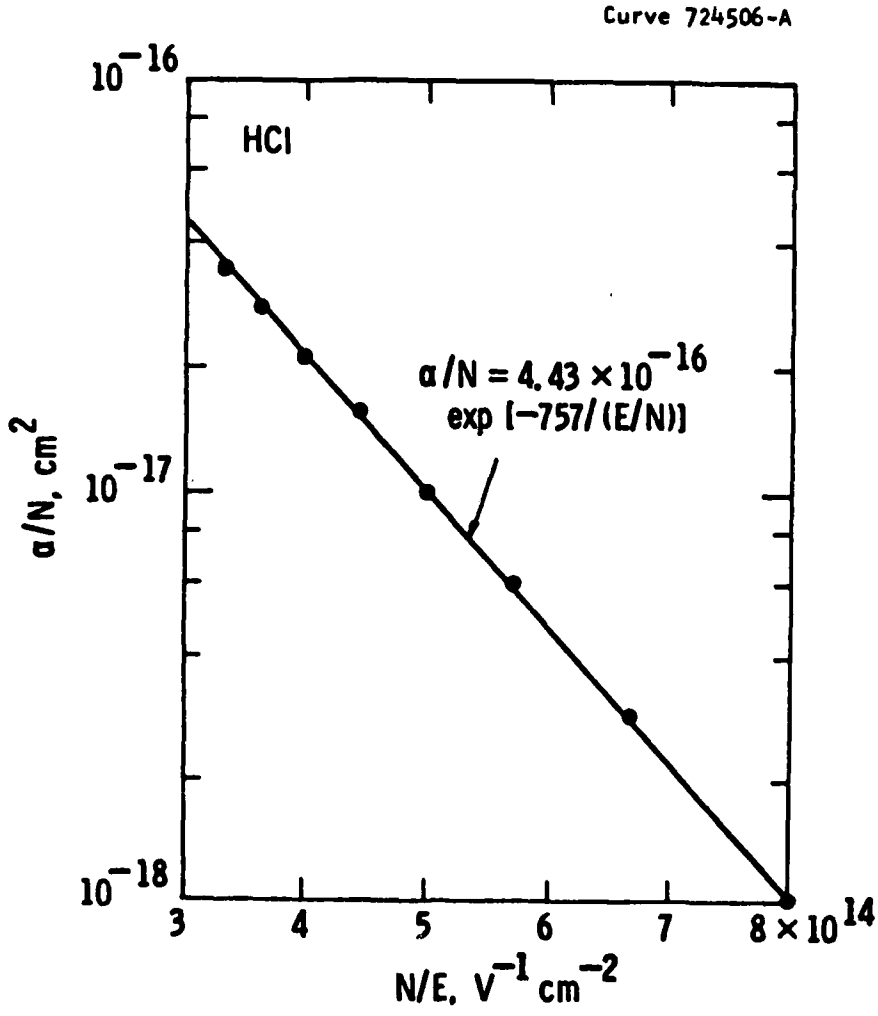

Fig. 16 - Present values of α/N in HCℓ plotted as a function of N/E.

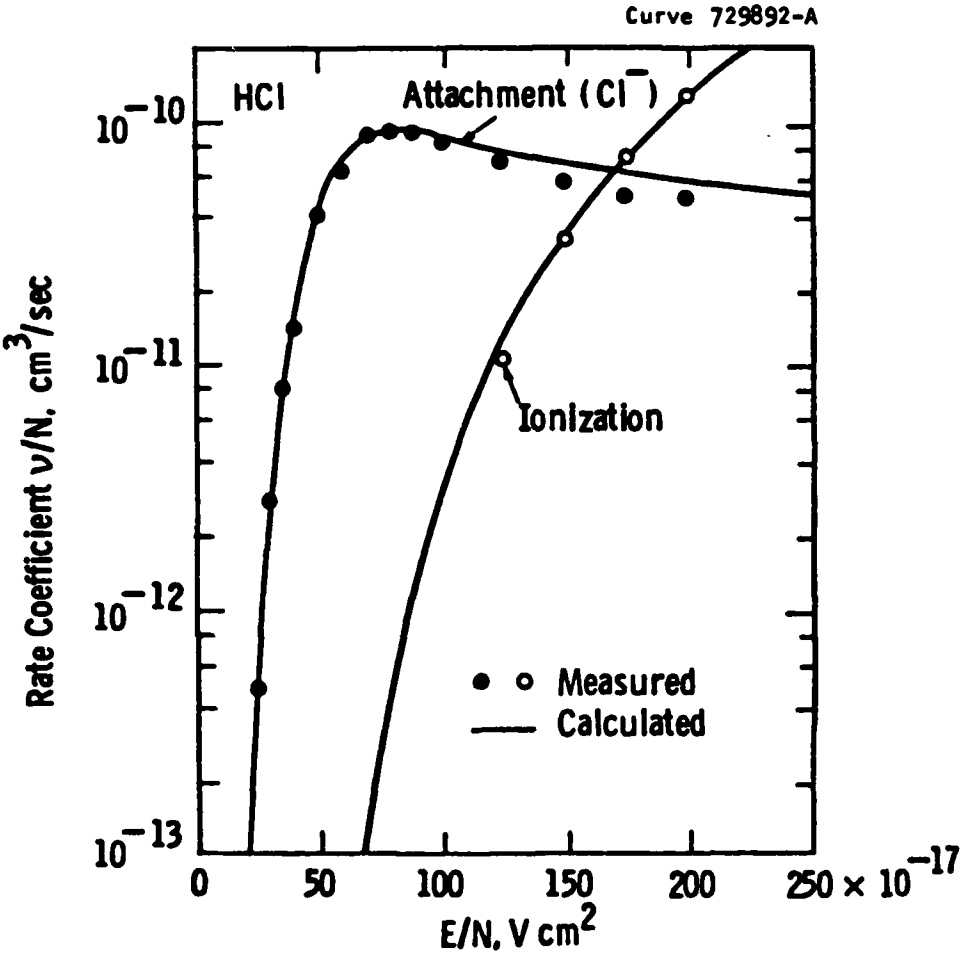

Fig. 17 - The rate coefficients for attachment k_a and ionization k_i in HCℓ as a function of E/N. The points denote the present measurements and the solid lines represent the predicted values obtained from the Boltzmann code using the set of cross sections discussed in Section 3.4.

of 10^{-14} cm^3/sec is placed on the attachment rate coefficient for thermal electrons in HCℓ. This result is consistent with the measurements at thermal energy of Davis et al[22] who were also unable to detect negative ion formation; these authors placed an upper limit of 3×10^{-12} cm^3/sec on the thermal electron attachment rate coefficient. However, the result contradicts the earlier measurements in dilute mixtures of HCℓ with N_2 of Christophorou et al[23] who reported an increasing attachment rate coefficient with decreasing E/N (governed by the nitrogen density) below $\sim 1 \times 10^{-17}$ V cm^2 with a thermal value $> 4 \times 10^{-10}$ cm^3/sec.

The solid lines in Figure 17 represent the predictions of the Boltzmann code using the set of cross sections discussed in the next section.

3.4 ELECTRON COLLISION CROSS SECTIONS

A set of electron collision cross sections has been derived from iterative solutions of the Boltzmann transport equation (discussed in Section 2.6) which yields results consistent with the measured swarm parameters. The derived set of cross sections is shown in Figure 18 and the values of each cross section as a function of electron energy are tabulated in Table 2. Values of the cross sections at electron energies intermediate between the quoted values are derived in the Boltzmann code by linear interpolation. The resulting fits between the values of the swarm parameters predicted using this set of cross sections and the present measurements are shown in Figures 11 and 17.

The momentum transfer cross section is derived in the present analysis by fitting the experimental data on electron drift velocity as a function of E/N. The difference between predicted and measured values of w_e is within 2% over the whole range of E/N with the exception of two small regions. For $E/N > 1.5 \times 10^{-15}$ V cm^2 the difference increases to 6% and in the range of 5 to 7×10^{-16} V cm^2 the difference varies up to 9%. In this latter region further adjustment of the cross section is required to more closely reproduce the observed structure in the drift data. The first structure is associated with the contribution to the momentum transfer cross section by the first vibrational cross section and the second structure to the Ramsauer minimum. At low electron energies the cross section decreases as ε^{-1} in accordance with theoretical predictions[24] for polar molecules while at electron energies in

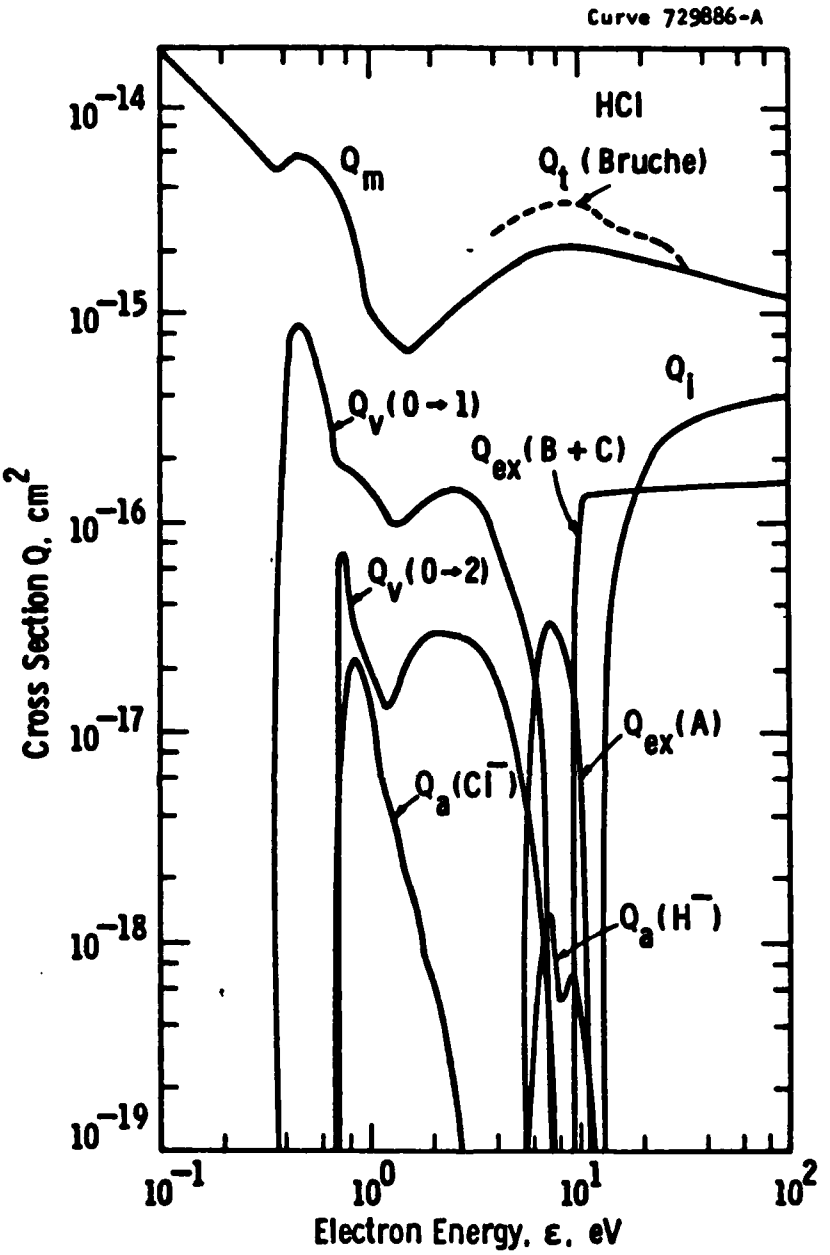

Fig. 18 - The set of electron collision cross sections for HCl derived from iterative solutions of the Boltzmann equation.

TABLE 2. FINAL CROSS SECTIONS FOR HCℓ

Momentum Transfer

ε, eV	Q_m, 10^{-16} cm^2	ε, eV	Q_m, 10^{-16} cm^2
0	1880	1.0	10
0.01	1880	1.5	6.6
0.015	1240	2.0	8.3
0.02	930	2.5	9.9
0.03	620	4.4	16.0
0.04	465	5.7	18.0
0.05	375	8.6	22.0
0.07	265	13	20.0
0.10	188	17	18.5
0.15	124	20	18.0
0.20	93	25	17.0
0.30	62	38	15.2
0.35	50	60	13.7
0.46	60	80	12.8
0.70	40	100	12.0

TABLE 2. CONTINUED

Inelastic

Process	Energy Loss, eV	Threshold, eV
Vibration (v = 1)	0.36	0.36
Attachment ($C\ell^-$)	0.67	0.67
Vibration (v = 2)	0.70	0.70
Excitation (A)	5.50	5.50
Attachment (H^-)	5.60	5.60
Excitation (B + C)	9.30	9.30
Ionization	12.74	12.74

Vibration (v = 1)

ε, eV	$Q_v(v = 1)$, 10^{-16} cm^2	ε, eV	$Q_v(v = 1)$, 10^{-16} cm^2
0.36	0	2.30	1.40
0.46	8.70	3.05	1.40
0.70	1.95	4.40	0.60
1.30	0.95	7.00	0

TABLE 2. CONTINUED

Attachment ($C\ell^-$)

ε, eV	$Q_a(C\ell^-)$, 10^{-16} cm^2	ε, eV	$Q_a(C\ell^-)$, 10^{-16} cm^2
0.67	0	1.20	0.0529
0.80	0.198	1.32	0.0391
0.84	0.230	1.40	0.0253
0.88	0.219	1.78	0.0092
0.92	0.200	2.04	0.0058
1.10	0.0736	2.70	0

Vibration (v = 2)

ε, eV	$Q_v(v = 2)$, 10^{-16} cm^2	ε, eV	$Q_v(v = 2)$, 10^{-16} cm^2
0.70	0	3.20	0.26
0.73	0.71	3.90	0.185
0.85	0.30	4.70	0.090
1.05	0.18	5.30	0.045
1.20	0.13	7.20	0

Excitation (A)

ε, eV	$Q_{ex}(A)$, 10^{-16} cm^2	ε, eV	$Q_{ex}(A)$, 10^{-16} cm^2
5.50	0	7.95	0.308
6.90	0.308	11.00	0
7.45	0.336		

TABLE 2. CONCLUDED

Attachment (H^-)

ε, eV	$Q_a(H^-)$, 10^{-16} cm^2	ε, eV	$Q_a(H^-)$, 10^{-16} cm^2
5.60	0	9.00	0.0069
6.75	0.0115	9.25	0.0071
7.00	0.0129	9.50	0.0069
7.20	0.0138	10.00	0.0058
7.50	0.0115	10.50	0.0037
7.85	0.0074	11.00	0.0022
8.30	0.0053	12.00	0
8.50	0.0055		

Excitation (B + C)

ε, eV	$Q_{ex}(B + C)$, 10^{-16} cm^2	ε, eV	$Q_{ex}(B + C)$, 10^{-16} cm^2
9.30	0	10.60	1.344
9.60	0.396	100.00	1.800
10.30	1.104		

Ionization

ε, eV	Q_i, 10^{-16} cm^2	ε, eV	Q_i, 10^{-16} cm^2
12.74	0	40.00	3.21
20.00	1.60	50.00	3.41
25.00	2.46	75.00	3.75
30.00	2.86	100.00	4.07
35.00	3.07		

the range 4 to 30 eV the shape of the cross section approximates that of the total cross section measurements of Bruche[25] which are included in Figure 18 for completeness. The position of the minimum in the cross section occurs at an electron energy of 1.5 eV. The present cross section is in very good agreement (within 30%) with the completely independent theoretical calculations of Norcross[26] over most of the common range of electron energy except in the regions of the vibrational resonance and the minimum. In particular, the position of the minimum is in exact agreement.

Rotational excitation is included in the present analysis through the continuous approximation including contributions due to the permanent dipole only. The measured value[27] of 1.11 Debye is used in the analysis for the permanent dipole moment of HCℓ.

Vibrational excitation to the first two levels only is included in the analysis. The shapes of these cross sections are those measured by Rohr and Linder.[28] However, it has been found necessary to reduce the magnitudes of the cross sections uniformly by a factor of two, the value at the peak of the $v = 1$ cross section being 8.7×10^{-16} cm^2.

The shapes of the dissociative attachment cross sections for $C\ell^-$ and H^- production are taken from the experimental measurements of Azria et al.[29] In the case of the $C\ell^-$ cross section there is excellent agreement concerning the shape of the cross section among four independent measurements.[29-32] However, the magnitudes of the cross sections have been increased uniformly by approximately a factor of two from those reported by Azria et al. The dependence of the predicted attachment coefficient as a function of E/N and the position of the peak are critically dependent on the magnitudes of the vibrational as well as attachment cross sections. The adjustments in the magnitudes of these cross sections from the published beam measurements have been found necessary to account for both the shape and magnitude of the attachment coefficient as a function of E/N measured in the present work. The resulting magnitude at the peak of the $C\ell^-$ cross section is 2.3×10^{-17} cm^2 which is within 10% of preliminary measurements of this cross section by Chen and Chantry.[33]

In addition, the measured attachment coefficient is proposed to be due to Cl^- formation only, based on a comparison of the predicted and measured functional dependence of the attachment coefficient on E/N. Such a comparison is shown in Figure 19. Further evidence for this hypothesis is the observation of a single ion in the measurements of negative-ion waveforms discussed in Section 3.2. The fate of the H^- ions is not known at present; two possible reactions are

$$H^- + HCl \rightarrow Cl^- + H_2 \tag{36}$$

$$H^- + HCl \rightarrow H + HCl + e \tag{37}$$

The first of these reactions is exothermic but has not been reported in the literature. Although such a reaction would be consistent with the observation of a single ion species (provided the rate coefficient for the reaction is sufficiently large) the predicted attachment coefficient would then be the sum of the Cl^- and H^- contributions which is inconsistent with the measurements (Figure 19). The second of these reactions, i.e., collisional detachment of the H^-, is the reaction invoked on the basis of the present study. From the work of Azria et al,[29] H^- is formed with appreciable kinetic energy (> 3 eV) leading to a high probability for collisional detachment. Further, the production of H^- occurs at sufficiently high values of E/N for the ions to gain appreciable energy from the applied field.

The agreement between predicted and measured attachment coefficients (based on the contribution by Cl^- only) is within 20% for values of E/N in the range from 40 to 250 x 10^{-17} V cm^2 and within 2% at the peak. The position of the predicted peak is in exact agreement with experiment. The predicted threshold behavior (E/N < 40 x 10^{-17} V cm^2) is somewhat steeper than the measured behavior and at values of E/N > 250 x 10^{-17} V cm^2 the predicted attachment coefficient decreases more rapidly with increasing E/N than the measured values. The increasing discrepancy between predicted and measured values of η/N at values of E/N > 250 x 10^{-17} V cm^2 may be indicative of the presence of an additional process. The only likely process in this range of E/N is the pair-production process discussed in Section 3.3. Further analysis

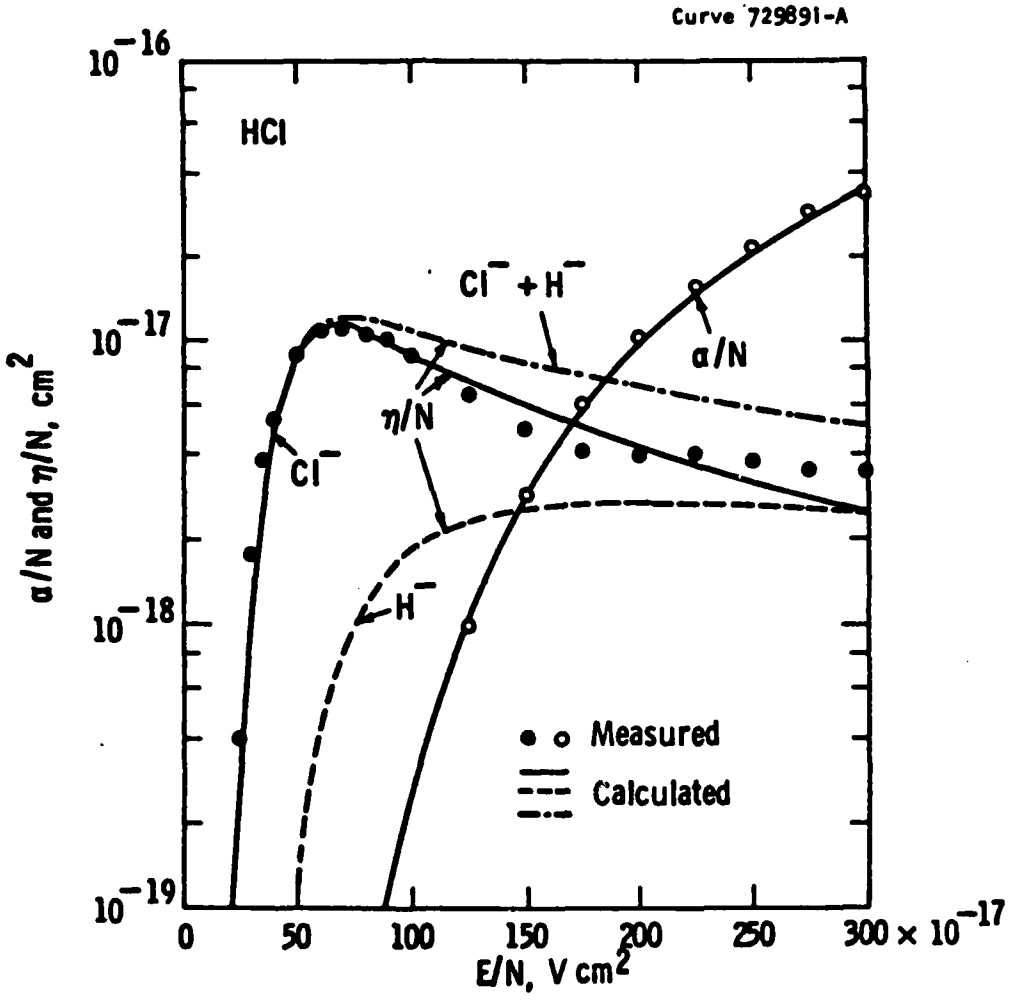

Fig. 19 - Comparison of predicted and measured values of the ionization and attachment coefficients in HCℓ as a function of E/N. Three predicted curves are shown for the attachment coefficient, one for $Cℓ^-$ formation, one for H^- formation, and the sum of the two.

is required to investigate whether the inclusion of such a process would lead to better agreement between measured and predicted attachment coefficients at high E/N.

A value of 38 is obtained from the present analysis for the ratio of the peak of the first vibrational cross section to the peak of the $C\ell^-$ cross section. This is within the limits of 32 to 64 determined experimentally for this ratio by Ziesel et al.[30] These authors indicate evidence which favors the ratio being closer to their lower limit.

The shape and magnitude of the ionization cross section is taken from the recent measurements of Chen and Chantry.[33] This cross section is in reasonable agreement with the earlier measurements of Compton and Van Voorhis[34] although the threshold dependence is somewhat steeper.

The cross sections for electronic excitation to the A and to the B and C states have been adjusted in shape and magnitude to give agreement between the predicted and measured ionization coefficients using spectroscopic values for the threshold energies. The only previous measurements of excitation cross sections are the relative measurements of Compton et al[35] using the SF_6 scavenger technique which provides information on the threshold behavior only. The predicted ionization coefficients are particularly sensitive to the excitation cross sections particularly those corresponding to the B and C states. The cross section for excitation to the A state is less uniquely determined; variation in the magnitude of the cross section by a factor of two can be compensated by adjustments to the momentum transfer cross section for comparable predictions of the swarm parameters measured in the present study. Further measurements of swarm parameters, e.g., diffusion coefficients or excitation coefficients, are necessary to resolve this question. However, as indicated in Figure 19 the degree of fit of the predicted and measured ionization coefficients is within 10% over the whole range of E/N.

The electron energy distributions determined using the set of cross sections derived in the present study and shown in Figure 18 are highly non-Maxwellian. Distribution functions corresponding to representative values of E/N over the range covered are shown in Figure 20 and a comparison of one of these (at $E/N = 60 \times 10^{-17}$ V cm^2) with a Maxwellian distribution of the same

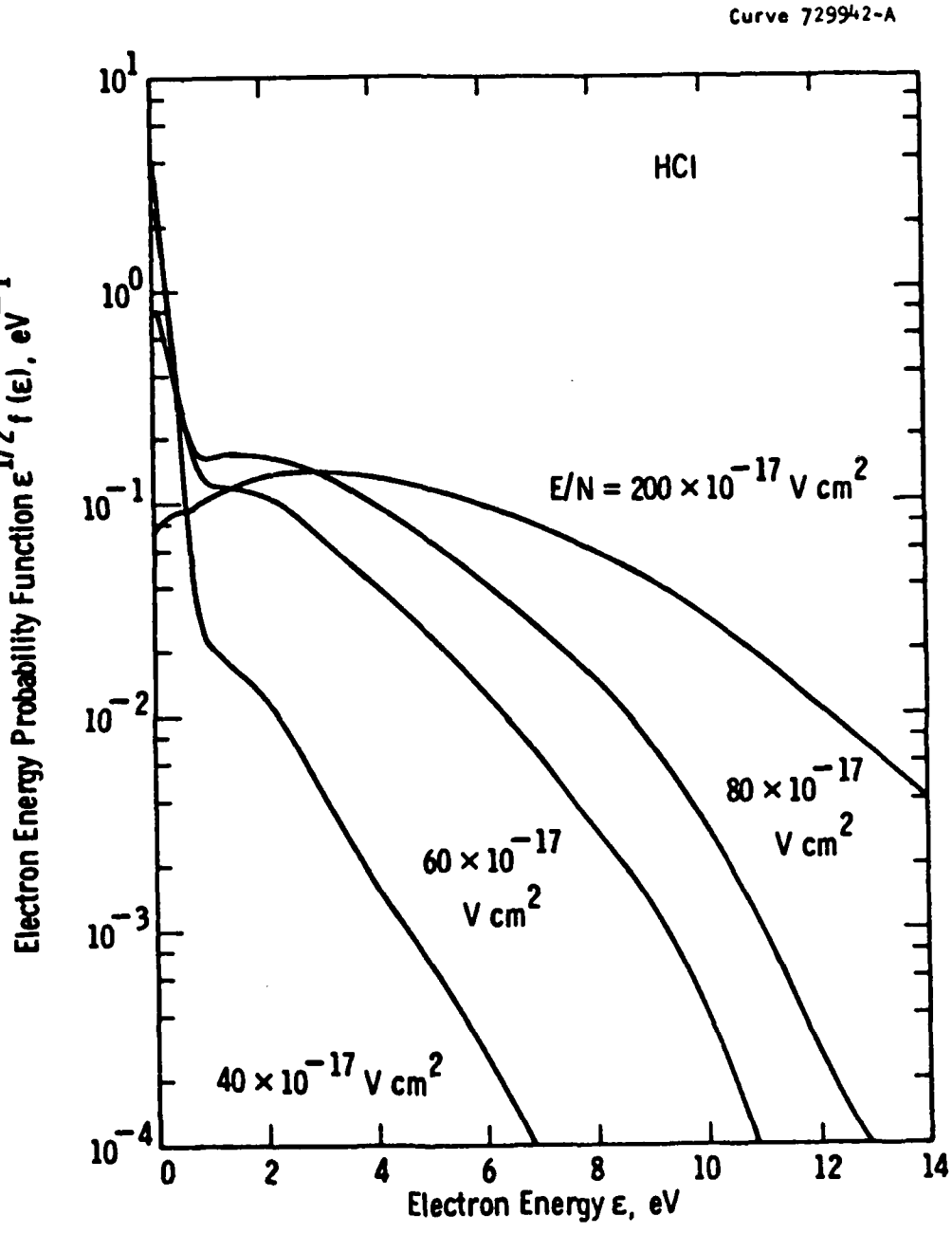

Fig. 20 - Electron energy distribution functions in HCℓ at values of E/N = 40, 60, 80, and 200 x 10^{-17} V cm^2.

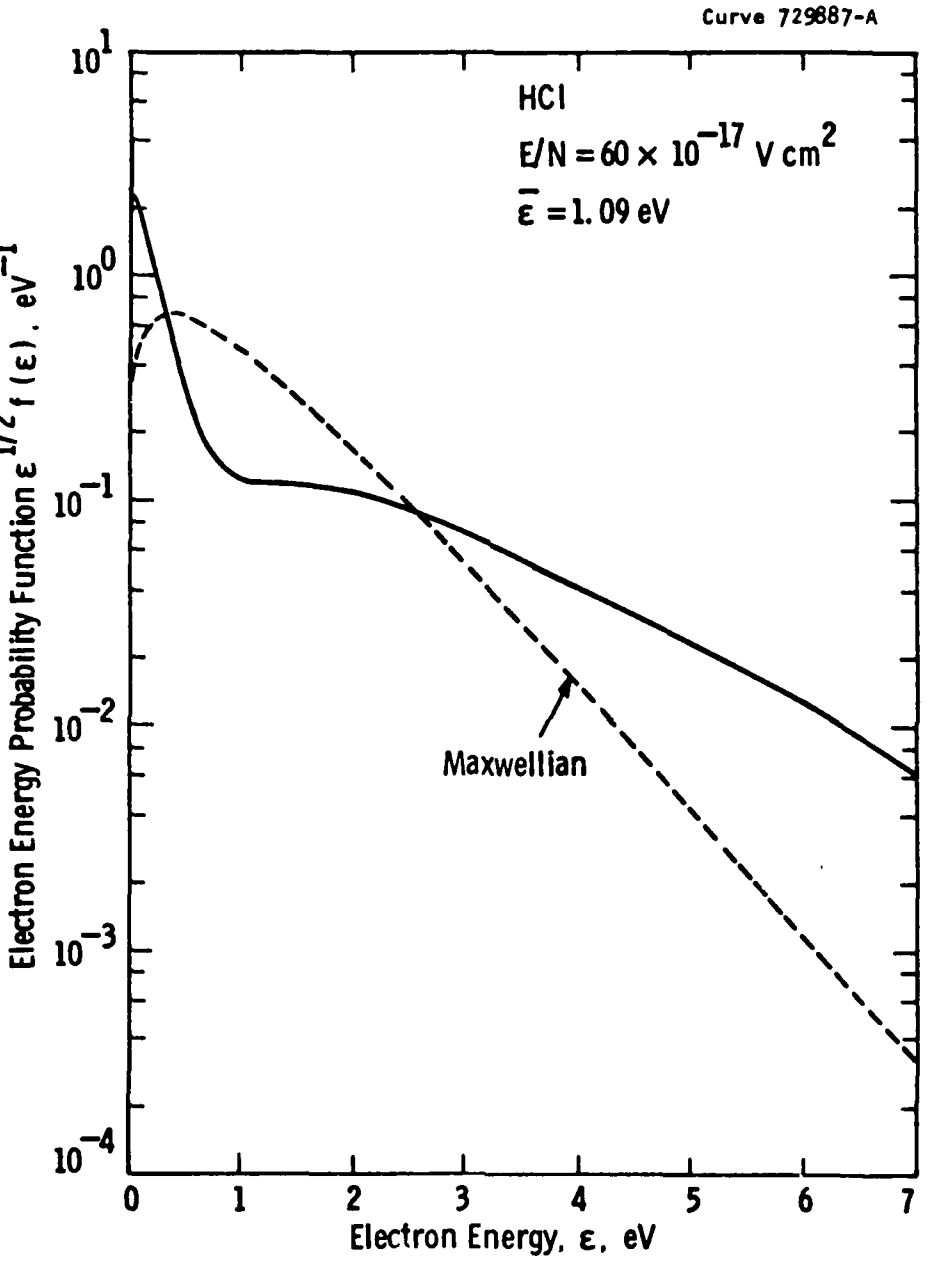

Fig. 21 - Electron energy distribution in HCℓ at E/N = 60 x 10^{-17} V cm^2 (solid line) compared with a Maxwellian distribution (dashed line) of the same mean energy.

mean energy is shown in Figure 21. At the lower values of E/N, the distributions show a larger number of electrons of energy less than 0.3 eV compared with a Maxwellian distribution, as a result of the effect of the large cross section for vibrational excitation to the first level. Correspondingly, there is a deficiency of electrons (compared with a Maxwellian distribution) over the range of energy for which $C\ell^-$ formation occurs.

Predicted values of D_T/μ_e, D_L/μ_e, and electron mean energy $\bar{\varepsilon}$, as a function of E/N are shown in Figure 22. At low values of E/N the ratio $D_L/D_T > 1$, characteristic of gases having a Ramsauer minimum in the momentum transfer cross section. The non-Maxwellian behavior for mean energies above thermal is also evident from a comparison of the curves of $\bar{\varepsilon}$ and D_T/μ_e.

Calculated values of rate coefficients for vibrational excitation, electronic excitation, attachment, and ionization as a function of electron mean energy are shown in Figure 23. These curves are calculated according to Equation (24) using the predicted curve of $\bar{\varepsilon}$ versus E/N shown in Figure 22 to establish the mean energy scale.

The predicted fractional power inputs to elastic and inelastic processes according to Equation (25) are shown in Figure 24 as a function of electron mean energy. For mean energies below ~ 0.2 eV most of the input energy is lost in elastic and rotational excitation collisions. Further measurements, e.g., of drift velocity in mixtures of $HC\ell$ with gases whose cross sections are known in this energy range, are required to separate elastic and rotational losses in this energy range. Since the percentage power input to attachment is at most 1%, the assumption made in the analysis of treating attachment as an energy-loss process only without taking into account the loss of the electron is not expected to introduce significant errors in the results.

3.5 DISCUSSION

The derivation of a set of cross sections for $HC\ell$ enables predictions of swarm parameters to be made in mixtures of $HC\ell$ with other gases whose cross sections are known. Thus, further evaluation of the validity of the derived cross sections may be made by comparing predicted parameters with published data in such mixtures.

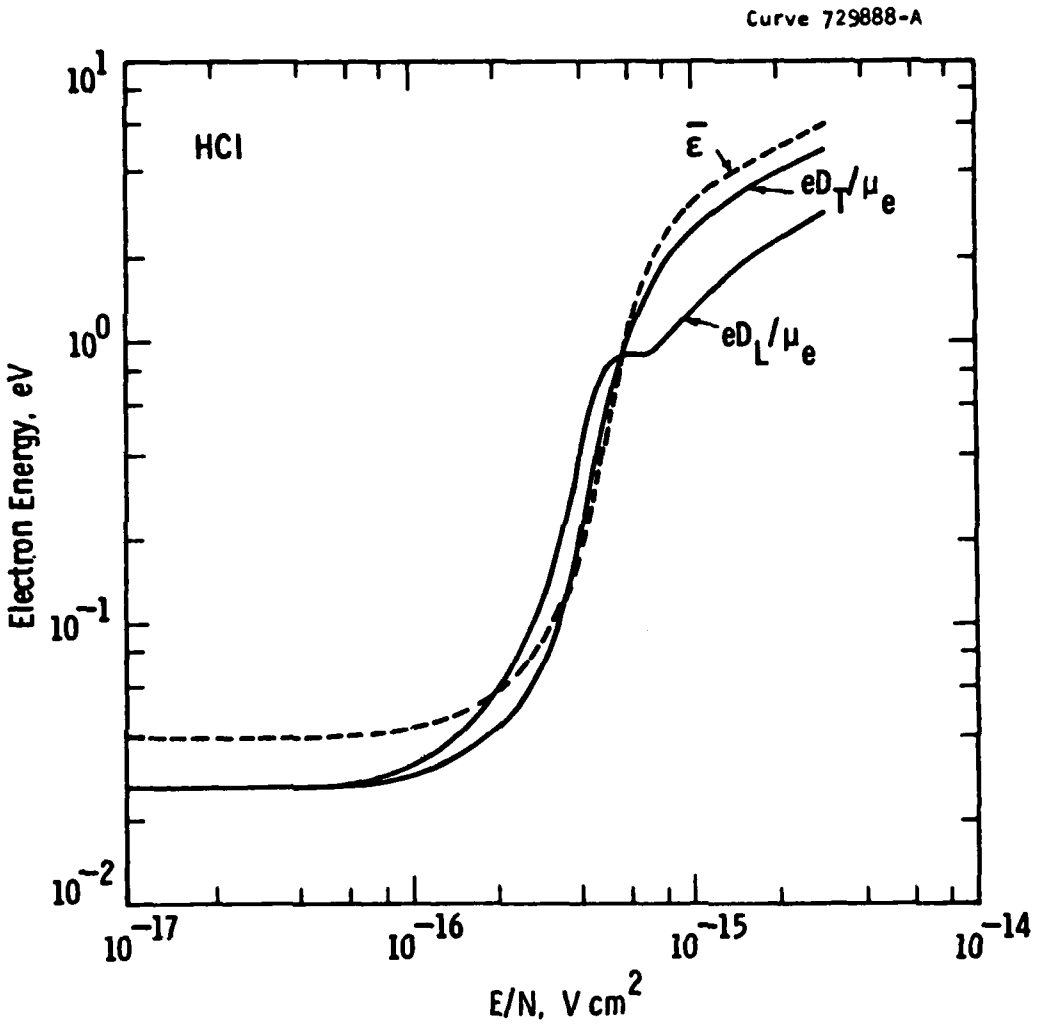

Fig. 22 - Predicted values of eD_T/μ_e, eD_L/μ_e, and $\bar{\varepsilon}$ in HCℓ as a function of E/N.

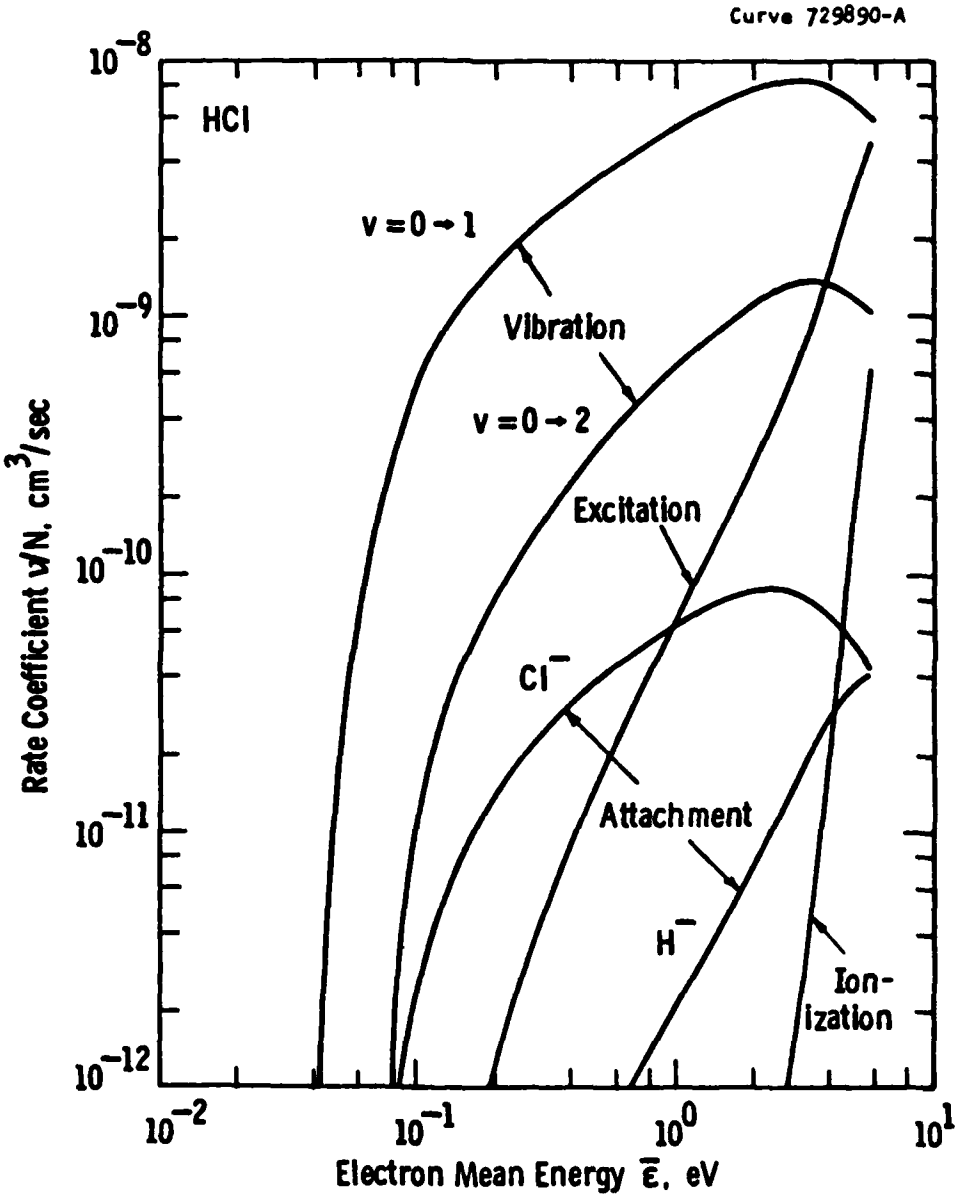

Fig. 23 - Predicted values of rate coefficients for vibrational excitation, attachment, and ionization in HCℓ as a function of electron mean energy.

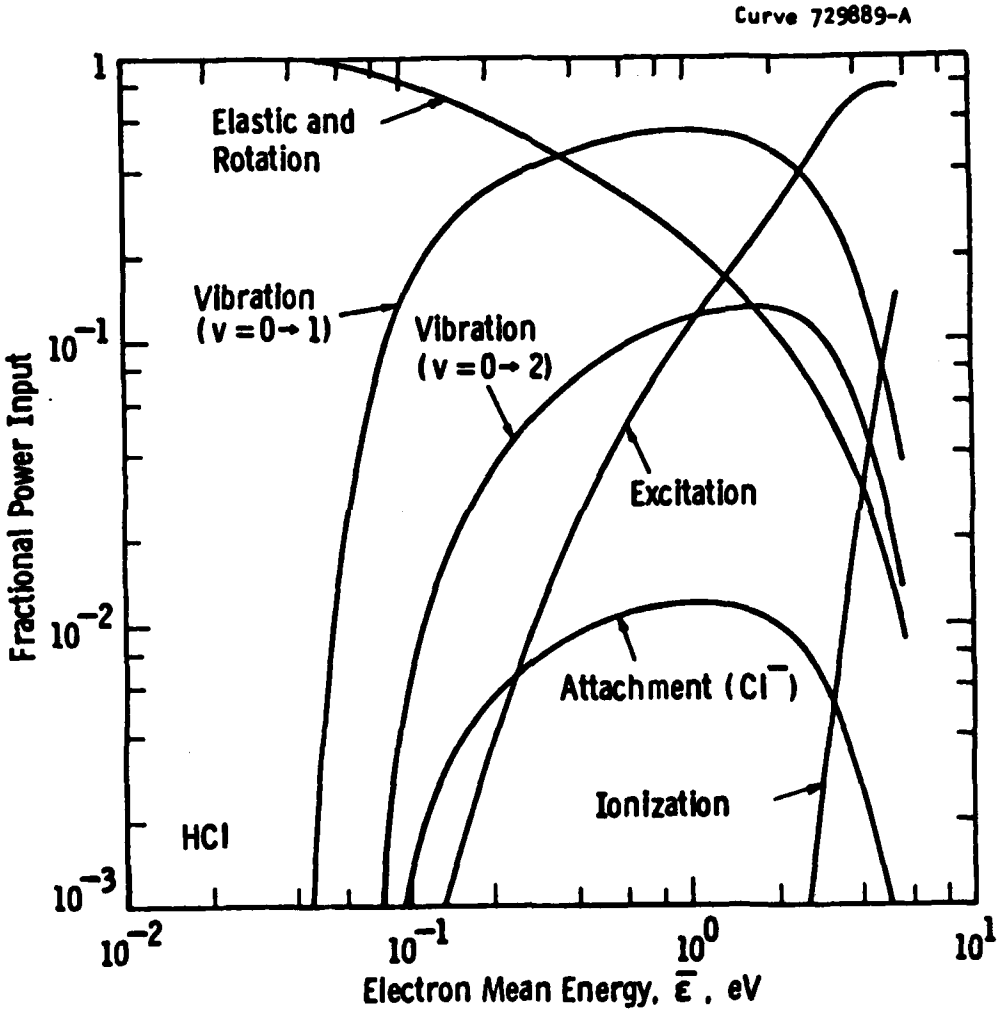

Fig. 24 - Predicted fractional power input to elastic and inelastic processes in HCℓ as a function of electron mean energy.

Measurements have been reported[23,36,37] previously of the attachment rate coefficient of dilute mixtures of HCℓ with N_2. In these measurements, the concentration of HCℓ is reported to be sufficiently low that the electron energy distribution is governed by the N_2 only. A comparison of these measured values with those predicted from solutions of the Boltzmann code is shown in Figure 25. The calculated values for $HC\ell/N_2$ mixtures have been obtained using the cross section set for HCℓ derived in the present work and the cross section set for N_2 reported by Engelhardt et al.[38] For these calculations the concentration of HCℓ in the mixture is chosen to be sufficiently low that the calculated transport coefficients w_e and D_T/μ_e are within 1% of those calculated for pure N_2. The concentration of HCℓ required to satisfy this condition decreases with decreasing E/N (or electron mean energy) and for $\bar{\varepsilon} < 0.6$ eV a concentration of less than 50 ppm is necessary. The calculated curve shows very good agreement with the data of Kligler et al[36] and of Sze et al[37], where the bars on the experimental points denote scatter in the data rather than confidence limits. The agreement with the data of Christophorou et al[23] is less satisfactory. However, as shown in Figure 25, these authors report an anomalously high attachment rate at low energy (which has already been discussed in Section 3.3) and it is difficult to assess whether the source of this anomalous behavior at low mean energy also influences the data at higher mean energy. Thus, the good agreement obtained with the other two sets of measurements is taken as further evidence in support of the absolute magnitude of the attachment cross section for HCℓ derived in the present study.

The measured and calculated attachment rate coefficients as a function of mean energy for pure HCℓ are also shown for comparison in Figure 25. It is noted that there is a large difference between the magnitude and shape of the attachment rate coefficient for $C\ell^-$ production in pure HCℓ compared with dilute mixtures of HCℓ with N_2. The peak value in the mixture is about a factor of four larger than that in pure HCℓ and the position of the peak in the mixture occurs at a lower mean energy (~ 0.83 eV) compared with that (~ 2.5 eV) in the pure gas. These large differences are due entirely to the differences in the electron energy distributions in N_2 and HCℓ particularly in the energy range where the cross section for $C\ell^-$ formation is appreciable. It

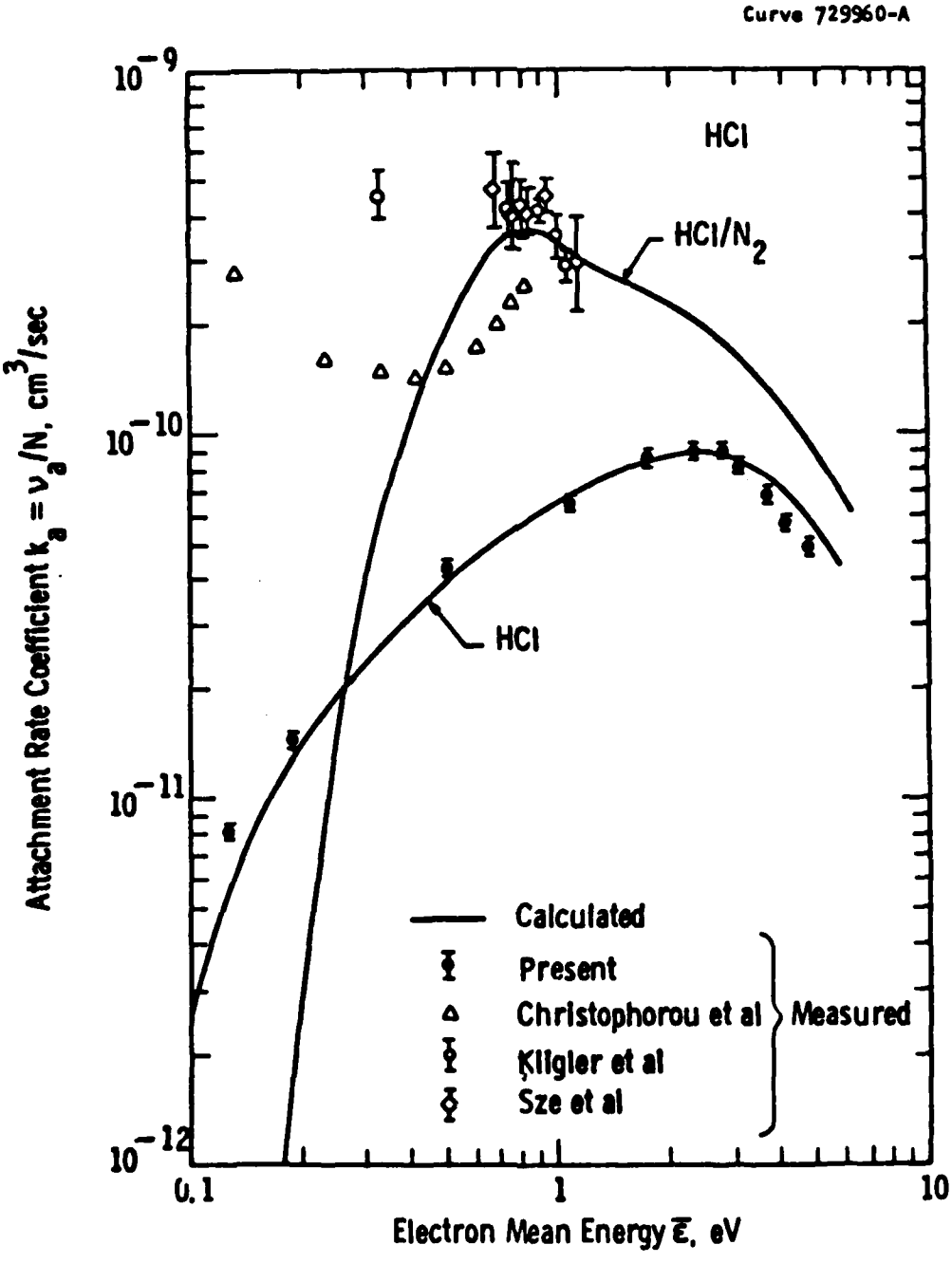

Fig. 25 - Comparison of predicted and measured values of the attachment rate coefficient as a function of electron mean energy in pure HCℓ and dilute mixtures of HCℓ with N_2.

has already been noted in Section 3.4 that the large vibrational cross section in HCℓ introduces a barrier for electrons at an energy below the onset for $Cℓ^-$ formation. On the other hand the large vibrational cross section in N_2, which occurs at an energy of 2.2 eV causes a relatively higher electron population at energies in the range of the $Cℓ^-$ cross section thereby leading to a larger attachment rate coefficient. Thus, the apparent discrepancy between the measurements in HCℓ and those in $HCℓ/N_2$ mixtures is resolved.

Calculations have also been carried out for a typical XeCℓ laser mixture comprising Ne/Xe/HCℓ in the proportions 97.9%/2%/0.1%. For these calculations, the cross sections for HCℓ derived in the present study have been combined with cross section sets[39] for Ne and Xe. The rate coefficients for vibrational excitation to the first level of HCℓ and attachment ($Cℓ^-$ formation) are shown in Figure 26 as a function of E/N and electron mean energy. The limiting value of E/N, (E/N)*, is indicated by the arrow on the abscissa and corresponds to the operating condition for an attachment-dominated self-sustained discharge in this mixture. The fractional power input to various elastic and inelastic processes involving the three components of the mixture is shown in Figure 27.

From Figure 26 it is seen that the attachment rate coefficient as a function of electron mean energy is intermediate between that for pure HCℓ and that for dilute $HCℓ/N_2$ mixtures (cf. Figure 25). On the other hand, the rate coefficient for vibrational excitation to the v = 1 level is similar to that in pure HCℓ (cf. Figure 23). From Figure 27 a major fraction of the input energy goes into vibrational excitation to the first level for electron mean energies ~ 1 eV.

For conditions corresponding to the high current density discharges used for excitation of the XeCℓ laser system, the high electron densities coupled with the large vibrational rate coefficient are expected to lead to a significant production of vibrationally excited HCℓ molecules in the laser mixture. In view of the large increase in the attachment cross section of HCℓ with each additional quantum of vibrational excitation of the target,[32] the effective attachment rate coefficient will be increased unless there are competing processes for quenching the vibrational states which have comparable or larger rate coefficients. Indeed, a value ~ 10^{-9} cm^3/sec has been

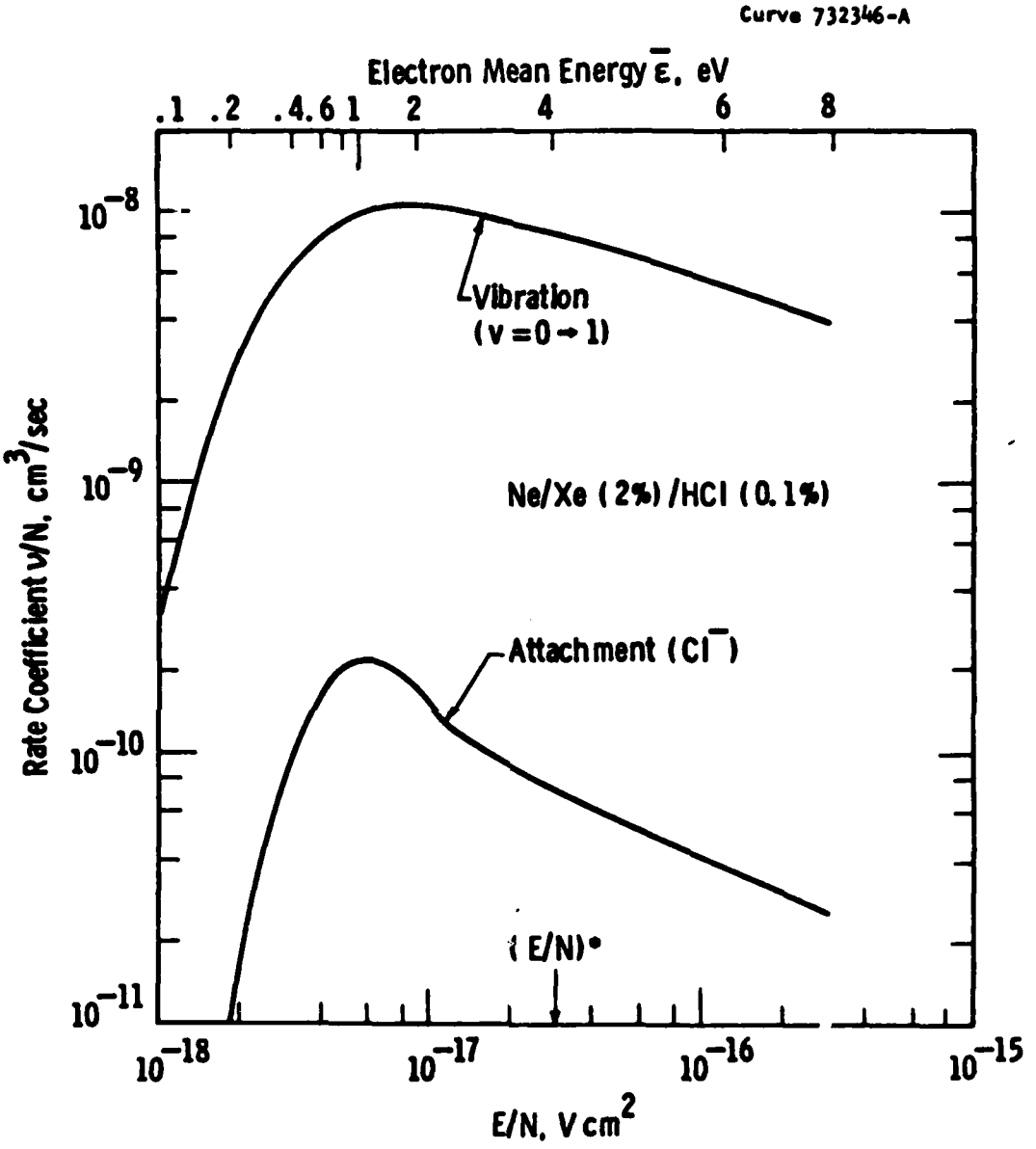

Fig. 26 - Predicted rate coefficients for vibrational excitation to the first level and for attachment ($C\ell^-$ formation) of HCℓ in a typical XeCℓ laser gas mixture, Ne/Xe (2%)/HCℓ (0.1%) as a function of E/N and electron mean energy. The limiting value of E/N is denoted by the arrow on the abscissa.

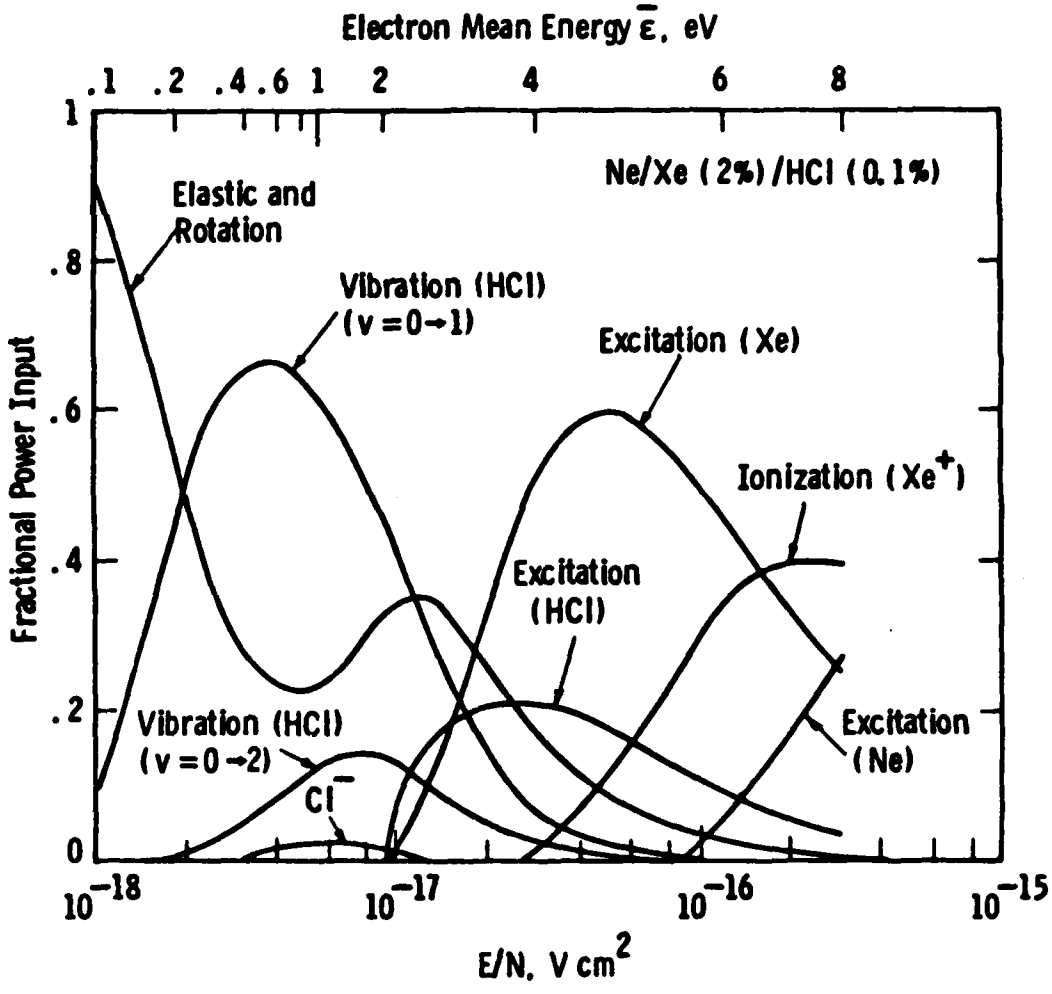

Fig. 27 - Predicted fractional power input to elastic and inelastic processes of the component gases in a typical XeCl laser mixture, Ne/Xe (2%)/HCl (0.1%), as a function of E/N and electron mean energy.

estimated[40] for the effective attachment rate coefficient of HCℓ under high current-density discharge conditions.

However, recent measurements have been made by Kligler et al[36] using an e-beam discharge device at e-beam current densities ~ 5A/cm^2, typical of laser discharge conditions. (These current densities are two orders of magnitude larger than those used in the HCℓ/N_2 measurements discussed earlier in this section). These measurements have been carried out in Ne/Xe/HCℓ mixtures of composition similar to that appropriate to Figures 26 and 27. Kligler et al obtain values ~ 10^{-10} cm^3/sec for the attachment rate coefficient at values of E/N ~ 10^{-17} V cm^2, i.e., in agreement with the predicted rate coefficient for attachment from HCℓ molecules in the ground vibrational state. If these measurements are correct, an additional quenching mechanism for the vibrationally excited states must be invoked which has comparable efficiency to that of dissociative attachment.

An upper limit for the loss rate of vibrationally excited HCℓ by attachment may be made for the experimental conditions of Kligler et al. Based on an attachment rate coefficient of 2 x 10^{-10} cm^3/sec (cf. Figure 26), a value for the electron density ~ 10^{14} cm^{-3} is found during the time of the excitation e-beam pulse. If a value ~ 5 x 10^{-9} cm^3/sec is taken for the rate coefficient for attachment to the v = 1 state, the loss rate by attachment is ~ 5 x 10^5 sec^{-1}.

The rate coefficients[41] for quenching of vibrationally excited HCℓ by Ne, Xe, and HCℓ lead to loss rates which are at least an order of magnitude smaller than that due to attachment. However, calculations[42] of the rate coefficients for V-T replacement by H atoms yield a value of 5 x 10^{-11} cm^3/sec for relaxation of the v = 1 state to the ground state. Thus, for a density of H atoms in the mixture of ~ 10^{16} cm^{-3}, a V-T quenching rate ~ 5 x 10^5 sec^{-1} is predicted. This implies that at least 5% of the HCℓ must be dissociated during the e-beam excitation pulse for the quenching rate by H atoms to be comparable to the attachment loss rate. The three most likely sources of H atom production are dissociative attachment to ground state HCℓ, dissociative attachment to vibrationally excitated HCℓ, and direct dissociation. For the latter process, a rate coefficient ~ 10^{-9} cm^3/sec at a mean energy ~ 1 eV is determined from the solutions of the Boltzmann code appropriate to Figures 26

and 27. Thus, production rates of H atoms of 2×10^4 sec^{-1}, 5×10^5 sec^{-1}, and 1×10^5 sec^{-1}, respectively, are estimated from the above three sources. In the experiments of Kligler et al, the e-beam pulse duration is 350 nsec, which leads to the result that ~ 20% of the HCℓ is dissociated during the pulse.

Clearly, a more quantitative analysis of the reaction kinetics is required to resolve this question. However, the above considerations together with the experimental measurements of Kligler et al, would appear to indicate that dissociative attachment to vibrationally excited HCℓ under laser excitation conditions may not be as significant as is currently thought. In this context, a more quantitative determination of the dissociation (A state) cross section would be desirable in view of the lack of uniqueness of this cross section as determined from solutions of the Boltzmann code in the present work (cf. Section 3.4).

4. RESULTS OF MEASUREMENTS IN $CC\ell_4$

The present measurements have been carried out using spectranalyzed grade carbon tetrachloride supplied by Fisher Scientific Co. To contain the liquid sample, a stainless steel valved sample cylinder was fabricated and thoroughly degassed by baking at 350°C for 20 hours on an auxiliary ultrahigh vacuum system. After obtaining a residual pressure in the low 10^{-9} Torr range about 30 cc of liquid $CC\ell_4$ was siphoned into the cylinder. The sample was then subjected to further pumping in order to remove any dissolved gas.

4.1 ELECTRON DRIFT VELOCITY

A summary of the measurements of electron drift velocity as a function of E/N is given in Table 3. These values have an estimated uncertainty of ±2%. Because of the very large attachment coefficient in $CC\ell_4$ measurements in the pure gas have been restricted to the range of E/N for which appreciable ionization occurs, i.e., for E/N > 850 x 10^{-17} V cm^2. Over the range of E/N covered, the electron mobility has an approximately constant value ~ 109 cm^2/sec V. No previous measurements of electron drift velocity in $CC\ell_4$ are available for comparison.

4.2 ION MOBILITIES

From the exponential temporal dependence of the measured negative-ion component of the total anode-collected current, it is concluded that only one dominant negative ion species is observed over the range of E/N studied. The values of the negative-ion mobility as a function of E/N are given in Figure 28 and in Table 3; the uncertainty in these measurements is estimated to be ±1%. There is general agreement among many studies[43-46] that the dominant ion species produced by electron impact on $CC\ell_4$ under single collision conditions is $C\ell^-$ formed by a dissociative attachment reaction. Although there is little doubt that the primary ion formed in the present work is $C\ell^-$, the identity of the final ion species recorded is undetermined.

The positive-ion arrival spectra recorded at the cathode also show the presence of only one dominant positive-ion species. The values obtained for the positive-ion mobility are given in Figure 28 and in Table 3 and are

TABLE 3. SUMMARY OF VALUES OF THE SWARM PARAMETERS DETERMINED FOR $CC\ell_4$[a].

E/N 10^{-17} V cm^2	w_e 10^6 cm/sec	η/N 10^{-18} cm^2	α/N 10^{-18} cm^2	$(\alpha - \eta)/N$ 10^{-18} cm^2	α/η	μ_o^- cm^2/sec V	μ_o^+ cm^2/sec V
300.0		453 ± 3%				0.685	
350.0		312 ± 3%				0.739	
400		248 ± 3%				0.788	
450		206 ± 3%				0.819	
500		167 ± 3%				0.846	
550		138 ± 3%				0.867	
600		110 ± 3%				0.868	
650		89 ± 3%				0.871	
700				-69		0.878	
725				-60		0.889	
750		59 ± 4%	9.2 ± 6%	-50	0.155	0.892	
775		52 ± 4%	11.9 ± 6%	-40	0.23	0.896	
800		46 ± 4%	15 ± 7%	-31	0.33	0.897	
825				-21		0.906	0.499
850	25.0	35 ± 6%	24 ± 8%	-11.6	0.67	0.919	0.492
880	26.0			0	1.00		
900	26.3	28 ± 14%	35 ± 12%	7.5	1.27	0.880	0.489
925	26.9	26 ± 8%	42 ± 6%	16.6	1.65	0.863	0.486
950	27.2	22 ± 6%	49 ± 5%	26.5	2.19	0.847	0.474

[a]Estimated uncertainties in the measured quantities are:

E/N: ± 0.2%

w_e: ± 2%

μ_o^-, μ_o^+: ± 1%

$(\alpha-\eta)/N$: ± 3%

α/η: ± 2%

η/N, α/N: As noted in table

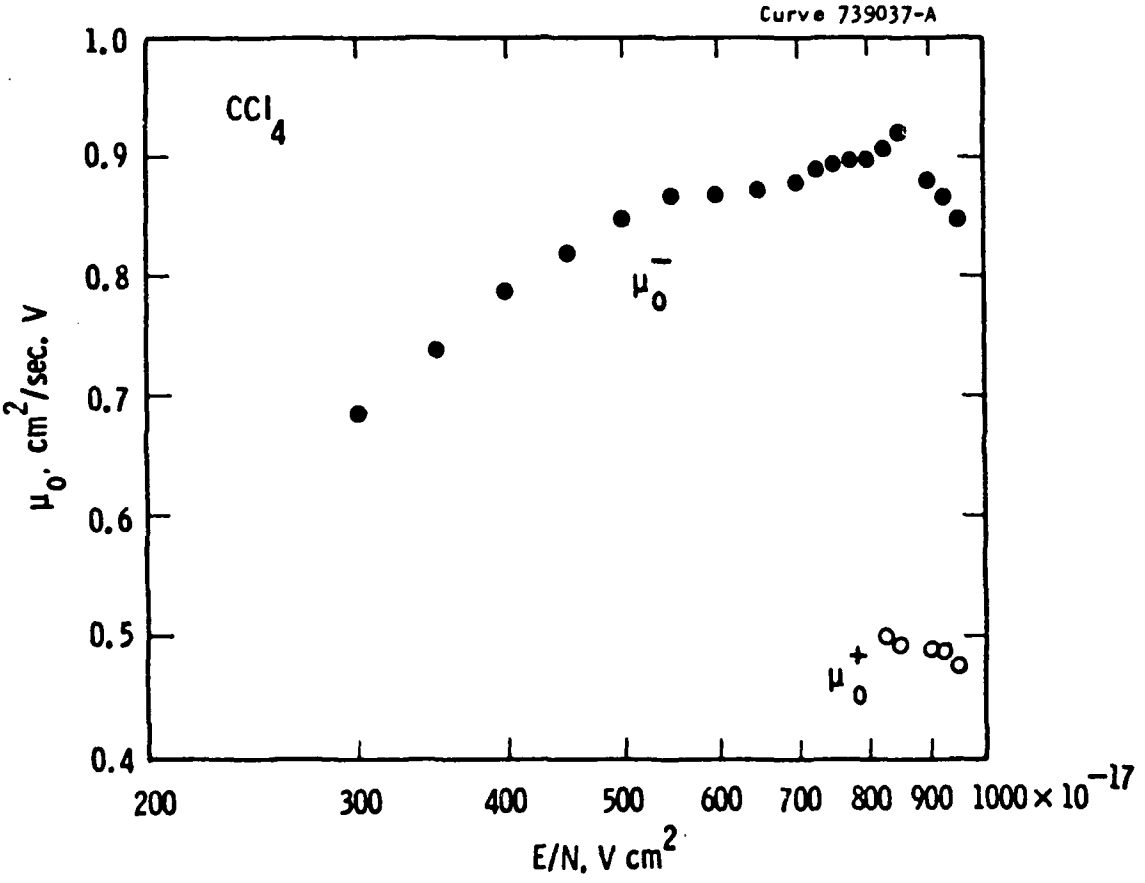

Fig. 28 - Measurements of the reduced negative-ion mobility (solid points) and positive-ion mobility (open points) in $CC\ell_4$ as a function of E/N.

approximately half the values of negative-ion mobility over the common range of E/N. The dominant positive ion formed is expected[44] to be CCl_3^+; however, the identity of the ion species to which the mobility values obtain remains uncertain.

4.3 ATTACHMENT AND IONIZATION COEFFICIENTS

The values of the net ionization coefficient $(\alpha - \eta)/N$ determined as a function of E/N from either the negative-ion or positive-ion waveforms are given in Table 3 and plotted as absolute values in Figure 29. The limiting value of E/N, $(E/N)^*$, is determined to be $(880 \pm 2) \times 10^{-17}$ Vcm^2 and is denoted by the dashed line in Figure 29. For values of E/N $< 650 \times 10^{-17}$ V cm^2 no positive ions are detected and the data in this region correspond to pure attachment coefficients.

The present measurements are compared in Figure 29 with the only other set of previous measurements, those of Geballe and Harrison.[47] There is a considerable difference between the two sets of measurements over the common range of E/N covered, i.e., in the vicinity of the limiting value of E/N. In particular, the limiting value found by Geballe and Harrison is ~ 6% larger than the present value and is considered to be well outside the uncertainty in the present measurement.

The same data are replotted in linear form in Figure 30. The linear dependence of $(\alpha - \eta)/N$ on E/N in the vicinity of $(E/N)^*$ observed in the present work is typical of the behavior found in a number of strongly attaching gases. Over the range of E/N from 650 to 950 $\times 10^{-17}$ V cm^2 the present data are described to within ± 3% (the uncertainty of the measurements) by the relation

$$(\alpha - \eta)/N = 3.81 \times 10^{-19} [(E/N) - (E/N)^*] \qquad (38)$$

where $(\alpha - \eta)/N$ is in cm^2, E/N and $(E/N)^*$ are in units of 10^{-17} V cm^2, and $(E/N)^* \equiv 880$.

Measurements of the ratio α/η as a function of E/N over the range 750 to 950 $\times 10^{-17}$ Vcm^2 are shown in Figure 31 and also in Table 3. The

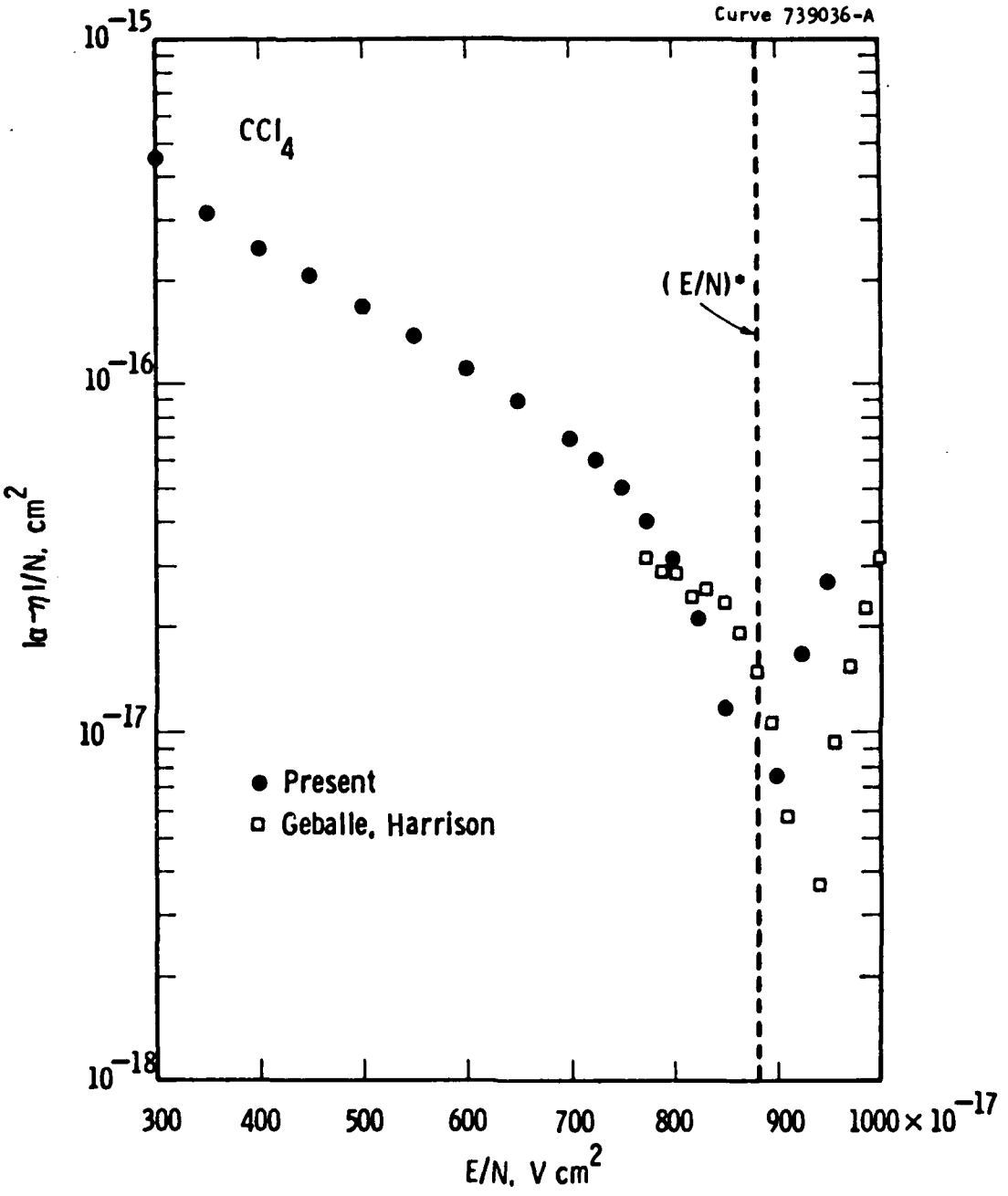

Fig. 29 - Comparison of the present values (solid points) of the net ionization coefficient $(\alpha - \eta)/N$ in $CC\ell_4$ as a function of E/N with previous measurements (open points).

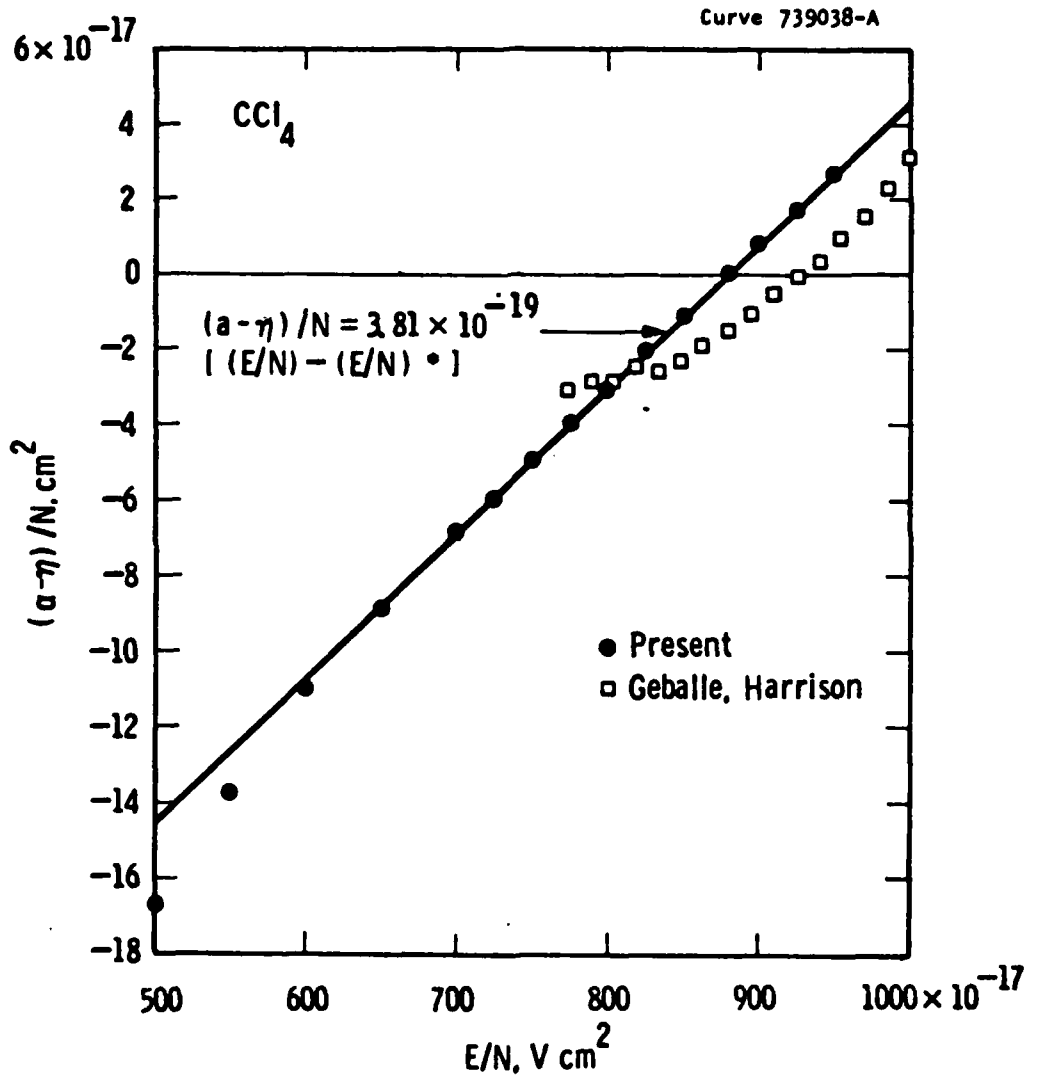

Fig. 30 - Linear plot of the values of $(\alpha - \eta)/N$ in $CC\ell_4$ as a function of E/N in the region of the limiting value of E/N.

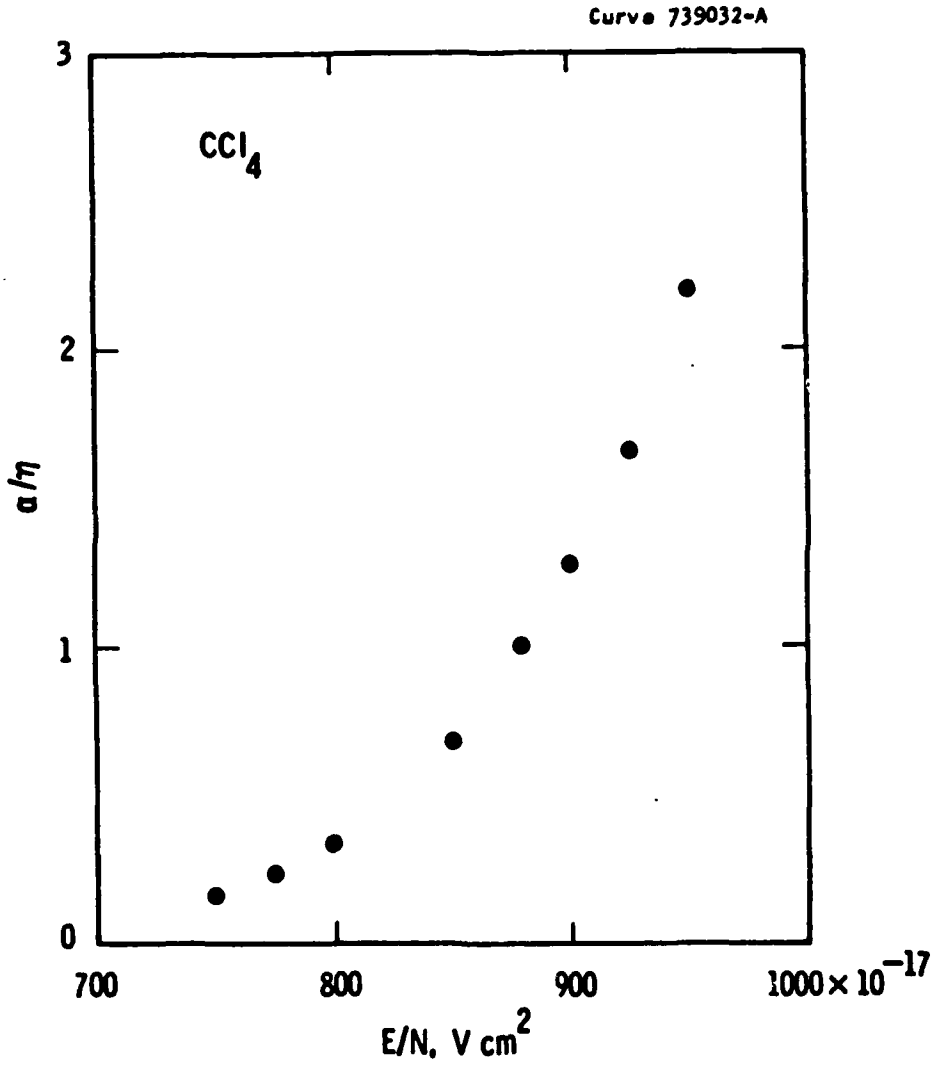

Fig. 31 - Present measurements of the ratio α/η in $CC\ell_4$ as a function of E/N.

uncertainty in these measurements is estimated to be ± 2%. In the case of $CC\ell_4$, the pair-production cross section is reported[44] to be very small, and if this is the case there is no ambiguity in identifying the ratio $(Q_+^C/Q_o)/(Q_-^A/Q_o)$ with α/η (cf. Section 3.3).

The values of α/N and η/N determined by combining the present values of $(\alpha-\eta)/N$ and α/η are given in Figure 32 and in Table 3. By comparison, the values of α/N and η/N obtained by Geballe and Harrison from their spatial current growth measurements exhibit anomalous behavior. Their data for the dependence of α/N and η/N as a function of E/N both show a minimum in the vicinity of the limiting value. Such behavior is difficult to understand, particularly the increasing ionization coefficient with decreasing E/N below $(E/N)^*$. The values of α/N determined in the present study are plotted as a function of N/E in Figure 33. Over the range of the measurements from $E/N = 750$ to 950×10^{-17} V cm^2, the experimental values agree to within ±2% with the relation

$$\alpha/N = 2.73 \times 10^{-14} \exp\,[-6000/(E/N)] \qquad (39)$$

where α/N is in cm^2 and E/N is in units of 10^{-17} V cm^2.

4.4 DISCUSSION

The present measurements of swarm parameters in pure $CC\ell_4$ have been confined to values of $E/N > 300 \times 10^{-17}$ V cm^2 which, based on previous experience with other gases, probably corresponds to electron mean energies in excess of 1 eV. Consequently, the electron energy distributions in this range are expected to be strongly influenced by processes having relatively large threshold energies, e.g., electronic excitation and ionization.

Unfortunately, very little information is available on either the shape or absolute magnitude of collision cross sections in $CC\ell_4$. No information is available concerning elastic, vibrational excitation, electronic excitation, or ionization cross sections. The only data that have been reported relate to the attachment cross section. The $C\ell^-$ cross section has a large peak at zero energy followed by a much smaller peak centered at an energy ~ 0.55 eV.[44-46,48,49] The magnitude of the first peak shows no change with

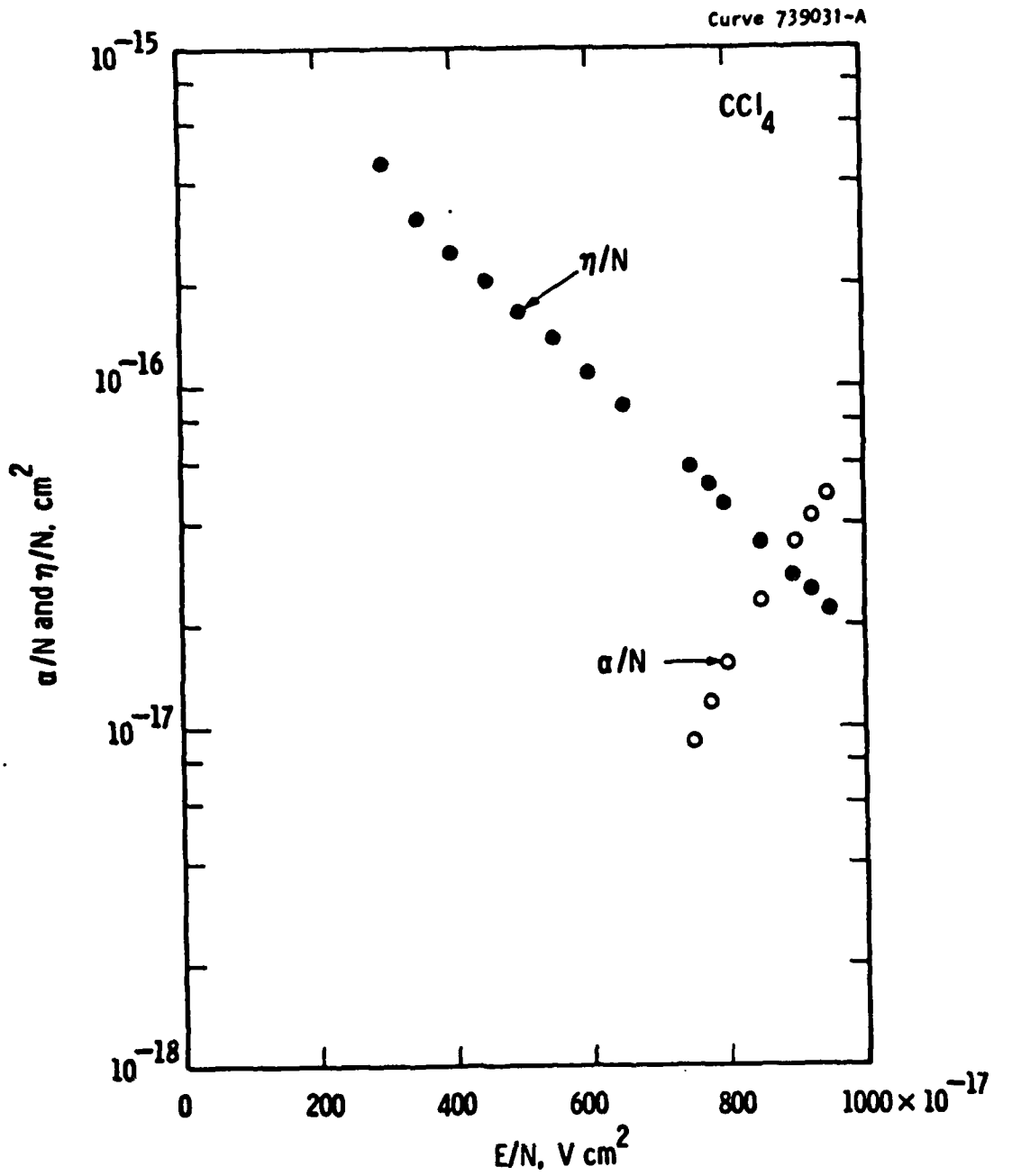

Fig. 32 - Values of the ionization (α/N) and attachment (η/N) coefficients in CCl_4 as a function of E/N measured in the present study.

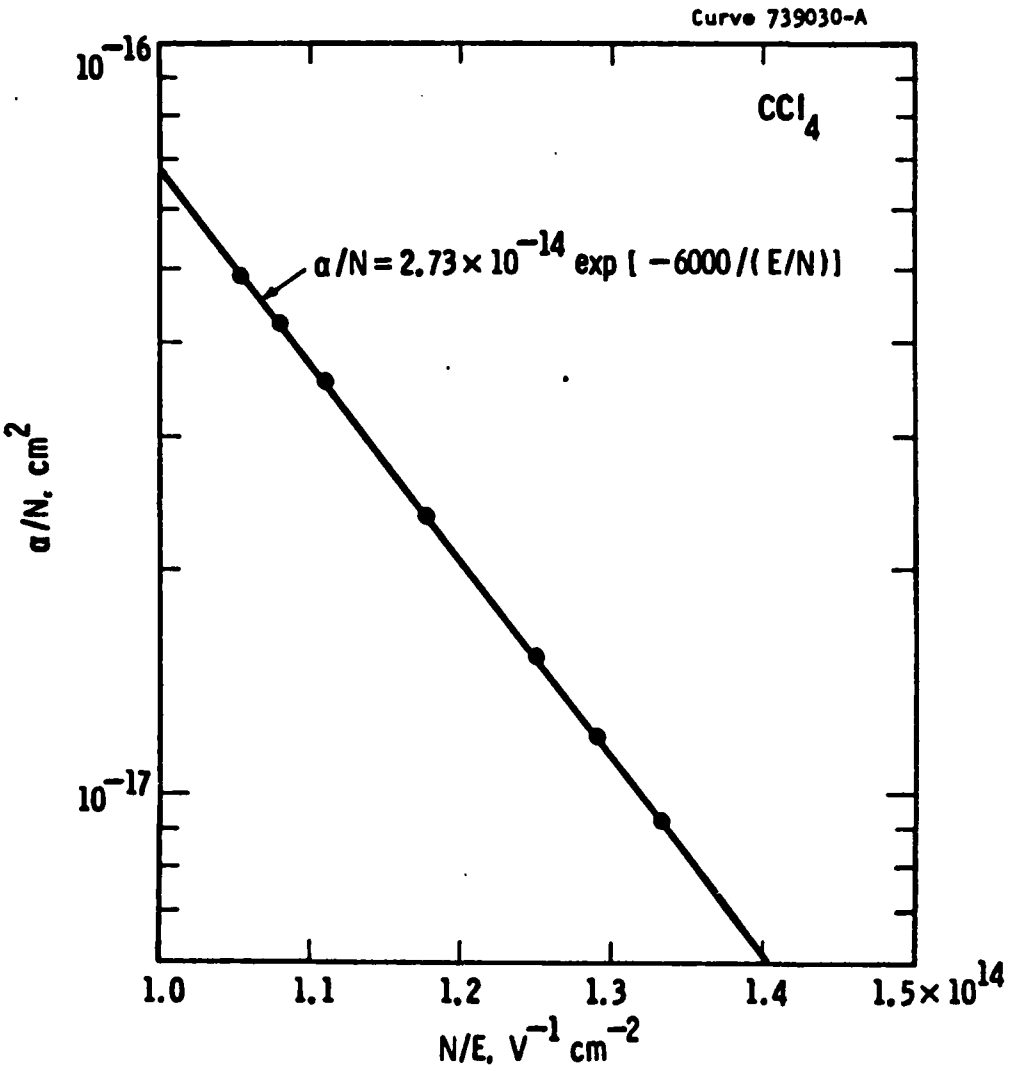

Fig. 33 - Present values of α/N in $CC\ell_4$ plotted as a function of N/E.

variation of gas temperature over the range 300 to 1060°K whereas the magnitude of the second peak almost doubles and shifts to lower energies over this temperature range.[49] The independence of the energy integrated cross section with temperature[49] is consistent with the independence of the thermal attachment rate on temperature observed[50] over the temperature range from 300 to 473°K. Measurements of the attachment rate coefficient have been made by Christodoulides and Christophorou[51] in dilute mixtures of $CC\ell_4$ with N_2 over the range of electron mean energy from thermal to 0.7 eV. They have analyzed these data, assuming known electron energy distribution functions for N_2 and a shape for the attachment cross section of the form $Q = A\varepsilon^{-\gamma}$, to obtain an absolute cross section over the range from 0.05 to 0.6eV. The derived cross section is given by $Q(cm^2) = 3 \times 10^{-16}\ \varepsilon\ (eV)^{-1.226}$, and yields a value of 1.2×10^{-14} cm^2 at 0.05 eV but, by virtue of the assumed shape, ignores the secondary peak. The value of the cross section at 0.6 eV is 5.6×10^{-16} cm^2 which compares with the value of 1.0×10^{-16} cm^2 determined by Buchel'nikova. The ratio of these values is similar to that reported by these workers for the peak cross section in $HC\ell$. The only further information available for $CC\ell_4$ is that of the thermal attachment rate coefficient which has been determined in a number of investigations[22,51-54] using dilute mixtures of $CC\ell_4$ in a variety of buffer gases; the values reported range from 2.9×10^{-7} to 4.1×10^{-7} cm^3/sec.

In view of the lack of information concerning cross sections in $CC\ell_4$, particularly at the higher electron energies, it is felt that a meaningful analysis of the present swarm data in $CC\ell_4$ is untenable at the present time. However, the availability of an absolute ionization cross section in the future will allow the present data to be analyzed to provide cross sections for electronic excitation and attachment. In the case of the latter, the high energy tail of the first $C\ell^-$ peak together with the secondary peak are expected to contribute substantially to the attachment coefficient over the range of E/N covered by the present measurements.

With respect to the low-energy region further measurements of drift velocity and attachment coefficient in mixtures of $CC\ell_4$ with gases whose cross sections are known would be desirable to attempt extraction of elastic and inelastic cross sections. Two sets of such measurements are required, one using sufficiently dilute mixtures so as not to perturb the energy

distribution of the buffer gas in order to determine the attachment cross section, and the other using sufficiently strong mixtures to deliberately perturb the distribution of the buffer in order to determine the other cross sections.[55]

5. INVESTIGATIONS IN $C\ell_2$ AND $BC\ell_3$

5.1 CHLORINE

The investigation in $C\ell_2$ has been carried out using research grade gas supplied by Matheson Co. The gas is quoted by the manufacturer to be 99.96% pure, the main impurities being CO_2:200 ppm, N_2: 100 ppm, O_2: 50 ppm, and H_2O: 50 ppm.

5.1.1 Initial Study

The introduction of $C\ell_2$ into the freshly-baked drift tube has presented two problems not encountered in the study of $HC\ell$ and $CC\ell_4$. First, the density of $C\ell_2$ in the valved-off system, monitored both by the Baratron gauge and by the optical absorption system set at λ 3650Å, decreases rapidly with an initial rate ~ 0.1 Torr-ℓ/min. Second, the photoelectron yield from the semitransparent gold-film cathode in the presence of $C\ell_2$ is more than three orders of magnitude less than that obtained in the presence of either $HC\ell$ or $CC\ell_4$.

The rate of disappearance of $C\ell_2$ in the drift-tube system decreases with the amount of gas consumed and is attributed to passivation of the system whereby reaction of the $C\ell_2$ with internal surfaces leads to the generation of surface layers which are relatively more inert to further reaction. Thus, after consumption of approximately 100 Torr-ℓ of $C\ell_2$, the rate of decrease of $C\ell_2$ in the system drops to ~ 0.01 Torr-ℓ/min. This reduced rate is low enough that the gas density in the drift tube can be maintained constant to 0.1% (the uncertainty in the pressure measurement) for the duration of a series of waveform measurements by continuously bleeding gas into the system.

The decreased photoelectron yield from the cathode of the drift tube results in an unacceptably low signal/noise ratio in the averaged current waveforms obtained using either the spark source or the deuterium lamp as UV light sources. The electron yield does not recover following re-evacuation of the system and deteriorates slowly on further admission of $C\ell_2$. Attempts to restore the yield either (i) by introducing H_2 into the system and allowing the H_2 to remain in contact with the gold-film cathode for a period of several

hours, or (ii) by bombardment of the film with low-energy hydrogen positive ions produced by operating the drift tube at a sufficiently high value of E/N, both proved unsuccessful. Rebaking the system restores the original vacuum photoelectron yield; however, upon introduction of $C\ell_2$ into the drift tube, the same reduction in yield is observed. In view of the importance of $C\ell_2$ in the overall perspective of the study, it was decided to divert effort into overcoming this major problem so that measurements in $C\ell_2$ could be carried out.

5.1.2 Development of an Electron Source For Measurements in $C\ell_2$

Methods of producing a pulsed electron source using a completely different technique have not been considered. Such an approach would have necessitated a major redesign of part of the drift tube and was considered impractical in the time allotted to the study. With this constraint, two approaches have been followed to improve the pulsed electron yield using the original photoelectric method: (i) to increase the quantum yield of the photocathode, and (ii) to increase the intensity of the pulsed UV source used to irradiate the cathode.

The observation that the photoelectron yield from the gold-film cathode which has been subjected to $C\ell_2$ can be restored by baking in vacuum suggests that contact of $C\ell_2$ with the gold-film cathode increases the work function of the cathode surface. Thus, other cathode materials have been tried, chosen for compatibility with $C\ell_2$, good vacuum processing properties, and lower vacuum work function. In addition, the quartz window in the chamber envelope has been replaced with a sapphire window in order to extend the transmission of radiation from the UV source to shorter wavelength.

Cathodes composed of thin films (300Å) of tantalum and platinum have been fabricated in the same manner as described in Section 2.1 for the gold-film cathode, with the exception that the tantalum film is sputtered rather than evaporated onto the sapphire substrate. The tantalum-film cathode is found to exhibit anomalous behavior even before exposure to $C\ell_2$. The vacuum current leaving the cathode structure is observed to be a factor of thirty larger than that collected at the anode, most of the current being emitted from the side opposite the drift region. No explanation for this behavior is available at

present. The platinum-film has a similar vacuum yield to the gold-film cathode. However, after exposure to $C\ell_2$, no anode current is detectable.

In order to investigate whether the low yield observed from thin-film cathodes is characteristic of bulk behavior, a different type of cathode has been tried. This cathode, designed as a direct replacement for the thin-film cathode, relies on photoemission from direct photon bombardment of the surface while retaining the desirable geometry of the thin-film cathode and is illustrated in Figure 34. The central region of the cathode plate consists of a raised portion 2.5 cm square with parallel slots 0.16 cm wide cut at an angle of 45° to the cathode plane. The face of each slot is used to support a strip of gold foil 0.48 cm wide and 0.008 cm thick strung across the central aperture of diameter 1.6 cm. In Figure 34, the upper drawing shows a plan view of the cathode plate (without the strips of gold foil), the center drawing shows a cross-section view along the edge of the raised center portion of the cathode plate, and the lower drawing shows a cross-section view through the center of the plate with the strips of gold foil attached. The upper edges of the foils are coplanar with the upper surface of the raised central region of the cathode and after installation in the drift tube are located 0.1 cm from the cathode screen, as in the case of the thin-film cathode. The cathode aperture presents a louvred appearance, the louvres being designed to be opaque to radiation at normal incidence. The photoelectron yield from the "louvre" cathode is found to be a factor of twenty larger than that from a gold-film cathode.

Attempts to increase the intensity of the pulsed UV source have focussed on the xenon discharge because of its rich UV continuum extending to 1470 Å. A xenon flashtube having a suprasil quartz window (EGG Type FX-265UV) has been used for this purpose. The flashtube has a maximum dissipation of 7W and a maximum input energy per pulse of 5 J. This allows the input pulse energy to be varied from 10 mJ to 1 J while maintaining a reasonable pulse repetition rate. Over this range, the vacuum photoelectron yield per pulse is found to be approximately proportional to input energy and is larger than that obtainable from the spark and deuterium sources by factors ranging from 10 to 1000 depending on the input energy. The photoelectron pulse width varies from 145 nsec to 1 μsec for input energies to the flashtube ranging from 10 mJ to 1 J. Thus, this source provides a considerable increase in UV intensity

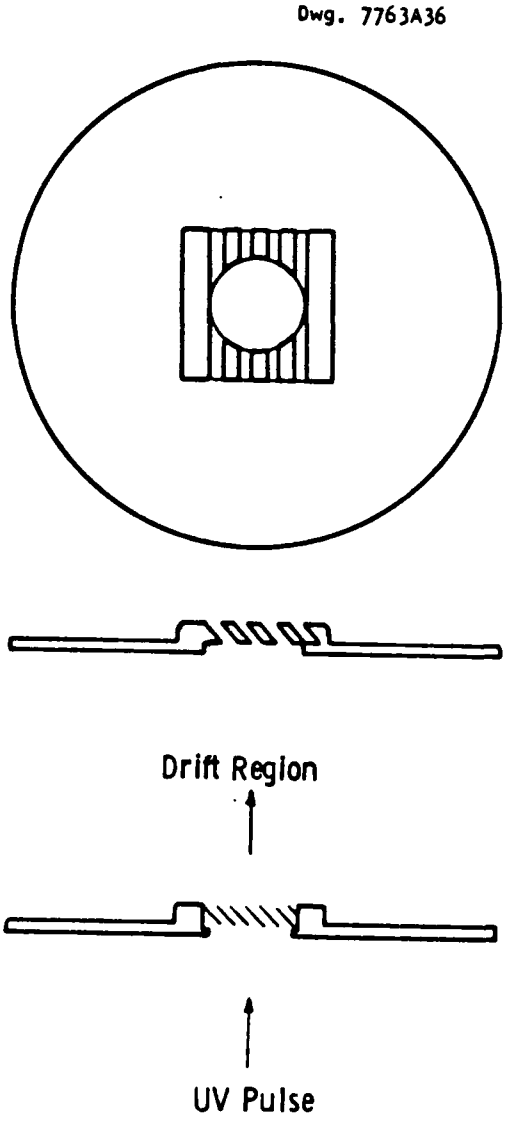

Fig. 34 - Drawing of the "louvre" cathode developed [illegible]

AD-A122 026 MEASUREMENTS OF SWARM PARAMETERS IN CHLORINE-BEARING MOLECULES(U) WESTINGHOUSE RESEARCH AND DEVELOPMENT CENTER PITTSBURGH PA D K DAVIES AUG 82 DYD-11008-CE 2/2

UNCLASSIFIED AFWAL-TR-82-2083 F33615-79-C-2074 F/G 20/8 NL

END

FILMED

DTIC

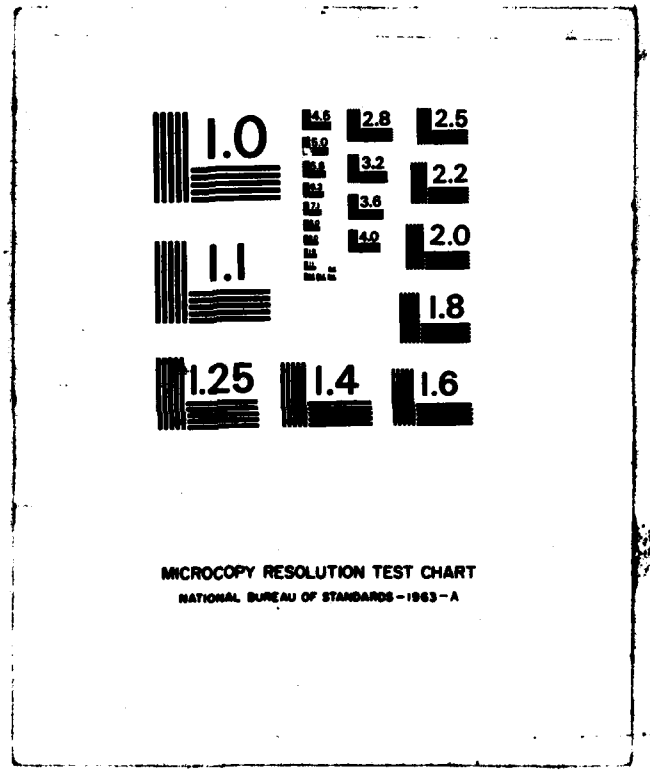
1.0
1.1
1.25
1.4
1.6
1.8
2.0
2.2
2.5
2.8
3.2
3.6
4.0
4.5
5.0
MICROCOPY RESOLUTION TEST CHART
NATIONAL BUREAU OF STANDARDS - 1963 - A

compared with the sources initially used while retaining an adequately narrow pulse width.

The combination of the "louvre" cathode and the xenon flashtube source is found to provide a vacuum photoelectron yield approaching 10^9 electrons/pulse for an input energy to the flashtube of 100 mJ. After exposure to $C\ell_2$, a photoelectron yield ~ 10^5 electrons/pulse is observed. This is found to be adequate for measurements of current waveforms in pure $C\ell_2$ as may be seen from the preliminary observations discussed below.

5.1.3 Preliminary Observations of Current Waveforms in $C\ell_2$

A sample of the averaged (10^4 pulses) anode waveforms recorded in pure $C\ell_2$ are shown in Figure 35, taken at values of E/N = 100 x 10^{-17} V cm^2, 290 x 10^{-17} V cm^2 (approximately the limiting value), and E/N = 300 x 10^{-17} V cm^2, for the maximum drift distance of 5.2cm using an input energy of 100 mJ/pulse to the UV flashtube. Although the signal/noise ratio in the current waveforms is not as large as that obtained in either $HC\ell$ or $CC\ell_4$ it is clear that accurate values of the swarm parameters may be determined from the charge waveforms. It should be emphasized that, due to lack of time, no attempt has been made to optimize the experimental conditions and that the examples shown in Figure 35 are not considered to be the best data obtainable using the presently improved system.

A complete survey of the parameter space over which measurements in pure $C\ell_2$ are possible has not been made. However, current waveforms measured for the same conditions appropriate to Figure 35 show that the attachment is sufficiently low to permit measureable electron transmission to the anode for values of E/N down to at least 30 x 10^{-17} V cm^2. Thus, measurements of electron drift velocity, attachment coefficient, and ionization coefficient in pure $C\ell_2$ may be made over a range of E/N covering at least two orders of magnitude using the presently improved system. At low values of E/N corresponding to electron mean energies approaching thermal, it will probably be necessary to use mixtures of $C\ell_2$ with other gases due to the large attachment cross section in $C\ell_2$ at zero energy.

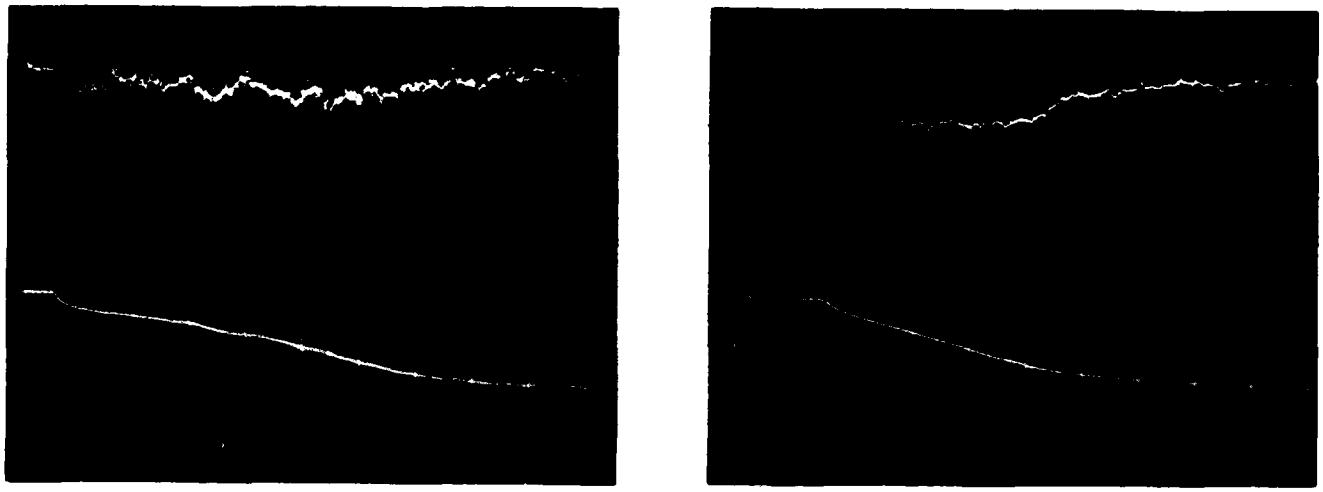

(a) (b)

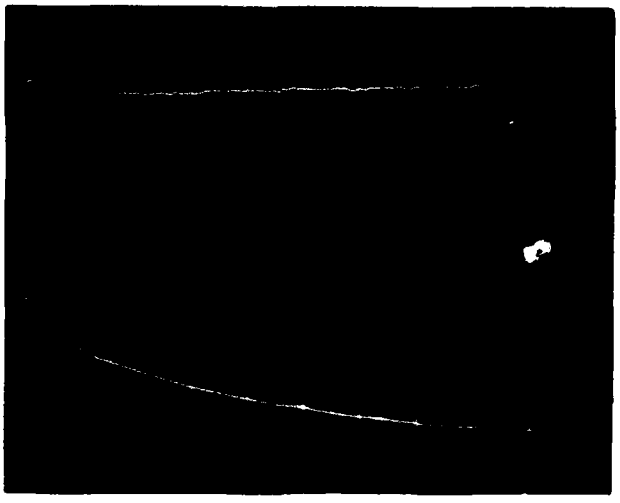

(c)

Fig. 35 - Samples of total anode current (upper trace) and charge (lower trace) waveforms recorded in pure $C\ell_2$ for a drift distance of 5.2 cm. (a) E/N = 1.000 x 10^{-15} V cm^2, N = 2.111 x 10^{16} cm^{-3}, 500 nsec/point (∿ 35 μsec/division); (b) E/N = 2.900 x 10^{15} V cm^2, N = 3.95 x 10^{16} cm^{-3}, 500 nsec/point (∿ 20 μsec/division); (c) E/N = 3.000 x 10^{-15} V cm^2, N = 2.111 x 10^{16} cm^{-3}, 200 nsec/point (∿ 10 μsec/division).

5.1.4 Discussion

The only previous swarm measurements in pure Cl_2 that have been reported are those of Bozin and Goodyear[56] in which attachment and ionization coefficients are given over the range of E/N from 212 to 455 x 10^{-17} V cm^2. Measurements of electron drift velocity, electron mean energy, and attachment coefficient have been made in mixtures of Cl_2 with He and with CO_2 by Bailey and Healey.[57] More recently, measurements of the attachment rate coefficient in Cl_2/N_2 and Cl_2/Ar mixtures at room temperature and at 250°C have been made by Rokni et al.[58] corresponding to electron mean energies ~ 1 eV and ~ 5.2 eV, respectively. Similar measurements at room temperature in the same mixtures have also been reported by Sze et al.[59] Values of the thermal attachment rate coefficient that have been reported[60,61] differ by an order of magnitude.

The availability of precision swarm measurements over an extended range of E/N in pure Cl_2 and in Cl_2/N_2 mixtures for the low energy region would allow an attempt to obtain a self-consistent set of cross sections for Cl_2 in the manner already carried out for HCl. In the case of Cl_2, absolute cross section measurements for both positive and negative ion formation have been reported by Kurepa and Belic[62] for electron energies from 0 to 100eV. The shape of the dissociative attachment cross section in the region from 0 to 8 eV is in good agreement with the relative measurements of Tam and Wong.[63] No measurements have been reported of elastic, vibrational excitation, or electronic excitation cross sections in Cl_2. However, the availability of both attachment and ionization absolute cross sections provides a good basis for determination of the other cross sections from swarm data.

5.2 BORON TRICHLORIDE

Because of the effort devoted to solving the problem associated with providing an adequate electron pulse source for drift-tube studies in Cl_2, no time was available for measurements in BCl_3. At present it is not known whether BCl_3 will present special problems for operation of the drift tube. However, the production of an adequately large electron pulse from the cathode is not likely to be as difficult as that experienced in the study of Cl_2, particularly since a pulsed photoelectron source has been used previously[64] in BCl_3/N_2 mixtures.

The available information on cross sections in $BC\ell_3$ is both meagre and conflicting, and is confined to studies of negative ion formation[48,64,65] and to studies of the threshold behavior of excitation cross sections[64] using the SF_6 scavenger technique. The production of $C\ell^-$ and $C\ell_2^-$ ions by dissociative attachment has been observed by Stockdale et al.,[64] both peaking at an energy ~ 1.1eV, the $C\ell^-$ peak intensity being an order of magnitude larger than the $C\ell_2^-$ peak. Secondary peaks for $C\ell^-$ production at ~ 2.5 eV and ~ 8 eV and for $C\ell_2^-$ production at ~ 8eV are found to vary as the square of the $BC\ell_3$ pressure. In contrast the low-energy peak is observed by Buchel'nikova[48] at an energy ~ 0.4 eV. The value of the cross section at the low-energy peak is reported[48] to be a factor of seven larger than that for $HC\ell$. No information on other cross sections is available. The only swarm measurement which has been reported is that of the thermal attachment rate coefficient[64]; the value 2.7×10^{-9} cm^3/sec found would appear to be anomalously large in view of the relatively high threshold, ~ 0.2 eV, of the attachment cross section.

It is clear that the determination of a self-consistent set of cross sections for $BC\ell_3$ not only requires extensive swarm measurements but also information on some of the cross sections, particularly the attachment and ionization cross sections.

6. SUGGESTED FURTHER WORK

Operation of discharges in XeCℓ laser mixtures leads to the production of $Cℓ_2$ as a result of reactions involving the chlorine-donor molecule. Thus, the availability of a set of cross section for $Cℓ_2$ is particularly desirable for modelling the effects of $Cℓ_2$ build-up in the laser gas mixture. The successful solution to the problems associated with operation of the drift tube in the presence of pure $Cℓ_2$ now enables measurements of swarm parameters in $Cℓ_2$ to be carried out. Further, it is considered that sufficient information is available on some of the key cross sections to enable a set of cross sections for $Cℓ_2$ to be determined from iterative solutions of the Boltzmann equation.

With respect to the chlorine-donor molecules, some questions remain to be addressed concerning HCℓ, further measurements are required in $CCℓ_4$ to cover the region of low electron mean energy, and measurements in $BCℓ_3$ have yet to be undertaken.

The prime chlorine-donor molecule currently used in the XeCℓ laser system is HCℓ and the present work has provided an extensive data base for this gas. However, further measurements of swarm parameters in mixtures of HCℓ with other gases, such as N_2, whose cross sections are known would be desirable to (i) separate the effects of rotational excitation from elastic scattering at low electron mean energy and (ii) more uniquely determine the cross section for dissociation (the A state). Both of these considerations bear on the attachment rate of HCℓ under conditions used for laser pumping. The attachment rate to rotationally[66] or vibrationally[32] excited HCℓ is known to be substantially higher than that to ground state HCℓ. Thus, prediction of the populations of rotationally and vibrationally excited states in the gas mixture enables the enhancement of the attachment rate to be predicted. Since quenching of vibrationally excited states by hydrogen atoms is particularly efficient, the dissociation rate of HCℓ is clearly significant.

Regarding the other chlorine-donor molecules, the present work in pure $CCℓ_4$ has provided data covering the upper range of electron mean energy. Because of the very large attachment coefficient in $CCℓ_4$, further measurements in mixtures of $CCℓ_4$ with other gases are required to provide information on

swarm parameters for the lower range of mean energy. The molecule $BC\ell_3$ requires a complete investigation of swarm parameters over an extended range of E/N. The attachment coefficient for this gas is likely to be low enough to enable measurements in the pure gas to be made over the whole range of E/N. The successful solution to the measurement problems encountered in $C\ell_2$ provides confidence that the presently modified system can also be used to determine swarm parameters in the potentially difficult gas $BC\ell_3$.

From the present experience in predicting properties of HCℓ/Xe/Ne mixtures it is apparent that complete information on the gases Xe and Ne is not presently available. In particular, uncertainties in the excitation cross sections for Xe and Ne lead to uncertainty in predicting the ionization rate for Xe^+ which is one of the components in the reaction forming the upper laser state via the ion-ion recombination channel. This uncertainty would be considerably reduced if the momentum transfer cross section were known for electron energies above 7 eV. Thus, it is proposed that a systematic set of measurements of electron drift velocity be made in pure Xe and in pure Ne over a range of E/N extending into the ionization region. The availability of such data would then allow the momentum transfer and excitation cross sections for Xe and Ne to be determined from iterative solutions to the Boltzmann equation using available data for the ionization coefficient and ionization cross section which are already well established for these gases.

REFERENCES

1. Manufactured by Buckbee-Mears Company.

2. MKS Instruments, Inc.

3. J. Romand, Ann. de Phys. 4, 527 (1949).

4. G. E. Gibson and N. S. Bayliss, Phys. Rev. 44, 188 (1933).

5. D. Stelman, J. L. Moruzzi, and A. V. Phelps, J. Chem. Phys. 56, 4183 (1972).

6. G. S. Hurst, L. B. O'Kelly, E. B. Wagner, and J. A. Stockdale, J. Chem. Phys. 39, 1341 (1963).

7. J. Lucas, Int. J. Electron. 17, 43 (1964).

8. L. M. Chanin, A. V. Phelps, and M. A. Biondi, Phys. Rev. 128, 219 (1962).

9. L. S. Frost and A. V. Phelps, Phys. Rev. 127, 1621 (1962).

10. A. V. Phelps, Rev. Mod. Phys. 40, 399 (1968).

11. R. D. Hake and A. V. Phelps, Phys. Rev. 158, 70 (1967).

12. J. H. Parker and J. J. Lowke, Phys. Rev. 181, 290 (1969).

13. J. J. Lowke and J. H. Parker, Phys. Rev. 181, 302 (1969).

14. P. E. Luft, JILA Information Center Report No. 14 (University of Colorado, 1975).

15. L. C. Pitchford and A. V. Phelps, Phys. Rev. A25, 540 (1982).

16. L. C. Pitchford and A. V. Phelps, Bull. Am. Phys. Soc. II, 27, 109 (1982).

17. J. J. Lowke, A. V. Phelps, and B. W. Irwin, J. Appl. Phys. 44, 4664 (1973).

18. V. A. Bailey and W. E. Duncanson, Phil. Mag. 10, 145 (1930).

19. E. W. McDaniel and M.R.C. McDowell, Phys. Rev. 114, 1028 (1959).

20. R. J. Corbin, K. J. Nygaard, and W. R. Snow, Bull. Am. Phys. Soc. II, 22, 191 (1977).

21. J. S. Townsend, Phil. Mag. 5, 389 (1903).

22. F. J. Davis, R. N. Compton and D. R. Nelson, J. Chem. Phys. 59, 2324 (1973).

23. L. G. Christophorou, R. N. Compton, and H. W. Dickson, J. Chem. Phys. 48, 1949 (1968).

24. S. Altshuler, Phys. Rev. 107, 114 (1957).

25. E. Bruche, Ann. der Phys. 82, 25 (1927).

26. D. W. Norcross, private communication.

27. C. A. Burrus, J. Chem. Phys. 31, 1270 (1959).

28. K. Rohr and F. Linder, J. Phys. B 8, L200 (1975); J. Phys. B 9, 2521 (1976).

29. R. Azria, L. Roussier, R. Paineau and M. Tronc, Rev. Phys. App. 9, 469 (1974); M. Tronc, R. Azria, Y. LeCoat, and D. Simon, J. Phys. B 12, L467 (1979); R. Azria, Y. LeCoat, D. Simon, and M. Tronc, J. Phys. B 13, 1909 (1980).

30. J. P. Ziesel, I. Nenner, and G. J. Schulz, J. Chem. Phys. 63, 1943 (1975).

31. R. Abouaf and D. Teillet-Billy, J. Phys. B 10, 2261 (1977).

32. M. Allan and S. F. Wong, J. Chem. Phys. 74, 1687 (1981).

33. C. L. Chen and P. J. Chantry, private communication. These measurements have been carried out using total ion collection within a collision chamber which defines the interaction region of monoenergetic electrons with molecules under single-collision conditions. A description of the apparatus and method used may be found in P. J. Chantry, "Negative Ion Formation in Gas Lasers," in Gas Lasers, W. L. Nighan, Ed. (Academic Press, 1982), Ch. 2.

34. K. T. Compton and C. C. Van Voorhis, Phys. Rev. 26, 436 (1925).

35. R. N. Compton, R. H. Huebner, P. W. Reinhardt, and L. G. Christophorou, J. Chem. Phys. 48, 901 (1968).

36. D. Kligler, Z. Rozenberg and M. Rokni, Appl. Phys. Lett. 39, 319 (1981).

37. R. C. Sze and A. E. Greene, Bull. Am. Phys. Soc II, 26, 726 (1981).

38. A. G. Engelhardt, A. V. Phelps, and C. G. Risk, Phys. Rev. 135, A1566 (1964).

39. L. E. Kline, private communication.

40. W. L. Nighan and R. T. Brown, Appl. Phys. Lett. 36, 498 (1980).

41. D. J. Seery, J. Chem. Phys. 58, 1796 (1973).

42. R. L. Wilkins, J. Chem. Phys. 63, 534 (1975).